

LIDA MALANA

This is to certify that the

thesis entitled

FORMATION CONSTANT AND PHOTOLABELING OF GRAMICIDIN

CHANNELS IN LIPID BILAYER MEMBRANES

presented by

Hsiao Yung Guh

has been accepted towards fulfillment of the requirements for

Ph.D. degree in Chemistry

Major professor

Date May 19, 1981

O-7639

. 5513



OVERDUE FINES: 25¢ per day per item

RETURNING LIBRARY MATERIALS:
Place in book return to remove charge from circulation records

FORMATION CONSTANT AND PHOTOLABELING OF GRAMICIDIN CHANNELS IN LIPID BILAYER MEMBRANES

Ву

Hsiao Yung Guh

A DISSERTATION

Submitted to

Michigan State University

in partial fulfillment of the requirements

for the degree of

DOCTOR OF PHILOSOPHY

Department of Chemistry

ABSTRACT

FORMATION CONSTANT AND PHOTOLABELING OF GRAMICIDIN CHANNELS IN LIPID BILAYER MEMBRANES

Ву

Hsiao Yung Guh

Gramicidin, a polypeptide of 15 alternating D and L amino acids, has been shown to increase the cation permeability of biological membranes. Substantial evidence indicates that ion transport across the membrane is mediated by gramicidin via the pore mechanism and that the gramicidin channel consists of two molecules.

By use of the charge injection technique, we have successfully obtained the formation constants of gramicidin channels in lipid membranes as well as the partition coefficients of gramicidin between the bilayer and torus phases. It was found that both of the parameters depend greatly on the membrane thickness. The dimerization constant, for instance, increases from 1.9 x 10⁴ l·mole⁻¹ for decane membranes (46.5Å in thickness) to 9.9 x 10⁵ l·mole⁻¹ for hexadecane membranes (32.0Å in thickness). In addition, a correlation was discovered between the dimerization constant and partition coefficient between the membrane

and torus regions. It is of interest to note that although relaxation experiments have been performed on the membranes, the resulting physical parameters represent the equilibrium values for the same parameters prior to the charge perturbation.

In order to study the orientation of gramicidin channels in lipid bilayers, 2-nitro-5-azidobenzoic acid (NABA), a photolabeling reagent, was devised. In the presence of this reagent, a remarkable blocking effect on gramicidin-mediated ion transport was observed upon illumination. The reduction in membrane conductance is attributed to the steric hindrance imposed by photolabels attached to the channel opening. Unfortunately, the chemical analysis of photoaltered gramicidin failed to reveal the exact location of the photolabeling. As a result, no definite conclusion was made regarding the conformation of gramicidin channels in lipid membranes.

Due to the limited capacity of the existing charge injection instrument, a microprocessor-controlled charge injection device was developed. It surpasses the old unit in performance as well as in the system design. The new device is able to inject the charge onto a capacitor in less than 100 ns and monitor the resulting voltage transient at a rate up to 15 MHz for 1K data points. The signal-to-noise ratio is at least 256 for an input voltage of 0.67 V registered at 15 MHz. The recording system

responds to a step voltage change of 0.5 V within 400 nanoseconds.

Acknowledgements

I would like to express my sincere thanks to Professor Christie G. Enke for his guidance and encouragement throughout this study. Thanks go to Professor Michael Weaver for serving as the second reader.

Special thanks go to Dr. Tom Atkinson for his help.

Many thanks also go to Marty Raab and the membranes in the

Enke research group for their help and friendship.

Deep appreciation to my parents for their unfailing support and encouragement throughout my education. Special thanks to my wife, Min, for her love and patience.

TABLE OF CONTENTS

Chapter	Page
LIST OF TABLES	
LIST OF FIGURES	
I. INTRODUCTION	1
The Biological Membrane	1
Pore Transport System	4
Gramicidin Channels	9
II. CHARGE INJECTION INSTRUMENT	15
The Measurement Problem	16
Charge Injection Approach	18
Description of Microprocessor-Controlled Charge Injection System	21
1. Overview of the System	24
2. Electrochemical Cell	26
 Pulse Generator and Cell Amplifier	28
4. Digital Recorder	30
5. Microcomputer	35
6. Operation of the System	36
7. Performance	37

Chapter	
III. FORMATION CONSTANT OF GRAMICIDIN CHANNELS IN LIPID MEMBRANES	. 46
INTRODUCTION	. 46
Current Relaxation Approach	. 47
Analog Approach	. 51
Voltage Relaxation Approach	. 52
EXPERIMENTAL	• 55
Material and Apparatus	• 55
Membrane Formation	. 56
Membrane Data Collection	• 57
Data Treatment	. 58
RESULTS AND DISCUSSION	. 60
Membrane Capacitance Measurement	. 60
Voltage Relaxation across Gramicidin-doped Membranes	. 65
Formation Constant of Gramicidin Channels	. 68
Partition Coefficient of Gramicidin between the Membrane and Torus Phases	. 82
Comments on the Assumptions	. 85
Conclusion	. 86
IV. PHOTOLABELING OF GRAMICIDIN CHANNELS IN LIPID MEMBRANES	. 88
INTRODUCTION	. 88
Photolabeling	. 89
Arvlazides	. 91

Chapter	Page
2-Nitro-5-azidobenzoic Acid	9 3
EXPERIMENTAL	94
Reagent	94
Apparatus	95
Procedure	96
RESULTS AND DISCUSSION	99
Photolysis of NABA	99
Effect of Photolysis of NABA on Gramicidin-mediated Ion Transport	101
Chemical Characterization of Gramicidin Isolated from Irradiated Liposomes	106
APPENDIX A Peripheral Schematic Diagrams	118
APPENDIX B Program Listings	121
REFERENCES	144

•

LIST OF TABLES

Table		Page
3-1	The thickness and capacitance of 3% GMO-cholesterol/n-alkane membranes (w/v)	62
3-2	Relaxation time, membrane conductance and concentration of gramicidin-doped GMO-cholesterol/n-decane membranes at 24 ± 1°C	70
3-3	Relaxation time, membrane conductance and concentration of gramicidin-doped GMO-cholesterol/n-tetradecane membranes at 24 ± 1°C	71
3-4	Relaxation time, membrane conductance and concentration of gramicidin-doped GMO-cholesterol/n-hexadecane membranes at 24 ± 1°C	72
3-5	Dimerization constant, K, and partition coefficient, D, of gramicidin in bilayer lipid membranes	76
3-6	Free energy of dimerization and partition of gramicidin in alkane membranes	84
4-1	Molecular weight and characteristic mass peaks of identified eluents	110

LIST OF FIGURES

Figure		Page
1-1	Schematic representation of the Davson-Danielli lipid membrane model. The polar head groups of the lipids are included in the aqueous phase. The shaded areas represent membrane proteins	2
1-2	Simplified schemes for carrier and channel transport	5
1-3	Stepwise changes in conductance for gramicidin-doped membrane. The aqueous phase is 1 M KCl (37)	7
1-4	Membrane treated as a series of n activation energy barriers. The energy of barrier n is f _n	8
1-5	Structure of gramicidin A	10
1-6	Possible conformations of gramicidin channels in lipid membranes (58)	13
2-1	Electrical representation of electrodes placed in two aqueous compartments separated by a membrane	17
2-2	Membrane capacitance charging curve for the voltage step and high voltage pulse experiments	20
2-3	Block diagram of the old charge injection instrument	23
2-4	Block diagram of the microprocessor-controlled charge injection device	25

Figure		Page
2-5	Schematic of electrochemical cell	27
2-6	Schematic of pulse generator and cell amplifier	29
2-7	Schematic of timing circuit	32
2-8	Schematic of ADC section	34
2-9	Response of the digital recorder to a 0.5-V 100-KHz square wave. Data collection rate: 15 MHz	38
2-10	Signal-to-noise ratio of data collected at 15 MHz	39
2-11	Response of the digital recorder to a 0-1 v 2-KHz ramp wave	41
2-12	Voltage transient resulting from a pulse application to a resistor and capacitor in parallel	42
2-13	Voltage transient resulting from a pulse application to resistor and capacitor in parallel. Data collection rate: 5 MHz	45
3-1	Voltage transients resulting from pulse applications to 3% GMO-1% cholesterol/n-tetradecane membranes in 1 M KCl at 24 ± 1°C	61
3-2	Voltage transients resulting from pulse applications to gramicidin-doped membranes in 0.5 M CaCl ₂ at 24 ± 1°C	64
3-3	Voltage relaxations resulting from pulse applications to gramicidin-doped membranes in 1 M KCl at 24 ± 1°C	66

Figure		Page
3-4	The voltage relaxation time and membrane capacitance of gramicidin-doped membranes (3% GMO-1% cholesterol/n-hexadecane) as a function of film age	69
3-5	Dimeric channel concentration, N2, as a function of the gramicidin concentration, B, in GMO-cholesterol/n-decane membranes	73
3-6	Dimeric channel concentration, N ₂ , as a function of the gramicidin concentration, B, in GMO-cholesterol/n-tetradecane membranes	74
3-7	Dimeric channel concentration, N, as a function of the gramicidin concentration, B, in GMO-cholesterol/n-hexadecane membranes	75
4-1	Reactions open to a nitrene after its formation	92
4-2	The effect of photolysis at 320 nm on the UV spectrum of NABA. NABA was dissolved in 0.1 M phosphate buffer (pH 9.4) and irradiated at 320 nm for 10 min. until no further change in the spectrum	100
4-3	The effect of photolysis on membrane conductance. Gramicidin was added to the membrane forming solution. Membrane potential: 50 mV; electrolyte: 0.1 M phosphate (pH 7.6).	102
4-4	The effect of photlysis on voltage relaxation time resulting from pulse applications to the membrane	104
4-5	Experiments that would result in substantial amount of photolabeled gramicidin for chemical characterization	107
4-6	Gas cheomatogram of derivatized hydrolysate of gramicidin isolated from control liposome using mass spectrometer as the detector	108

Figur	e	Page
4-7	Gas chromatogram of derivatized hydroly- sate of gramicidin isolated from irradiated liposomes using mass spectrometer as the detector	109
4-8	The mass spectrum of derivatized tryptophan	111
4-9	GC trace of the derivatives of tryptophan which has been treated with trifluoro-acetic acid-const. distilled HCl at 110 C for 1.5 hours	113
A-1	4K RAM board schematic diagram	118
A-2	1K PROM board schematic diagram	119
A-3	USART board schematic diagram	120

CHAPTER I

INTRODUCTION

In the past twenty years, it has become plain that the biological membrane plays a crucial role in almost all cellular activities. Its ability to regulate the transport of substances into and out of cellular organelles underlies the basis for nerve conduction (1), muscle function (2), energy assimilation (3) and conduction of metabolites through cell walls (4, 5). Consequently, a thorough study of transport system across the membrane will contribute to the understanding of these physiological phenomena. In this research, gramicidin channel, an excellent model for the study of pore transport mechanism in lipid bilayers, was photolabeled and its formation constant determined.

The Biological Membrane

The first clue that the biological membrane contained lipids came in 1899 from Overton's observation (6) that cellular membranes were permeable to lipids and lipidlike substances. Since then, numerous efforts (7-9) have been made to elucidate the structure of biological membranes. It is now generally accepted (10) that the biological membrane (Fig. 1-1) consists of two back-to-back

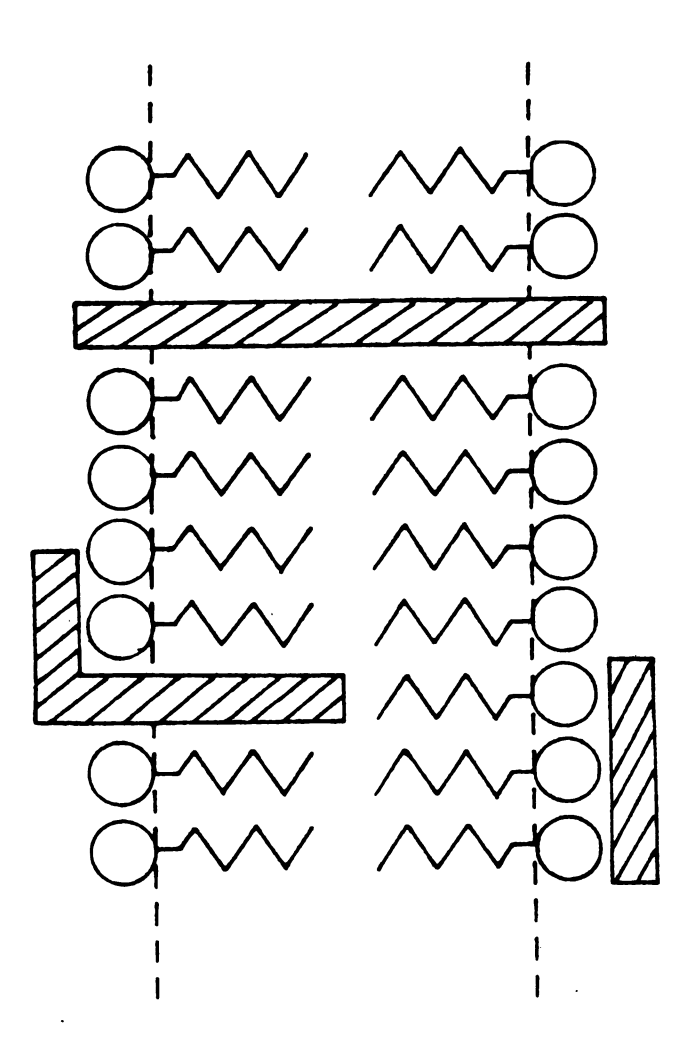


Fig. 1-1 Schematic representation of the Davson-Danielli lipid membrane model. The polar had groups of the lipids are included in the aqueous phase. The shaded areas represent membrane proteins.

layers of lipid molecules with the polar head groups pointing to the aqueous environment and the hydrocarbon tails buried inside the interior of the membrane phase. Proteins and other membrane constituents either reside on the surface of the lipid bilayers or penetrate deeply into the membrane interior. The bilayer model successfully accounts for the amphipathic nature of lipid molecules and the ultrathin membrane structure (less than 100Å) as well as for the versatile biological functions manifested by the associated proteins.

Experimentally, there are two approaches in the studies of biological membranes. One involves the utilization of spherical lipid vesicles, the so called liposomes (11), which can be prepared by sonicating lipids in aqueous solutions. The liposomes resemble the cellular membranes in that they have a curved closed form, a large surface to volume ratio and solvent-free lipid bilayers. The small physical size of liposomes (300-1000Å in diameter), however, presents obstacles to investigations where probes are required to be placed on both sides of the membrane.

This difficulty was circumvented in 1962 by Mueller et al. (12), when they successfully formed a planar bimolecular lipid membrane (BLM) by brushing a complex mixture of brain lipids, n-tetradecane, silicone fluid and mineral oil across a narrow orifice between two aqueous compartments. The planar geometry of BLM allows easy application of perturbations to and direct measurement of responses of

the membrane. As a result, a wealth of information regarding membrane permeability (13), membrane photochemicsty (14, 15), membrane transport mechanism (16-28) etc., has been learned in the past two decades.

Pore Transport System

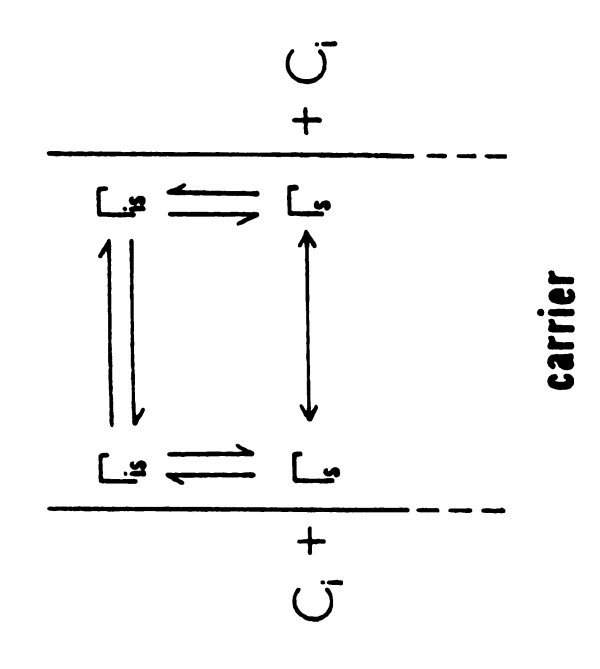
Due to the nonpolar nature of the hydrocarbon chains of lipid molecules, plain lipid membranes are not permeable to metal ions and exhibit an electrical resistance as high as 10^4 - 10^{10} ohm-cm².

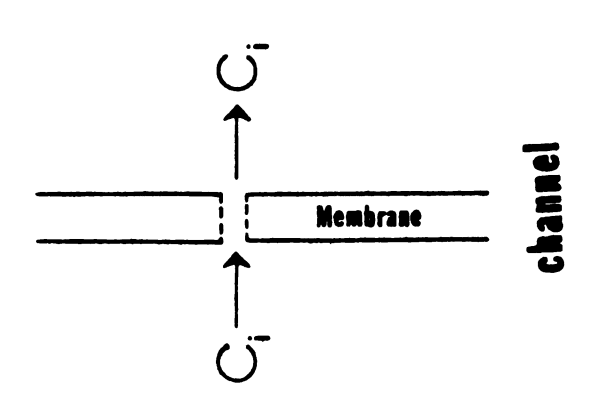
Upon the addition of some chemical substances, the resistance of lipid bilayers, however, can be reduced by several orders of magnitude. Depending on the way they facilitate the transport of ions across the membrane, these chemical modifiers can be classified into two categories: carriers (29-31) and pore formers (32-37).

In the carrier mechanism, as depicted in Fig. 1-2, the ions form complexes with carrier molecules and the subsequent diffusion of the complexes across the membrane translocates the ions from one side of the bilayer to the other side of the bilayer.

In the pore mechanism (Fig. 1-2), as the name implies, the chemical modifiers form transmembrane channels through which the ions diffuse across the membrane.

The ion translocation mediated by transmembrane





Simplified schemes for carrier and channel transport. Fig. 1-2

channels displays several interesting features not shared by the carrier system. It is observed that membranes doped with pore formers have very high ion transport rate ($4 \times 10^{-11} \Omega^{-1}$ for a single gramicidin channel in 1 M potassium chloride at 25°C) (37) and the membrane conductance is essentially independent of membrane thickness (38). Furthermore, the high conductance of a pore-doped bilayer membrane persists when the lipid film is solidified by lowering the temperature (39). The most striking aspect of the channel transport system is, however, the finding that when the concentration of pore formers in the bilayers is very low, the membrane conductance fluctuates in a stepwise fashion with definite heights (Fig. 1-3) (37). The commencement and termination of a transition corresponds to the opening and closing of a single conducting channel.

Over the years, a number of models have been proposed for the mechanism of pore transport system (21-28). Although they differ in sophistication, all the postulations are based on Eyring rate theory (40), in which the transmembrane channel has been considered as a sequence of energy barriers over which the ion has to jump (Fig. 1-4). The kinetics of pore mediated transport are governed by

- (1) the number and the heights of potential barriers in the channel and
- (2) the simulataneous occupancy of various ion binding sites.

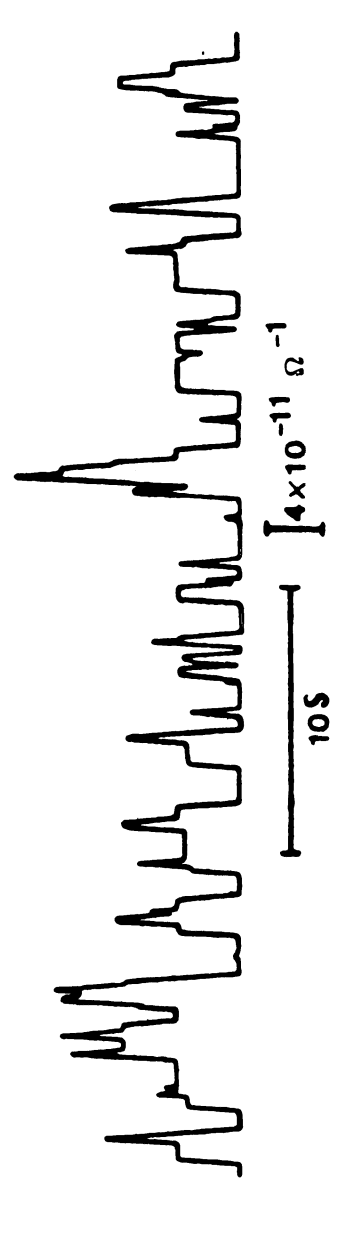


Fig. 1-3 Stepwise changes in conductance for gramicidin-doped membrane. The aqueous phase is 1M KCl (37).

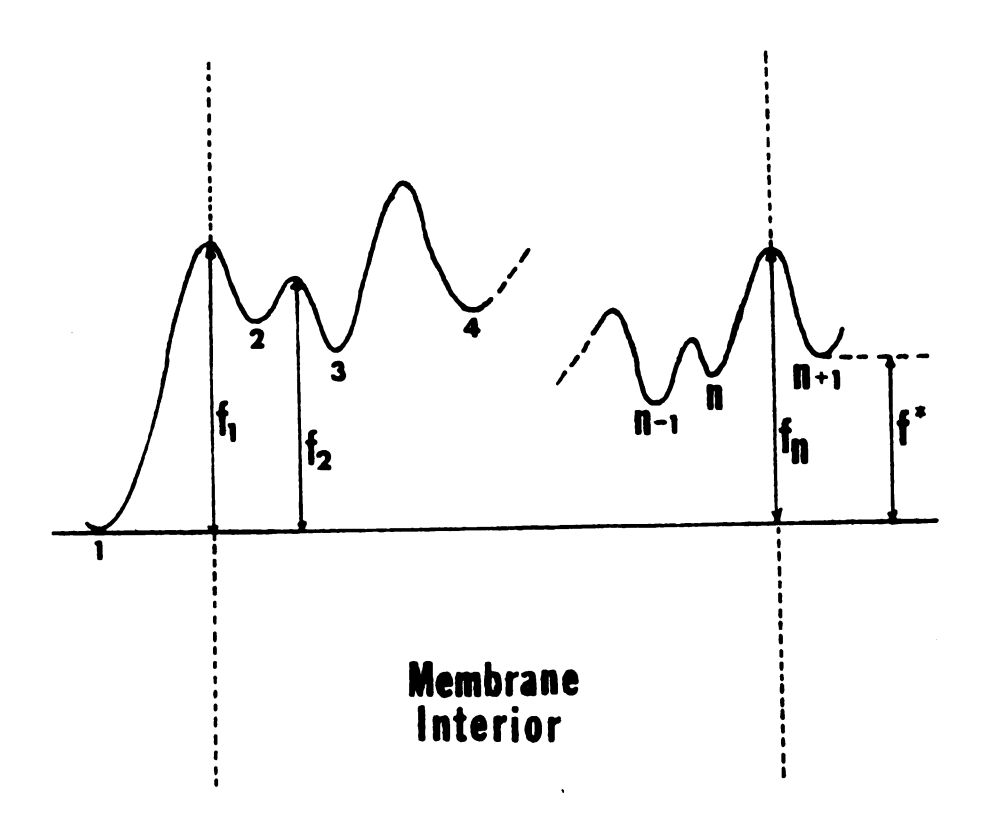


Fig 1-4 Membrane treated as a series of n activation energy barriers. The energy of barrier n is f_n .

The potential difference between the two aqueous phase is \mathbf{f}^* .

Recently, Haegglund et al. (28) put forth a three-site-four-barrier model, which successfully accounts for the observed concentration-dependences of flux-ratio, conductance, I-V characteristic and permeability displayed by gramicidin-doped membranes. As the membrane conductance induced by gramicidin is voltage-independent, it is obvious that a more sophisticated and elaborate model is needed before voltage-dependent conductance manifested by certain pore formers could be satisfactorily rationalized.

Gramicidin Channels

Of the various pore formers known today, gramicidin system is probably one of the most investigated because of

- (1) its commercial availability,
- (2) structural simplicity (both primary structure and channel structure) and
- (3) resemblance to physiological channels (Na⁺ and K⁺ channels in nerve, for example).

Historically, gramicidin was first isolated from Bacillus brevis by Hotchkiss and Dubos in 1941 (41). In 1965, Sarges and Witkop reported that gramicidin is a linear polypeptide, consisting of 15 alternating D and L amino acids (Fig. 1-5) with N-terminus blocked by a formyl group and C-terminus derivatized to an amino alcohol (42). It is noted that none of gramicidin's amino acid constituents is polar or ionic. As a result, gramicidin is

HCO-L-Val-Gly-L-Ala-D-Leu-L-Ala-D-Val-L-Val Try-L-Leu-D-Try-L-Leu-D-Try-L-Val-D D-Leu-L-Try-NHCH2CH20H

GRAMICIDIN

Fig. 1-5 Structure of gramicidin A. Gramicidin B and C differ from gramicidin A in that L-try in position 11 is replaced by L-phe and L-tyr, respectively. Commercially available gramicidin is a mixture of gramicidin A (85%), B (4%) and C (11%).

highly hydrophobic with a solubility of less than 10^{-10} M in aqueous solutions.

In 1972, through the measurement of biionic potentials and transference numbers of various electrolytic solutions partitioned by gramicidin-doped membranes, Haydon and Mayers (43) found that the gramicidin channel is not permeable to anions, is blocked by divalent cations and is selective for univalent cations with the following sequence: $H^+>NH_4^+>Cs^+>Rb^+>K^+>Na^+>Li^+>(CH_3)_4^N^+$.

Substantial evidence suggests that gramicidin channels in lipid bilayers are dimeric in nature. Tosteson (44) and Goodall (45) observed that the membrane conductance increases with the square of the gramicidin concentration in the aqueous phase. In 1973, by means of voltagejump experiments, Bamberg and Lauger (46) acquired results which are consistent with the hypothesis of an equilibrium in the membrane between a non-conducting monomer and a conducting dimer of gramicidin A. In 1975, based on the simultaneous measurements of membrane fluorescence and conductance. Veatch et al. (47) reported that dancyl gramicidin C, a highly active analog of gramicidin, forms a dimeric channel in lipid membranes. Similar results have also been obtained from an autocorrelation analysis of the conductance fluctuations (48). Recently, X-ray diffraction studies on a cation-containing gramicidin structure (49) shows a 26Å-length to the pore and a 3.4Å-length to the radius, which further supports the dimer concept of the

channel on the basis of the molecular size of monomeric gramicidin.

In the past decade, several structures have been proposed for the conformation of gramicidin channels in lipid membranes. The salient features of these conformations are depicted in schematic form in Fig. 1-6. Model A is the N-terminal-to-N-terminal single stranded helical dimer proposed by Urry et al. (50). Model B, a C-terminal-to-C-terminal helix, was considered by Bradley et al. (51), when they discovered that N-succinyldeformyl gramicidin methyl ester is able to induce membrane conductance.

Model C is the antiparallel double helix proposed by Veatch et al. (52-54) as one of the dimer conformations found for gramicidin in nonpolar organic solvents. Model D is a parallel double helix with both N-termini at one end of the channel.

examining their ability in inducing membrane conductance (51, 55-57), it was concluded that the double-stranded helics (model C and D) could not adequately represent the conformation of gramicidin channels in lipid membranes. More recently, Veatch et al. (58) incorported ¹³C and ¹⁹F nuclei at both N and C termini of gramicidin and carried out NMR experiments to determine the relative accessibility of these ¹³C and ¹⁹F nuclei to paramegnetic probes in the aqueous solution. They found that the chemical shifts and spin lattice relaxation rates of C-terminal labels are

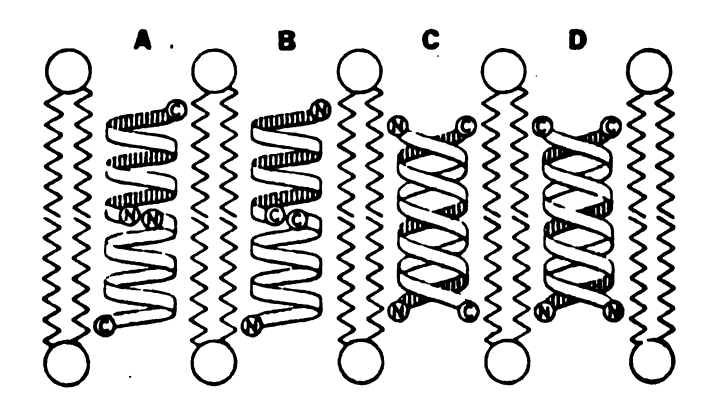


Fig. 1-6 Possible conformations of gramicidin channels in lipid membranes (58).

- A. N-terminal-to-N-terminal single-stranded helix
- B. C-terminal-to-C-terminal single-stranded helix
- C. antiparallel double-stranded helix
 D. parallel double-stranded helix

affected much more than those of N-terminal labels by the aqueous paramagnetic ions. It is thus believed that the most probable channel structure of gramicidin in membranes is model A.

The experiments mentioned above, however, suffer from one serious drawback, i.e., they all utilized chemically altered gramicidins. It is noted (51) that the polarity and physical size of chemical groups derivatized to gramicidin greatly affect the way the channel is formed. Consequently, in order to obtain unambiguous information regarding the channel conformation, some new techniques have to be developed which would use native gramicidin as the major investigating tool.

CHAPTER II

CHARGE INJECTION INSTRUMENT

An often-used technique to study ion transport across a lipid membrane is to make steady-state conductance measurements on a given membrane and transport system for a family of ions. However, in order to evaluate many of the kinetic parameters, it is necessary to perform measurements on a short time scale after a certain perturbation.

In 1977, a computer-controlled data acquisition system was developed in this laboratory (77). The device is able to monitor the voltage transient resulting from a pulse application to a membrane at a rate up to 10 voltage readings per microsecond. It was demonstrated that rate constants regarding monactin-and dinactin-mediated ion transport could be obtained from charge injection experiments by use of this instrument (78).

Recently, we have built a microprocessor-controlled charge injection device. It will be shown in this chapter that the new system surpasses the old device in performance as well as in the system design.

This chapter is organized into two sections. The first part includes a brief discussion of the measurement problems encountered in membrane kinetics and the advantages of the charge injection technique. The second

section is a description of the newly constructed system and its performance.

The Measurement Problems

One approach to study the kinetics of fast reactions is to apply a sudden perturbation to the system of interest and mointor the resulting relaxation. The most widely used method to date in the study of membrane kinetics has been the voltage step experiment. This technique has not been totally successful in measuring very fast parameters however, due to the membrane capacitance. The experimental set up for an electrical measurement on a membrane can be represented by Figure 2-1; where:

C_M = membrane capacitance,

G(V) = membrane conductance (function of voltage),

 C_T = membrane-solution double layer capacitance,

 R_S = solution resistance,

 $C_{\rm F}$ = electrode-solution double layer capacitance, and

 $R_{\rm F}$ = Faradaic resistance at the electrode.

Several disadvantages of the voltage step technique can be recognized from Figure 2-1. First, due to the fact that the membrane must be charged, the voltage perturbation is not a clean transition but rather a growing exponential curve whose time constant depends on the resistances and capacitances mentioned above. This slow growth of the forcing function completely obscures any information in

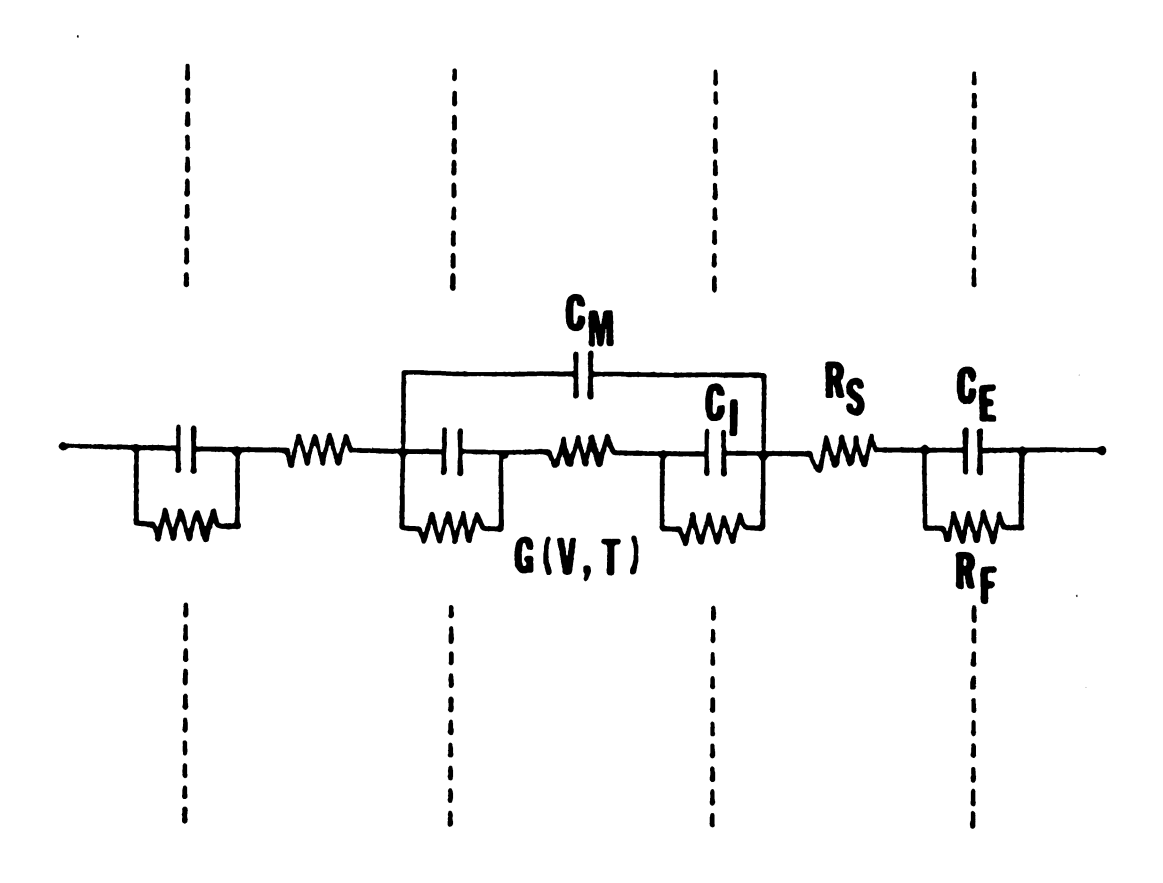


Fig. 2-1 Electrical representation of electrodes placed in two aqueous compartments separated by a membrane.

the early part of the relaxation. Second, in a voltage jump experiment the total current passing through the cell is measured instead of that due only to G(V,t). As a result, the current going to charge the membrane capacitance further obsures the relaxation. Third, because of the solution and Faradaic resistances the membrane potential is always less than the externally applied voltage.

Charge Injection Approach

The membrane capacitance problem has been avoided in the charge injection technique (76). This method uses the membrane capacitance to advantage by charging the membrane very rapidly and monitoring the voltage decay as the membrane's conductance (ion transport) depletes the charge stored on the membrane capacitance.

The advantages that accrue to this method are the following:

- 1. The entire conductance-voltage relationship can be deduced from data obtained by a single pulse on a single membrane and in a time short enough to minimize changes in membrane area and composition.
- 2. No current exists in the solution or external circuitry during the measurement. Thus, the solution resistance between the membrane and

the electrodes does not introduce an extraneous voltage drop.

- 3. The time course of the voltage decay depends on the ratio of the membrane capacitance to the conductance and therefore is independent of membrane area.
- 4. The voltage at any time after injection yields the amount of charge which has crossed the membrane since application of the charge pulse.
- 5. The fast charge injection allows measurements to be made on the system within a few hundred nanoseconds.

The primary disadvantage of the technique is that the relaxation occurs over a broad potential range and the voltage dependencies as well as the time dependencies must be determined. Furthermore, small amplitude relaxation will be difficult to observe and analyze.

Traditionally, there are two ways to achieve a rapid injection of charge onto a membrane. Both approaches utilize a pulse generator with a high output voltage compliance and rapid rise time. Since the pulse duration is very short, a high voltage level that would normally break the membrane can be successfully employed. When the pulse generator is operated in a current mode, the time necessary to charge the membrane to a given voltage would be given by t = VC/i, where V is the desired voltage, C is the membrane capacitance, and i is the amplitude of the current pulse.

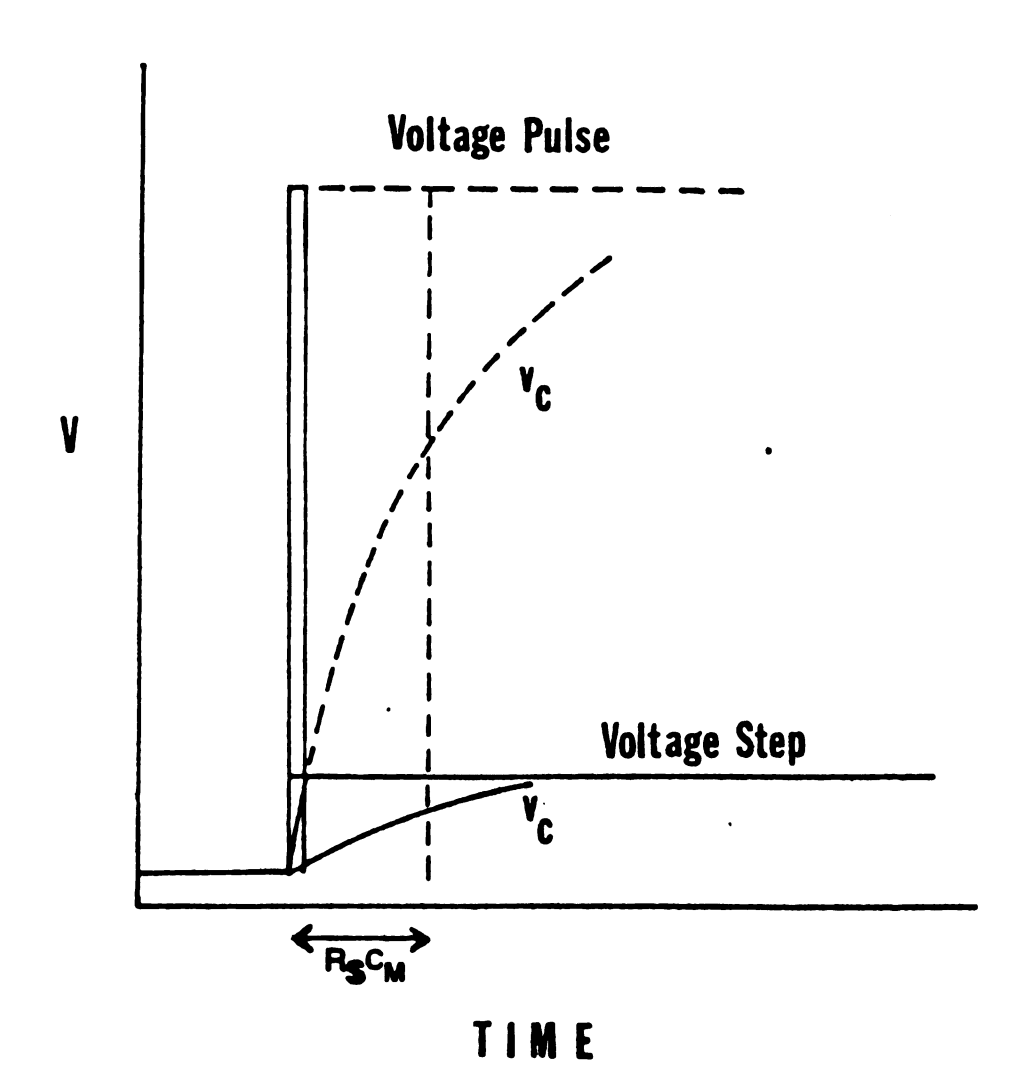


Figure 2-2. Membrane capacitance charging curves for the voltage step and high voltage pulse experiments. V is the voltage on the membrane capacitance.

As is evident from Figure 2-2, although the capacitance must be charged through the solution resistance, a voltage pulse of large amplitude can also bring the membrane potential to a desired value in much less than $R_S^C{}_M$ seconds. In practice this results in an improvement of the charging time from tens of microseconds for the voltage step method, to a hundred nanoseconds for the charge injection technique using a voltage pulse.

Recently, due to the advance in electronic technology, a third approach has been developed. In this method, a predetermined amount of charge is stored on a capacitor and then dumped onto the membrane capacitance by means of an ultrafast operational amplifier. The speed of the charging action depends greatly on the settling time of the output of the amplifier. With a state-of-the-art fast operational amplifier, it is now feasible to accomplish a charge injection in a few hundred nanoseconds. The advantages of this method over the use of a pulse generator are the low cost and structural simplicity of the charging device and the precision of the charge injection.

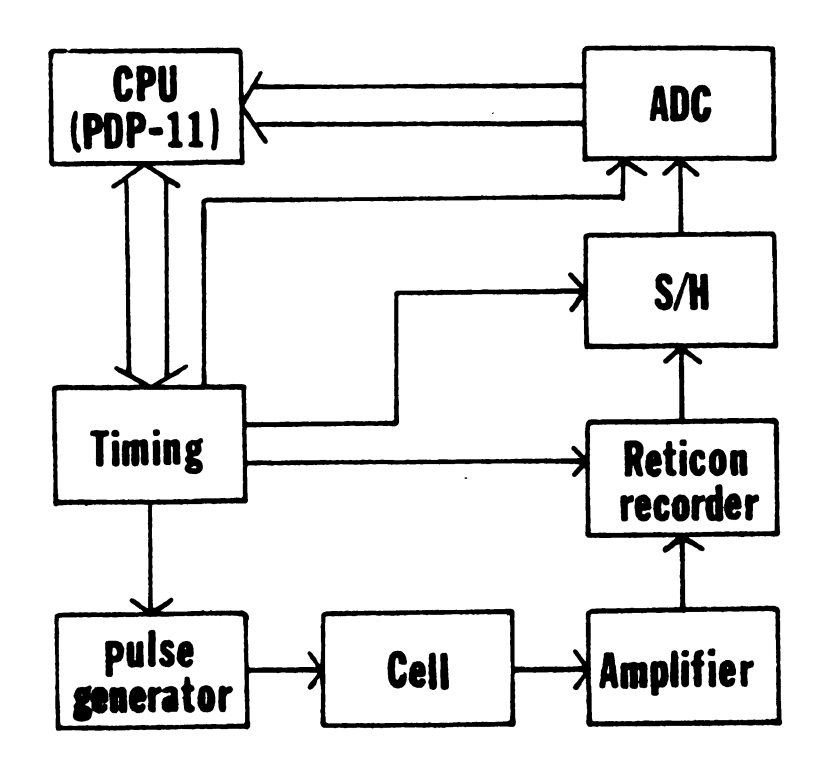
<u>Description of Microprocessor-Controlled Charge Injection</u> <u>System</u>

The first computer-controlled charge injection instrument designed for membrane kinetics studies was developed in this laboratory in 1977 (77, 78). The block

diagram of the instrument is shown in Figure 2-3. It consists of four major parts: a minicomputer, a pulse generator, a cell amplifier and a Reticon transient recorder. Two advantages of this system can be recognized. First, the employment of a minicomputer minimizes the human errors and the time to perform experiments, data acquisition and data analysis. Second, the rapid injection of charge onto the membrane and the ability of the Reticon recorder to collect data at 10 MHz makes possible the study of fast kinetics at microsecond level. However, a system that requires the constant attention of a minicomputer is rather expensive. In addition, the number of data points available at the fast collection rate (0.1 to 10 MHz) is limited to 100.

In the past few years, due to the advance in microelectronics, microcomputers have become very cost-effective
and are capable of performing most of the tasks previously
assigned to a minicomputer. Furthermore, high speed
electronic components such as operational amplifiers,
analog-to-digital converters (ADC) and random access memory
(RAM) are also available at moderate prices. It thus
appears that a significant improvement in the design and
cost/performance ratio of the charge injection system could
be accomplished by use of these recently developed
electronic devices.

In this section, the details of the newly constructed charge injection device, its operation and performance will be discussed.



Figrue 2-3 Block diagram of the old charge injection instrument.

1. Overview of the System

Figure 2-4 shows the block diagram of the newly constructed system. It consists of a microcomputer, a pulse generator, a cell amplifier, an electrochemical cell and a fast digital recorder. Several features can be recognized in this system. First, the control of the experiment and the data acquisition is accomplished by a microcomputer. This alleviates the working load of a minicomputer and allows it to perform more significant tasks such as data analysis. Second, a digital recorder capable of operation at 15 MHz with 1K memory has been implemented. It surpasses the Reticon analog recorder in speed, memory size, range of data collection rate and circuit design. Third, the charge pulse generator is composed of an ultrafast operational amplifier, a capacitor and a set of switches. This simple device replaces the conventional pulse generator which costs \$1400. Fourth, the whole system (including the microcomputer) is built on three circuit boards. The simplicity of the system design makes the construction and debugging relatively easy and reduces the overall cost to about \$1400. The only expensive component in the instrument is the analog-to-digital converter used in the digital recorder. It is an 8-bit device (0.39% resolution) and cost \$800.

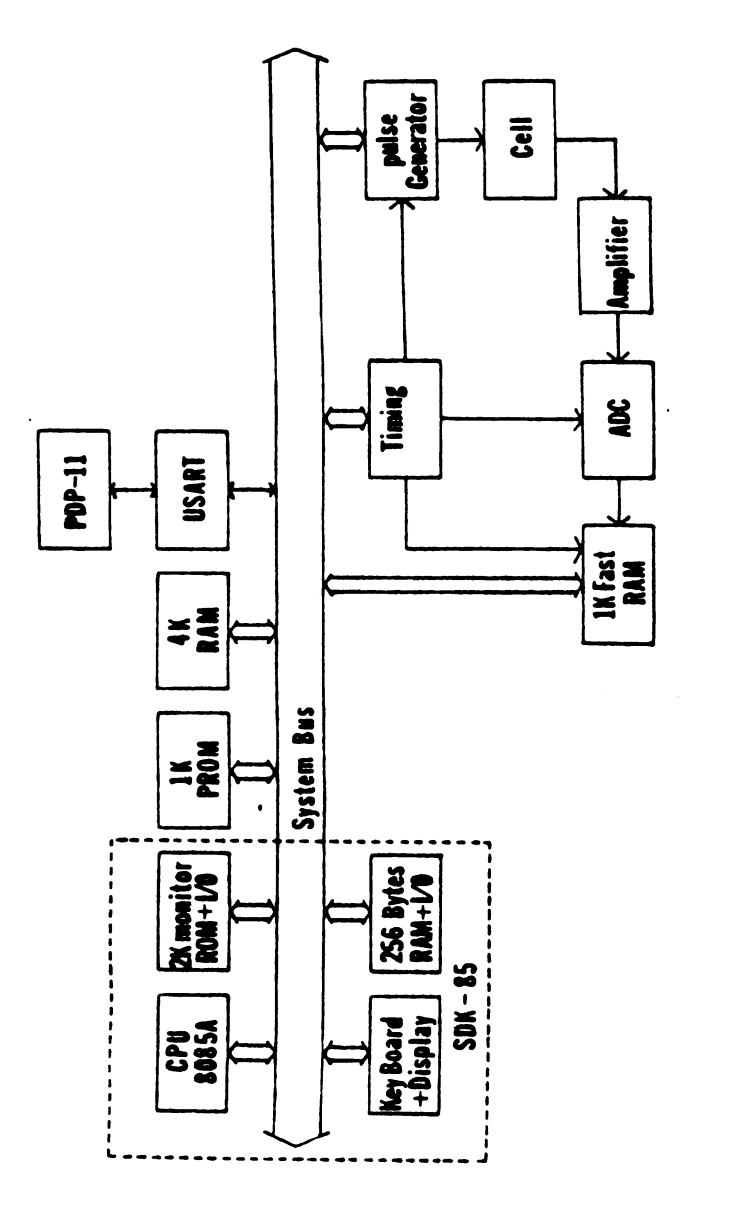


Figure 2-4. Block diagram of the microprocessor-controlled charge injection device.

2. Electrochemical Cell

The schematic of the electrochemical cell is shown in Figure 2-5. It consists of two Teflon compartments.

Each has a volume of 45 ml separated by a Teflon sheet (0.25 mm in thickness) with an orifice (1-2 mm in diameter) in the center. Two Viton "0" rings, each situated in a circular trough on the Teflon compartment, are used to ensure tightness when the cell parts are clampped together.

On the face opposite to the 0-ring trough side of the compartment there is 1-inch circular hole. The mounting of a glass window of the same size allows the visual examination of the formed lipid membrane through a microscope. To prevent solution leakage, a Teflon tape (0.5 inch in width) of proper length is employed to achieve tight fit of the glass window to the hole.

Two Ag/AgCl electrodes are shaped into coils and mounted on a piece of Teflon plate. The length and separation of the electrodes is such that when the plate is placed on top of the cell assembly, each electrode dips into the solution in a different compartment. The electrodes are made of silver wires coated with AgCl and have a surface area of about 3.5 cm². Since the AgCl on the cathode is consumed in the experiments, the coating must occasionally be reinforced by anodizing the electrodes in NaCl with a Pt counter electrode. It should be noted that each pulsing study uses approximately 5 nanocoulombs and therefore the coating is not depleted rapidly.

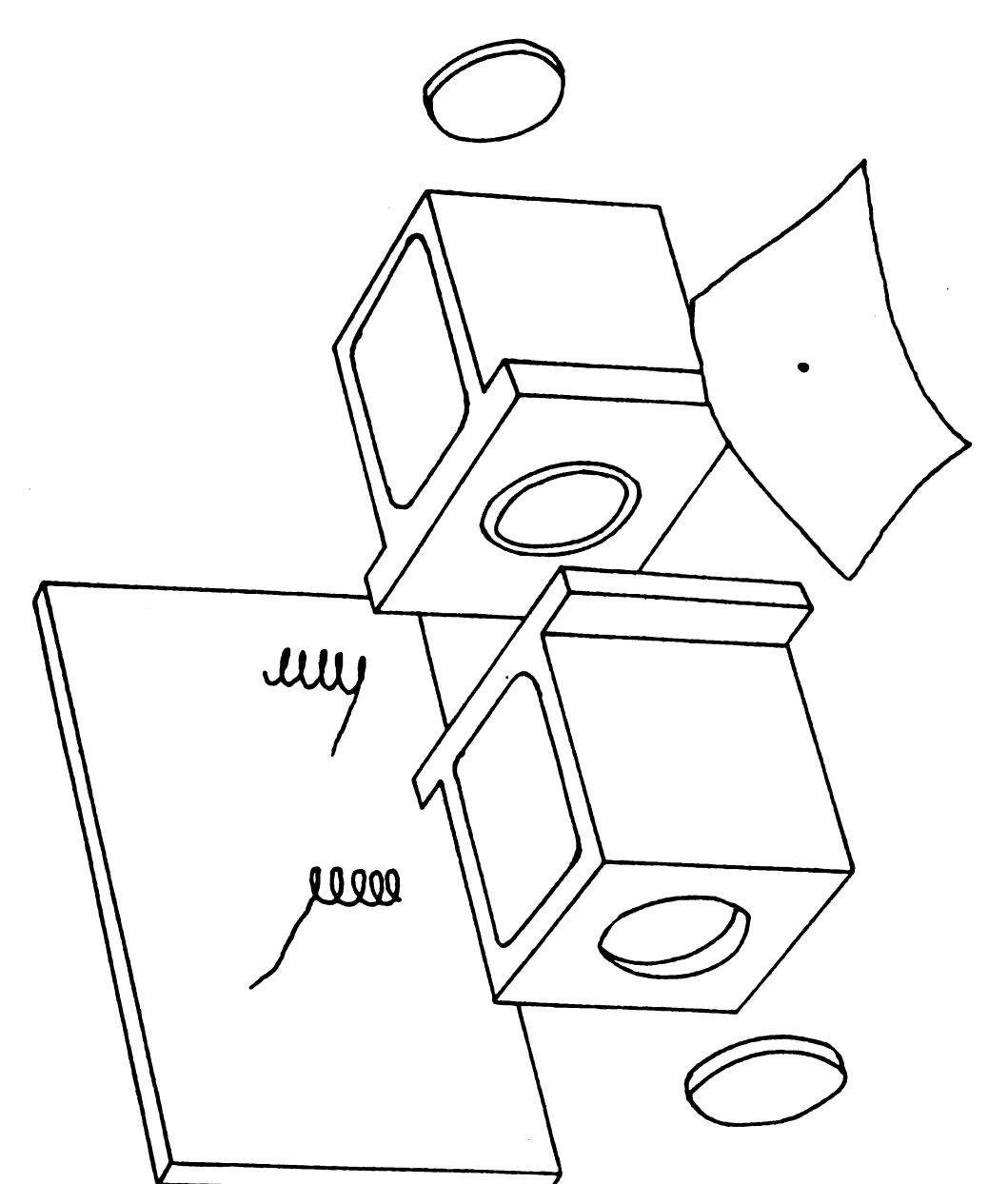


Figure 2-5. Schematic of electrochemical cell.

3. Pulse Generator and Cell Amplifier

The pulse generator and cell amplifier are shown in schematic form in Figure 2-6. The pulse generator and the amplifier are placed as close to the electrodes as possible in order to minimize capacitance and stray signal pickup in the connecting wires. The components are housed in a small aluminum box which rides "piggy back" on the electrochemical cell. The electrodes are attached through a 2 prong Cinch-Jones connector on the bottom of the housing.

The pulse generator is a digitally controlled source of charge pulses. It consists of a set of switches, a charging capacitor (capacitor D) and a charging amplifier (amplifier 1). The input voltage in Figure 2-6 comes from the microcomputer interface and is used to charge up capacitor D. The switches A, B and C are directly controlled by CPU through a buffer register. Normally, switch A and B are open and switch C is closed to prevent the charging amplifier from oscillating. When switch A is closed, capacitor D is charged up to V_{in} with a charge of $C_D^{V}_{in}$ C where $\mathbf{C}_{\mathbf{D}}$ is the capacitance of capacitor \mathbf{D} . Upon opening switches A and C, and closing B, the charge stored on capacitor D is injected by the action of charging amplifier onto the membrane which is situated between the two electrodes. The voltage transient produced is amplified by the LH0032 PET input amplifier (gain of X2) to produce a voltage excusion in the range of 0-1 volt at the output. Theoutput

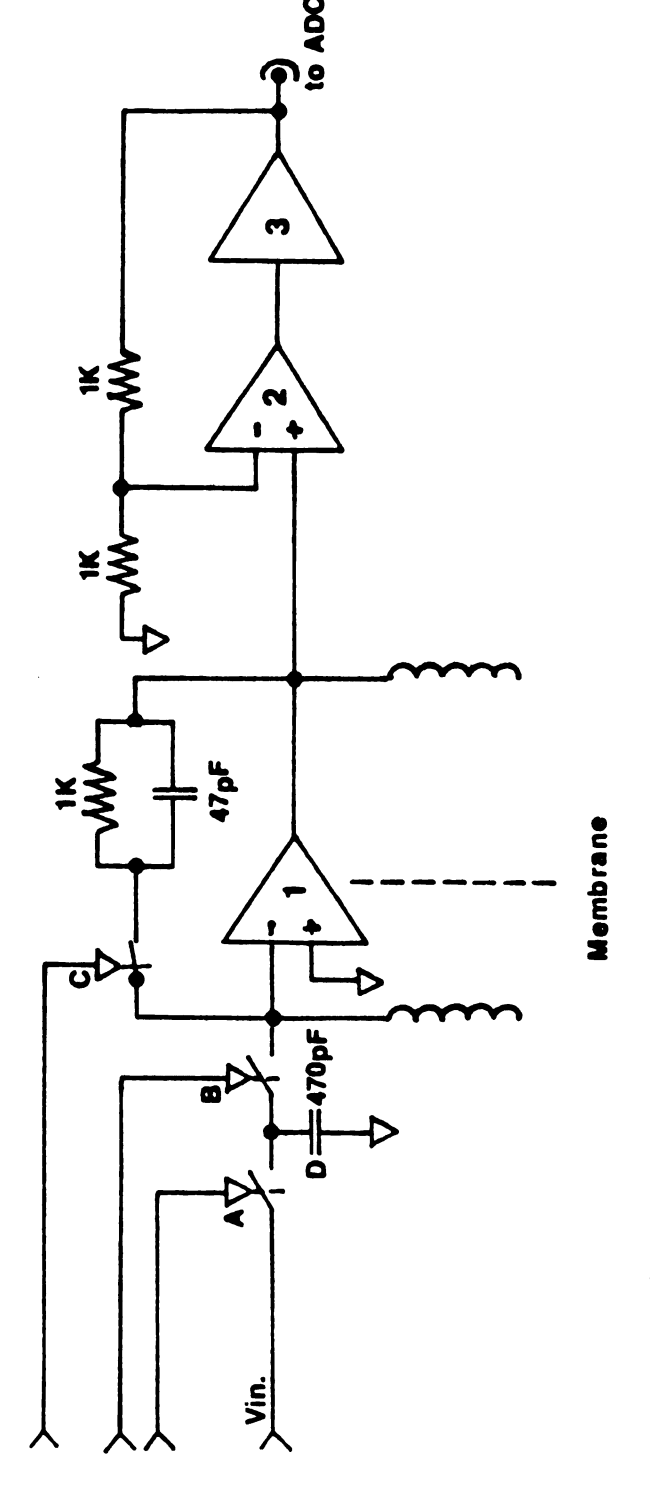


Fig. 2-6 Schematic of pulse generator and cell amplifier. 1 1025; 2: LH0032; 3: LM310; A,B,C, : SD5000(switch) and SD5200(driver).

signal is then buffered by a LM310 cable driver and sent via coaxial cable (terminated with 75 ohms) to the digital recorder. It should be noted that because electrode E is at virtual ground, a negative V_{in} will result in a positive voltage at electrode F.

To satisfy the "high speed" requirement of the pulse generator, a Teledyne Philbrick 1025 FET input operational amplifier was used for the charging amplifier. It has a high input impedance of 10¹¹ ohms and a very short settling time of 55 nanoseconds (to 1%). The switches are Signetics SD5000 (switch) and SD5200 (driver) with an on resistance of 30 ohms and an off resistance of 10¹⁰ ohms. The on and off times of the switch are both 5 nanoseconds.

Power (± 15 , ± 5 volts), common, and control signals from the microcomputer are connected to the pulse generator and cell amplifier by 6 and 4 prong Cinch-Jones connectors respectively located on the side of the housing. The power supply lines are decoupled to common with 6 μ F tantalum capacitors at the input, and with smaller ceramic capacitors near the amplifiers, to allow good transient response.

4. Digital Recorder

The digital recorder implemented in the present system consists of a timing circuit and an analog-to-digital converter with associated memory and address counters. The timing circuit provides necessary signals

for the operation of the ADC section. The ADC section converts the incoming analog signal (voltage) into digital form and stores it in the RAM. The device is a general data acquisition system and can be adapted to any instrument provided proper buffer circuit is available between the unit and the instrument.

a. Timing Circuit

The timing circuit provides the conversion signal for the ADC, the "write enable" for the RAM and the clock pulse for the address counter. The system is shown in schematic form in Figure 2-7. The operation of the circuit is as follows. The crystal controlled oscillator frequency (30 MHz) is divided by a set of flip flops to generate 5 different clock frequencies that determine the data collection rate (15, 10, 5, 2, 1 MHz). Due to the fact that the digital output of the ADC is delayed by one and half clock cycles, three flip flops (FF1, 2, 3) are employed to ensure proper timing among the signals for ADC, RAM and counter. Prior to the start of the experiment, the data acquisition rate is loaded into a register and a "clear" pulse issued by the microprocessor to reset the address counter and flip flops. When a start signal is received by the timing circuit, output Q of FF4 goes to "1" which places the CPU on hold. On sensing "hold acknowledge" from the microprocessor, the pulse generator is actuated (output of gate 4 goes to 1), and 1K RAM is selected,

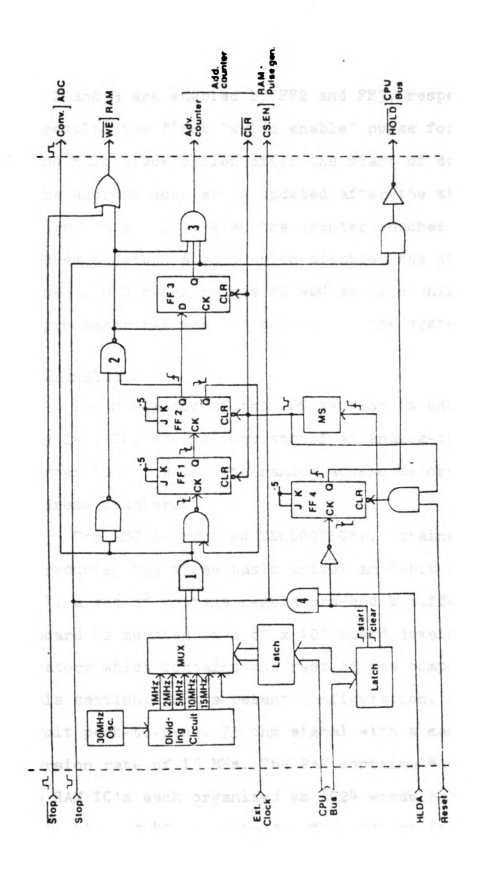


Figure 2-7. Schematic of timing circuit.

the ADC starts data conversion, and output Q of FF1 goes to "1". On the next rising clock edge (out of gate 1), gates 2 and 3 are enabled by FF2 and FF3, respectively.

As a result, the first "write enable" pulse for RAM occurs one and half clock cycles after the start of data conversion and the address counter is updated after the storage of the first data point. When the counter reaches 1024 (1K), it issues a "stop" signal which disables the clock circuit from sending further pulses to ADC section while the microprocessor resumes the control of the system bus.

b. ADC Section

The schematic of the ADC section is shown in Figure 2-8. The system consists of an analog-to-digital converter board, a 1K byte random access memory (RAM) and an address counter.

The ADC board (TRW TDC1007PCB), obtained from TRW LSI Products, has three basic units; an 8-bit ADC (TPC 1007J), a set of voltage regulators and a buffer circuit. The board is mounted on a 8" x 10" board developed in this laboratory which contains the rest of the components used in this section. In its pesent configuration, it digitizes a 1 volt peak-to-peak, 75 ohm signal with a maximum conversion rate of 15 MHz. The RAM contains 8 Fairchild 93425 RAM IC's each organized as 1024 words by one bit with a write time of 45 nanoseconds. The address lines of the RAM are connected to the system bus and a counter through

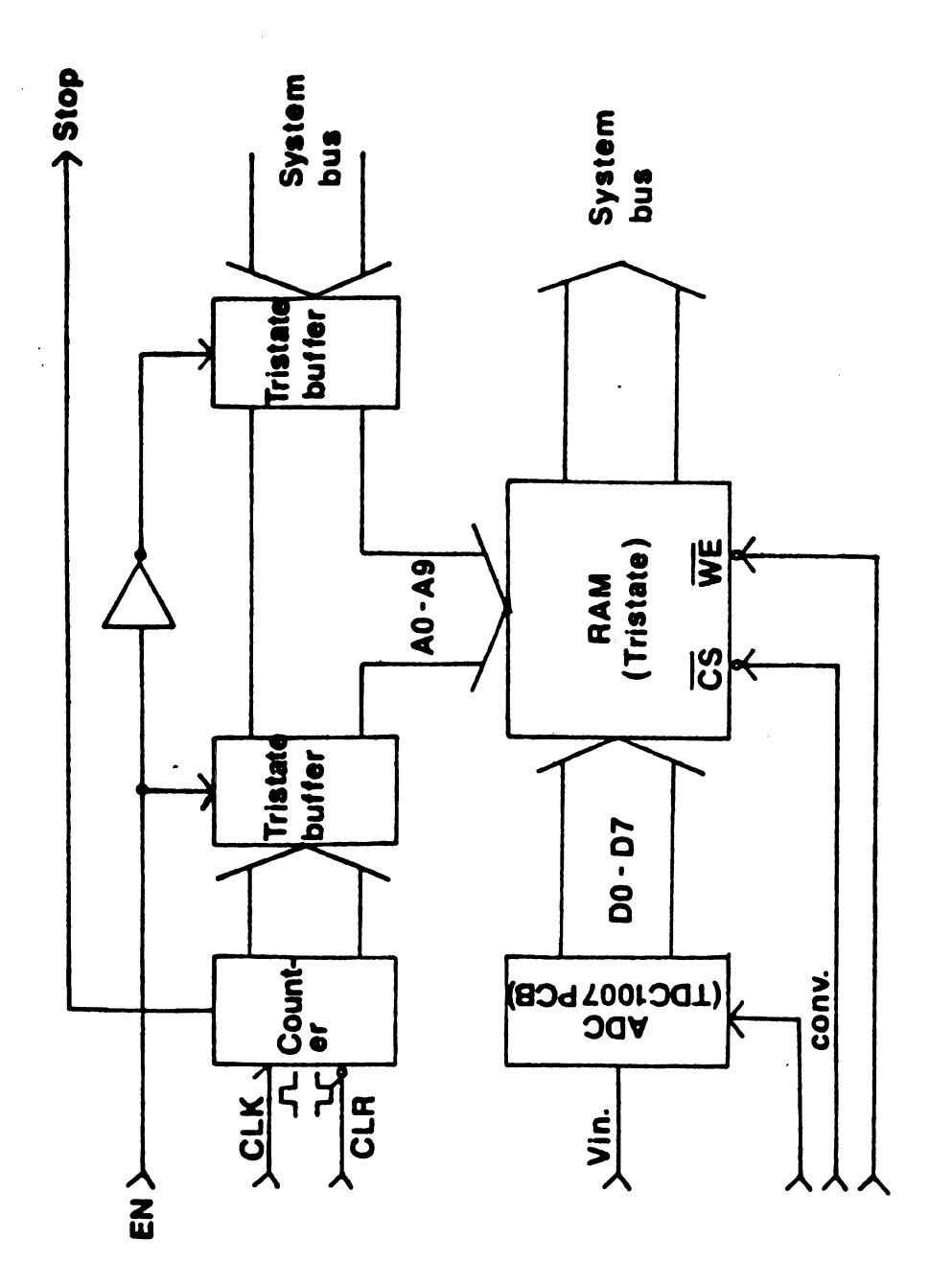


Figure 2-8. Schematic of ADC section.

tristate buffers. Due to the tristate nature of the RAM output, the data lines are directly coupled to the system bus. Briefly, the system operates as follows. Prior to the experiment, the counter is reset to zero. During the experiment, the clock circuit provides the conversion pulse to the ADC, the clock pulse to the address counter and the "write" pulse to the RAM to record the digitized voltage. After 1K data points have been recorded, the counter issues a flag to the microprocessor to indicate the end of data collection. The microprocessor then resumes control of the system.

5. Microcomputer

of the various microcomputers, the Intel SDK-85 system was chosen for the control of experiments and data collection because of its high performance (1.3 microsecond instruction cycle), popular instruction set and low cost. The system consists of an 8085A CPU, 2 kilobyte read-only-memory (ROM), 256 byte RAM, 38 parallel I/O ports, a serial port and an interactive keyboard and LED display. The system also has an excellent monitor program residing in the 2K ROM. It allows the operator to examine and load the registers and memory as well as to run and single-step user's program.

However, the memory capacity of SDK-85 is rather limited. To circumvent this problem, an additional 4K RAM and a 1K PROM (programmable ROM) were interfaced to the system. Also added to the system was a USART (Universal

Synchronous/Asynchrous Receiver Transmitter) to facilitate the communication between a minicomputer and the microprocessor. The schematic diagrams of these peripherals, which were designed by Bruce Newcome in our group, are shown in Appendix A.

6. The Operation of the System

To operate the microprocessor-controlled charge injection device, four programs are required. They are DOWNLD.FTN, DATAIN.FTN, LOAD.MAC, and MEMB.MAC. A listing of these programs is shown in Appendix B.

DOWNLD.FTN and DATAIN.FTN reside in the minicomputer (PDP-11). The former is used to send object files from the minicomputer to the microsystem through a serial link. For the present system, MEMB.MAC in binary codes is downloaded to the microcomputer when the charge injection device is powered up. DATAIN.FTN receives data from the microcomputer. It can then either plot the data on a graphic terminal or store them in a file on any mass storage device.

LOAD.MAC and MEMB.MAC reside in the microcomputer.

LOAD.MAC is situated in PROM and is available when power is on. It receives files from the minicomputer and stores them in RAM. MEMB.MAC controls experiments, data collection and data transfer from the device to the minicomputer.

The data collection rate and charging voltage for the charging capacitor in pulse generator are entered through

the keyboard to memory locations 2000H and 2001H (hexidecimal), respectively. When the pulse experiment is over, MEMB.MAC transfers data immediately to the minicomputer. This is done because at the moment the microprocessor lacks graphic terminals and mass storage devices. The examination of data can only be done on the minicomputer.

A program named EXPFIT.FTN can be used to exponentially fit the acquired data. To use EXPFIT.FTN, a data file name and two integers are given to the program. The integers specify the first and the last data points of a data block in the data file. EXPFIT.FTN will linearize the exponential data and calls a linear square fitting subroutine. The program will then return the fitted parameters.

7. Performance

The performance of the system is illustrated in the next five figures. Figures 2-9 to 2-11 demonstrate the rise time, signal-to-noise ratio, linearity and accuracy of the digital recorder. Figures 2-12 to 2-13 display the rise time and accuracy of the pulse generator.

Figure 2-9 shows the response of the digital recorder to a 100-KHz, 0.5-V square wave. It can be seen from the figure that the system responds to voltage steps within 3 data points and that it takes 3 to 5 data points for the system to settle down to a constant voltage. Based on the data collection rate (15 MHz), the rise and settling

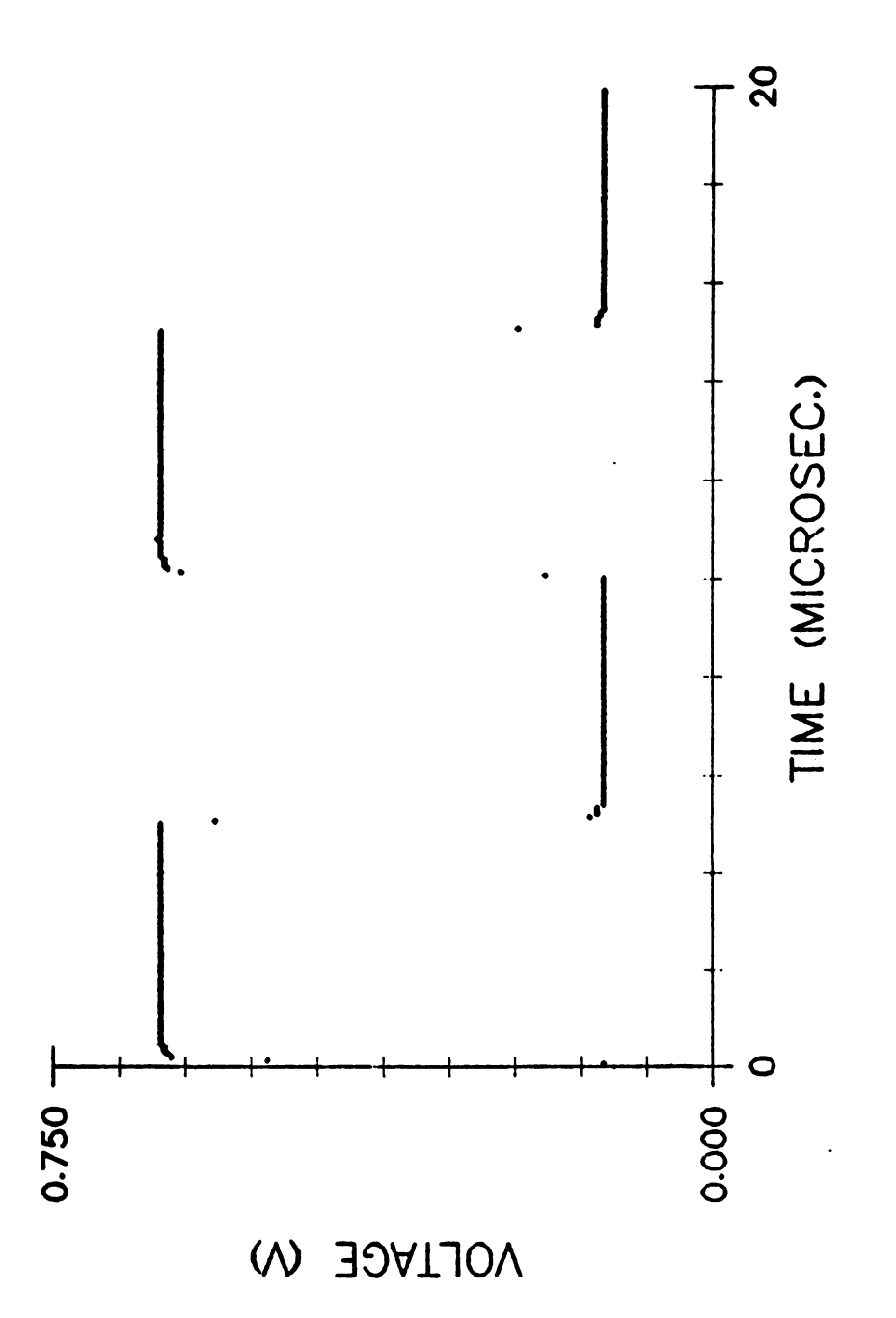


Figure 2-9. Response of the digital recorder to a 0.5-V 100-KHz square wave. Data collection rate: 15 MHz.

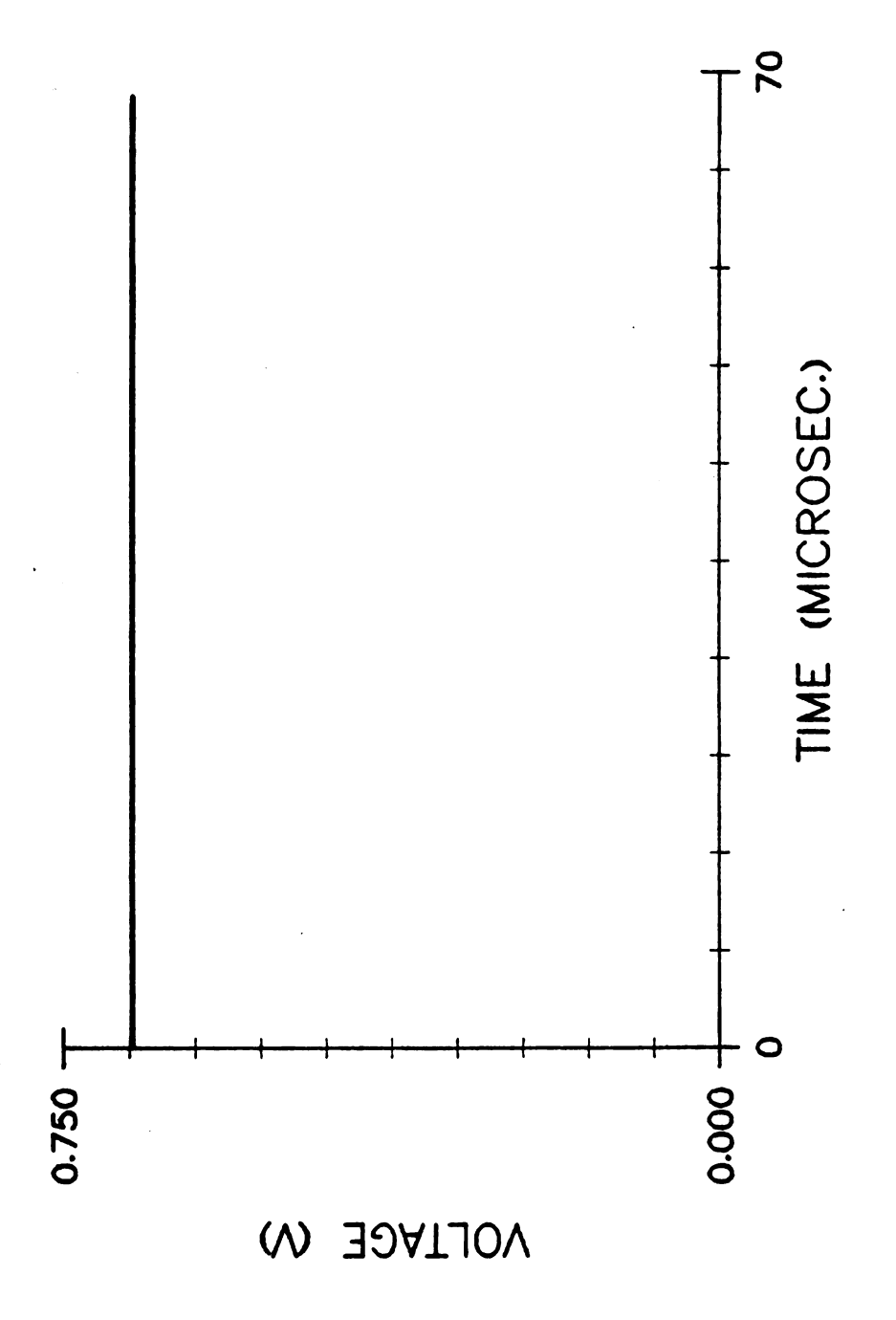
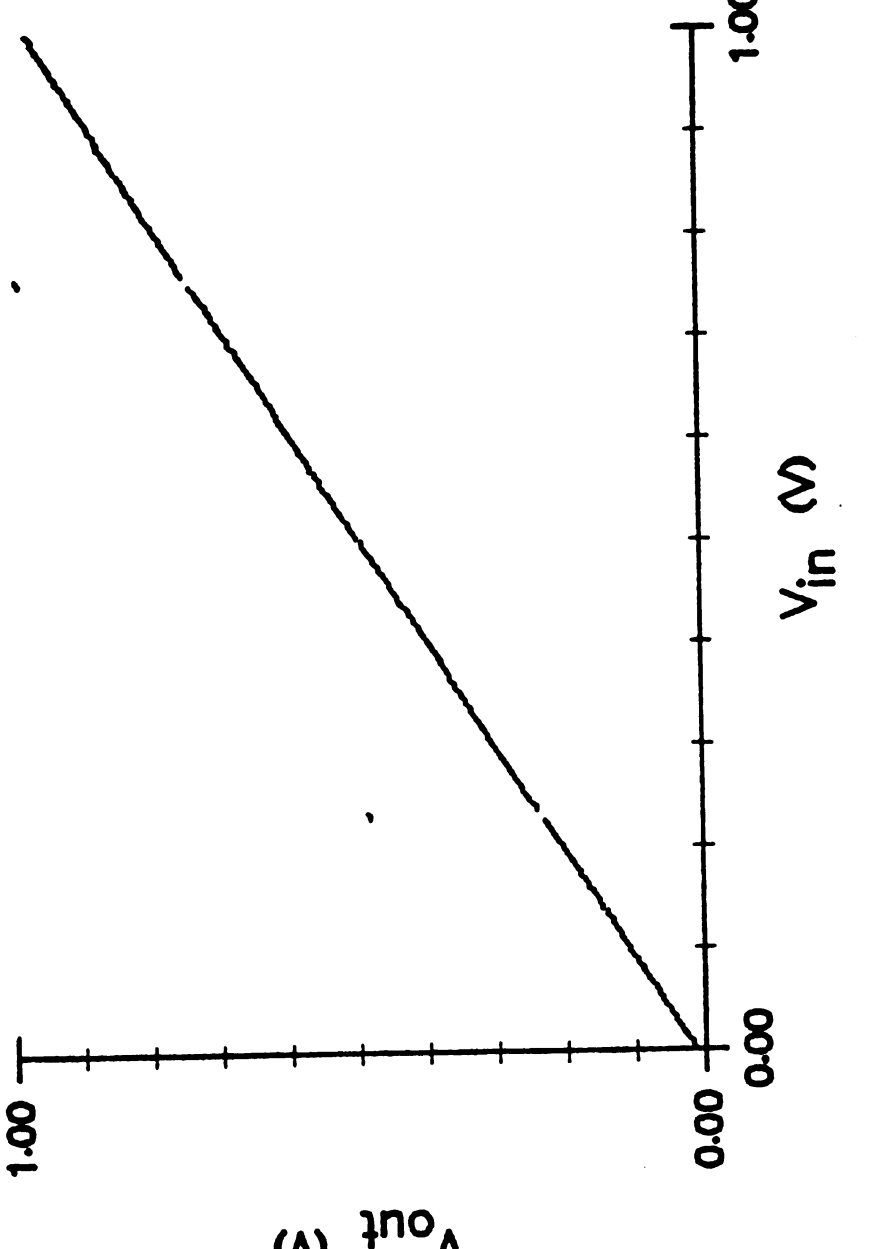


Figure 2-10. Signal-to-noise ratio of data collected at 15 MHz.

time of the recorder are approximately 0.2 and 0.3 microsecond, respectively.

The response of the digital recorder to a constant voltage is shown in Figure 2-10. Apparently, only one value for the voltage was recorded by the system. For an 8-bit analog-to-digital converter, the resolution is 0.39% which amounts to a quantization error of 3.9 mV for a 1-volt signal. It is therefore concluded that the signal-to-noise ratio is at least 256 and the actual fluctuations in output voltage are less than 3.9 mV.

Figure 2-11 shows the response of the recording system to a 0-1 V ramp wave at 2 KHz. The figure displays the rising half of the signal. Since a data collection rate of 2 MHz was used, each data point corresponds to a 2 mV resolution in V_{in} . As a result, a stepwise curve for V_{out} vs V_{in} is observed in Figure 2-11. It is noticed that the slope of the curve is one and Vout equals Vin within quantization error. These two facts demonstrate that the response of the system is linear and that the device has an accuracy of 3.9 mV. It is also observed in Figure 2-11 that two small groups of data points do not fall on the curve. These data points are attributed to instrumental errors which were not observed when a constant voltage was applied to the recorder (Figure 2-10). As the difference between the true value and the noise is much greater than that between the two adjacent data points, the noise can be eliminated from the data set by data treatment



 $V_{
m out}$ is the output of the recorder. Only the rising rising half of the wave is shown. Data collection rate: 2 MHz. Figure 2-11. Response of the digital recorder to a 0-1V 2-KHz ramp wave. $v_{\rm in}$ is the voltage of the signal and

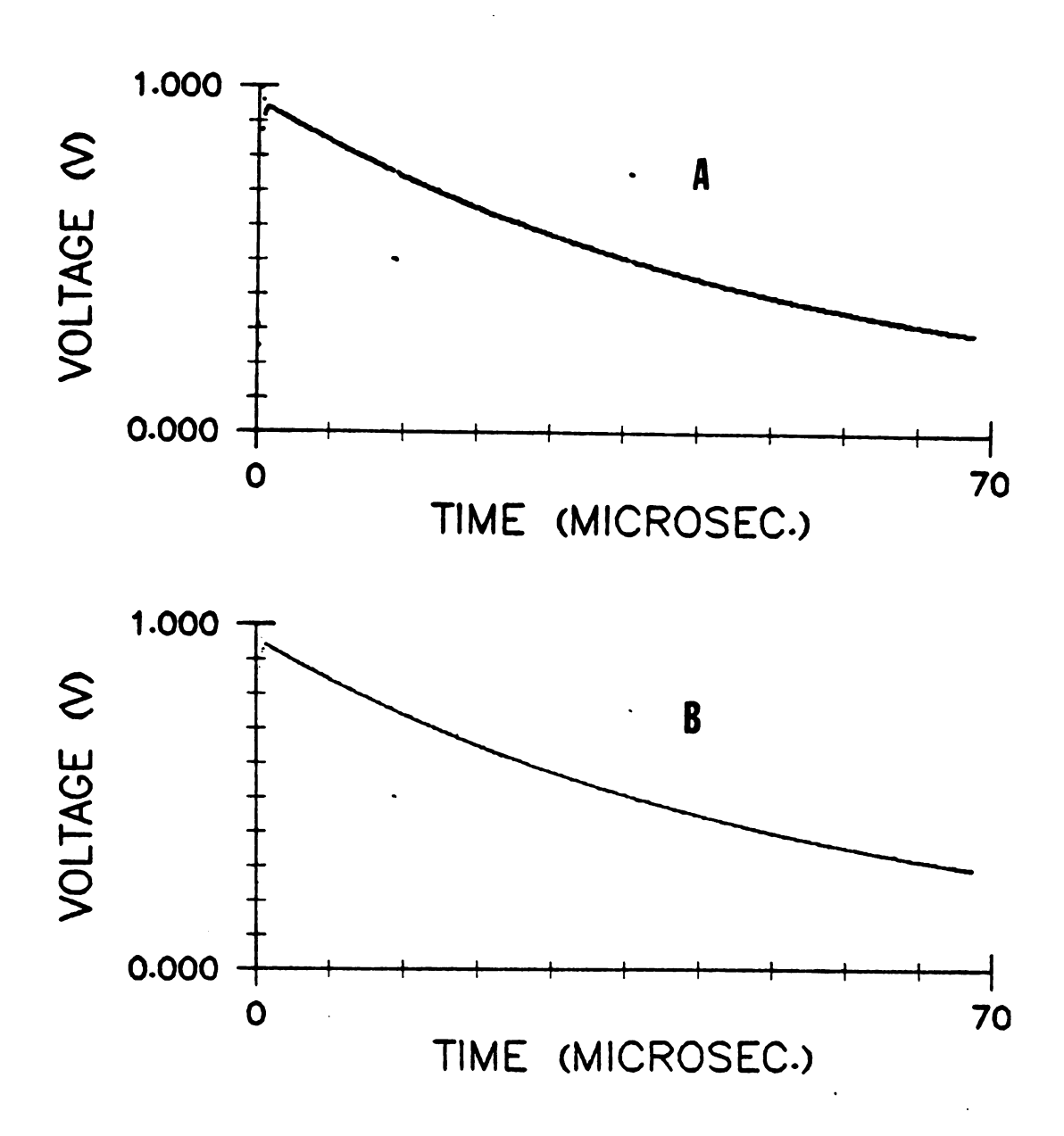


Figure 2-12. Voltage transient resulting from a pulse application to a resistor and capacitor in parallel. Data were collected at 15 MHz. A: transient, B: transient plus its exponential fit.

using software techniques.

To characterize the pulse generator, a predetermined amount of charge is applied to a resistor (10.0 \pm 0.1% k Ω) and a capacitor (5000 \pm 1% pF) in parallel (dummy cell) and the resulting voltage transient is monitored by the system. Figure 2-12A shows the voltage transient collected at 15 MHz. Its exponential fit plus the transient are illustrated in Figure 2-12B. Two parameters were obtained from fitting the curve: the initial voltage, Vo, and the time constant, τ , of the transient. The initial voltage can be used to calculate the amount of charge injected onto the dummy cell according to equation (1):

$$Q_o = CV_o/2$$
(1)

where: Q.: the amount of charge received by the dummy cell,

C : capacitance of the dummy cell,

Vo : initial voltage of the transient obtained by exponential fit,

2 : voltage gain of the cell amplifier.

For this experiment, Vo equals 0.809 V and Qo is 2.02×10^{-9} coul. The amount of charge issued by the pulse generator is equivalent to the product of the capacitance of the charging capacitor (470 \pm 10% pF) and the charging voltage (4.45 \pm 0.04 V). This is equal to

2.09 X $10^{-9} \pm 10\%$ coul. Apparently, the amount of charge received by the dummy cell is equal to that released by pulse generator within experimental error. The time constant acquired from exponential fit of the data is 50.23 microseconds. It is comparable to the RC constant (50.0 \pm 0.5 microseconds) of the dummy cell.

It is noted that it takes about 7 data points (Figure 2-12A) to reach the first valid data point. This amounts to about 0.5 microsecond. Since the recorder needs approximately 0.4 microsecond to rise and settle, this means the charging time of the dummy cell is probably less than 100 nanoseconds. This amount of time is close to the settling time of the charging amplifier specified by the manufacturer.

Figure 2-13 shows the results of the same experiment collected at 5 MHz. The Vo and decay constant of the transient obtained from curve fitting are 0.821 V and 50.02 microseconds, respectively. The variation in initial voltages acquired at different collection rates is attributed to the uncertainty in the validity of the first data point. As the decay constant is irrelevent to Vo, an excellent agreement between two experiments is observed for this quantity.

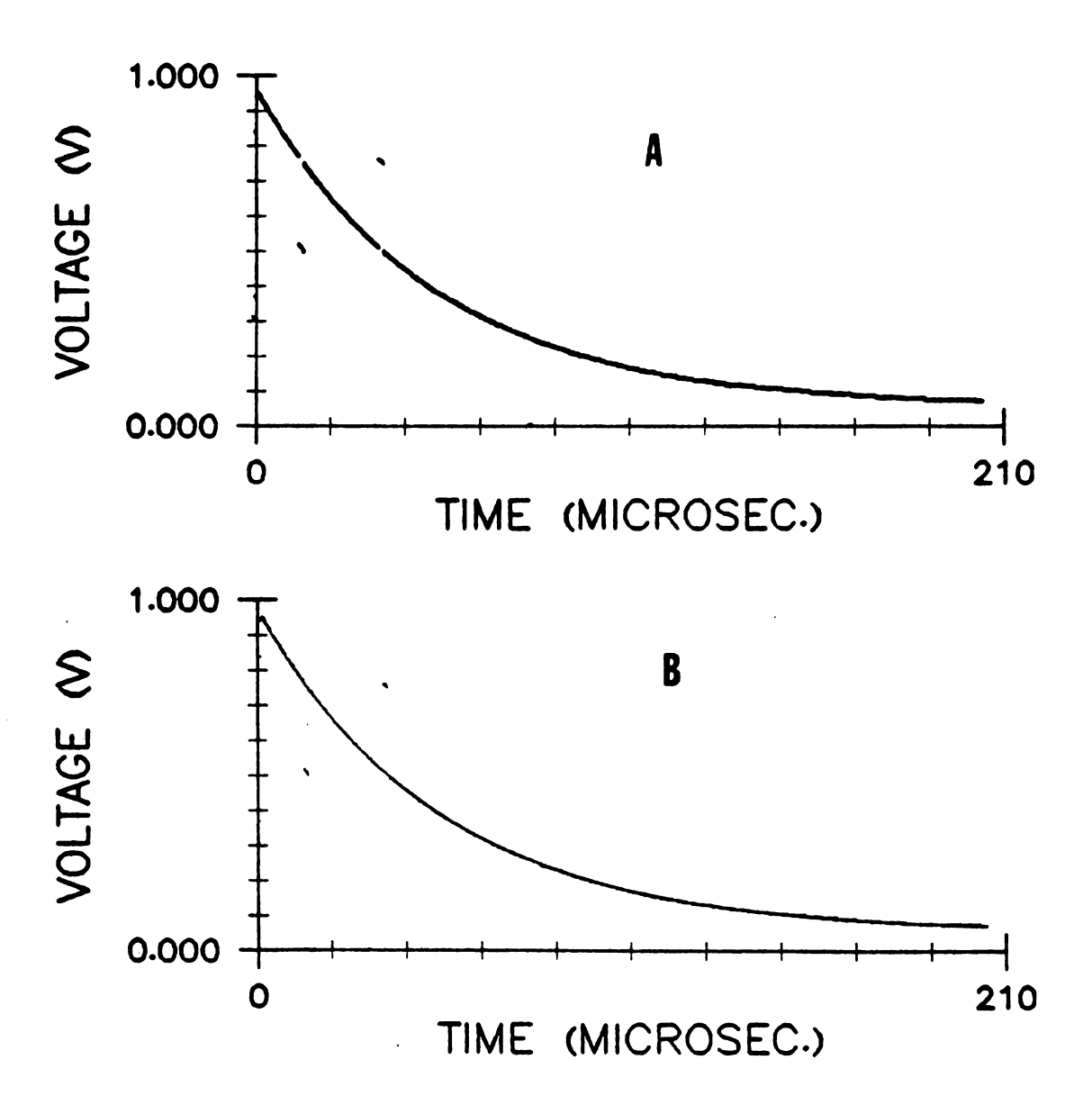


Figure 2-13. Voltage transient resulting from a pulse application to a resistor and capacitor in parallel. Data were collected at 5 MHz. A: transient, B: transient plus its exponential fit.

CHAPTER TIT

FORMATION CONSTANT OF GRAMICIDIN CHANNELS IN LIPID MEMBRANES

INTRODUCTION

In the past few years, two studies have been reported that concern the formation constant of gramicidin channels in bilayer lipid membranes. In Bamberg and Lauger's work (46), a voltage-jump relaxation method was used in which the rate constants for the formation and dissociation of the dimer were obtained from the time course of the current after a sudden change of the potential.

In 1975, based on the simultaneous measurements of membrane fluorescence and conductance, Veatch et al. (47) concluded that dancyl gramicidin C, a highly active analog of gramicidin, forms a dimeric channel and has a dimerization constant comparable to that of native gramicidin channels.

Recently, we have developed a new and unique approach to the problem. It is based on the observation that when lipid membrane is properly doped with gramicidin, the voltage discharge through the membrane

after a charge pulse is purely exponential. As a consequence, the number of dimeric channels in the membrane could be derived from the voltage relaxation time if the membrane capacitance is known. With this new method, we found that the formation constant of gramicidin channels depends greatly upon the membrane thickness. Furthermore, a constant partition coefficient of gramicidin between the membrane and torus phases exists.

In this chapter, Lauger et al. and Veatch et al.'s work will be discussed briefly. The major emphasis will be on the newly developed approach and the results therefrom. We will show that our data are in accordance with others and that the assumptions involved in the study are legitimate and justified.

Current Relaxation Approach

In all three approaches to the measurement of dimerization constant of gramicidin, it is assumed that an equilibrium between monomers (A) and dimers (A₂) exists in the membrane. This equilibrium may be characterized by an association rate constant k_R (sec⁻¹·l·mole⁻¹), a dissociation rate constant k_D (sec⁻¹) and an equilibrium constant k_D (sec⁻¹)

$$A + A = \frac{k_R}{k_D} A_2$$

$$R_R = k_R N_1^2$$

$$R_D = k_D N_2$$

$$K = \frac{k_R}{k_D} = \frac{N_2}{N_1^2} \dots (2)$$

where N_1 : concentration of monomers A in mole·1⁻¹

 N_2 : concentration of dimers A_2 in mole·1⁻¹

 R_R : rate of channel formation in molecular sec⁻¹

 R_D : rate of channel dissociation in mole:1-1.sec-1

It is further assumed that the exchange of A and A_2 between membrane and aqueous phases is sufficiently low, so that the total concentration N of gramicidin in the membrane remains constant during the experiment:

$$N = N_1 + 2N_2 \dots (3)$$

In Lauger and Bamberg's approach, a differential equation is set up which describes the rate of change in channel concentration after the voltage jump and the solution of this equation reads:

$$N_2(t) = N_2(\infty) - (N_2(\infty) - N_2(0)) \frac{q e^{-t/\tau}}{1+q-e^{-t/\tau}} .. (4)$$

with q =
$$\frac{(1+8NK)^{\frac{1}{2}}}{4K(N_2(\infty)-N_2(0))}$$
(5)

$$\tau = \frac{1}{k_D + 4k_R N_1(\infty)} \qquad (6)$$

At a given voltage, the current density J(t) is proportional to the concentration N_2 of conducting channels. Using equation (4), the time course of the current may be expressed by:

$$\frac{J(t) - J(0)}{J(\infty) - J(0)} = 1 - q \frac{e^{-t/\tau}}{1 + q - e^{-t/\tau}} \dots (7)$$

Equation (7) reduces to an exponential form, equation (8),

$$\frac{J(t) - J(0)}{J(\infty) - J(0)} = 1 - e^{-t/\tau} \quad (|q| \gg 1) \quad \quad (8)$$

for large values of the parameter, q, which implies either small displacements from equilibrium (i.e. $N_2(\infty)-N_2(0)$ 0) or low gramicidin concentration (NK>>1).

Via the use of single channel conductance, G , and Avogadro's number N_{Av} , equation (6) assumes the form:

$$\tau = \frac{1}{k_D^{+4}(1000k_Dk_R \lambda(\infty)/N_{Av}G d)^{\frac{1}{2}}} \dots (9)$$

where $\lambda(\infty)$ is the membrane conductance ar t = ∞ , and d is the membrane thickness in cm and G. the single channel conductance in Ω^{-1} .

It is thus evident that a plot of $1/\tau$ vs. $(\lambda(\infty))^{\frac{1}{2}}$ would result in the values of k_R and k_D . The dimerization constant K could then be calculated according to equation (2).

Within experimental error, Lauger and Bamberg found that the time course of membrane current after the voltage jump is indeed exponential. Accordingly, a value of $4.8 \times 10^5 \ l \cdot mole^{-1}$ was obtained for the formation constant of the dimer in lecithin membranes at V=205 mV. It is noteworthy that in this method no direct measurement of gramicidin concentration in the membrane is necessary, as is evident from equation (9). Furthermore, both kinetic and thermodynamic constants are readily available from the study. The disadvantage of the technique is that the parameters are acquired under the influence of an applied voltage. The rate and formation constants at $\Delta V=0$ mV could only be estimated by extrapolating to $\Delta V=0$ the parameters obtained at a series of nonzero ΔV 's.

Analog Approach

Equation (2) and (3) suggests that the dimerization constant of gramicidin channels can be expressed in terms of N and N_2 according to the equation:

$$K = \frac{N_2}{(N - 2N_2)^2} \dots (10)$$

In 1975, Veatch et al. devised dancyl gramicidin C (DGC), a highly fluorescent and active analog of gramicidin A. Assuming that monomeric and dimeric gramicidin have same excitation characteristics and quantam yield, N could be determined directly by measuring the fluorescence intensity of the membrane. With the knowledge of N₂, which is proportional to the membrane conductance, the dimerization constant, K, of DGC could be easily calculated according to equation (10).

In spite of structural differences, Veatch et al. obtained results comparable to those reported by Lauger and Bamberg. They found that the dimerization constant is greatly influenced by the membrane thickness. Furthermore, a constant partition coefficient of gramicidin between the torus and membrane phases exists when the concentration of gramicidin in the membrane forming solution is sufficiently low.

It is interesting to note that Veatch's approach

is thermodynamic in nature and not capable of yielding any kinetic information. Because of the requirement of the incorporation of a fluorescent probe into the channel former, the analog approach is not as convenient nor as universal as the voltage-jump experiment.

Voltage Relaxation Approach

In 1976, in an attempt to clarify the cause of the shift of the gramicidin monomer-dimer equilibrium in the membrane after a voltage jump, Bamberg and Lauger (69) discovered that the membrane capacitance and conductance begin to relax several milliseconds after the voltage perturbation. This finding is consistent with our observation that when the lipid membrane is properly doped with gramicidin, the time course of the voltage relaxation after a charge pulse is purely exponential.

On the basis of these two facts, the following conclusions were reached:

- (1) For a fast voltage relaxation (less than a few milliseconds), the membrane capacitance and conductance are independent of the membrane potential and can be deduced from the voltage relaxation time.
- (2) Assuming the interactions between gramicidin channels are insignificant, the density of gramicidin dimers can be estimated from the

membrane conductance according to the equations:

$$G = C/\tau \qquad (11)$$

where G : membrane conductance in $\Omega^{-1} \cdot \text{cm}^{-2}$

C: membrane capacitance in F·cm⁻²

T: relaxation time in sec.

G. : single channel conductance in α^{-1}

 N_2 : concentration of gramicidin channels in mole·1⁻¹

 N_{Av} : Avogadro's number

d: membrane thickness in cm.

(3) The dimer concentration, N₂, obtained from voltage relaxation experiments represents the equilibrium concentration of gramicidin channels in the membrane prior to the charge perturbation.

To utilize equation (10) to obtain K, we assume that the partition coefficient, D, of gramicidin between the membrane and torus phases is a constant:

$$D = N/B$$
(13)

where B is the gramicidin concentration in the membrane forming solution. Combining equation (10) and equation (13) and solving for N_2 , equation (14) is obtained:

$$N_2 = \frac{DB}{2} + \frac{1 - (1 + 8KDB)^{\frac{1}{2}}}{8K}$$
(14)

Equation (14) consists of two experimentally available variables, N_2 and N, and two physical parameters, K and D. By use of a weighted nonlinear least squares program, K and D could be estimated by fitting experimental data, N and N_2 , to equation (14).

Explicitly, the assumptions involved in our approach are as follows:

- (1) An equilibrium in the membrane between a nonconducting monomeric gramicidin and a conducting dimer exists.
- (2) There is no interaction between gramicidin channels so that single channel conductance could be used to calculate channel density from the membrane conductance.
- (3) Conservation of membrane bound gramicidin persists during the course of experiments.
- (4) The partition coefficient of gramicidin between the membrane and torus phases is a constant over the concentration range used in

the experiments.

EXPERIMENTAL

Material ans Apparatus

All chemicals and solvents used are reagent grade and used without further purification. The glycerol monocleate (GMO, technical grade) and cholesterol were purchased from Matheson, Coleman & Bell and Fisher Scientific Company, respectively. n-Decane was obtained from Sigma, n-tetradecane from Phillips Petroleum and n-hexadecane from Aldrich Chemical Company. Gramicidin (isolated from Bacillus brevis), a mixture of gramicidin A (85%), B (4%), and C (11%) (64), was purchased from Sigma and used without further purification.

The electrolyte solution used for the charge pulse experiments was 1M KCl. This was chosen because potasium ion gives rise to higher membrane conductance than lithium and sodium ion. The membrane solution was prepared by adding GMO (3% by weight) and cholesterol (1% by weight) to n-alkanes. A stock solution of gramicidin in methanol was kept in the freezer. Appropriate amounts of this solution were added to the membrane forming solution. The resulting solution was sonicated for 30 minutes and used immediately. In this chapter, unless specified, "the gramicidin concentration in the membrane"

is equivalent to "the gramicidin concentration in the membrane forming solution".

The old instrument (see Chapter II and references (77, 78)) was used to perform the charge pulse experiments because membrane experiments and the construction of the new instrument were carried out at the same time. A 200 nanosecond current pulse of appropriate amplitude was applied to the membrane so that the initial membrane potential is around 300 mV. Since no thermostate was used, the temperature of the solution was checked before and after each pulse experiment to ensure it is within 1° of 24°C. Usually, two to three measurements could be made before the readjustment of solution temperature was necessary.

Membrane Formation

The electrochemical cell used for the membrane ion transport was described in Chapter II. The membranes were formed on a 1.6 mm orifice in a thin Teflon barrier which was sandwiched between the two electrolyte compartments. The membrane formation was accomplished using a Pasteur pipet to apply approximately 1-5 μ l of the membrane forming solution to the lip of the orifice. By using the Pasteur pipet to gently create air bubbles along the barrier, just below the orifice, the membrane solution can be repeatedly swept across the orifice until a membrane forms. The

membrane area was measured with a microscope and graticule and was kept about $1.6 \times 10^{-2} \text{ cm}^2$ (80% of the total area) for all the experiments. Depending on the membrane composition, it usually takes about 30 seconds for n-hexadecane membranes to thin and 1.5 minutes for n-decane membranes. Tetradecane membranes thin in a time intermediate between these values.

Membrane Data Collection

The program used to control data collection is named "MEMBRN.FTN; 2". It is a modification of "MEMBRN. FTN; 1" (78) to suit our recently installed multiuser operating system (RXS-11) on a Digital PDP-11/40 computer. A listing of the program is shown in appendix B. This program can be used to collect, plot, list, exponentially fit and store data in a file on any mass storage device. To collect data, the recording and readout rates of the transient recorder, as well as the number of data points collected at the fast recording rate are entered in a 16bit word through the terminal. The bit assignments are shown in the program listing under "Data Collection Section". It should be noted that a base line scan (n average) must be acquired before the program will honor a store command. This is necessary to allow correction for the transient recorder's background noise (see references (77, 78)). After the data have been stored, a plot command

will plot the baseline corrected data. To exponentially fit data, a data file name and two integers that specify the first and last data points of a data block in the data file must be provided to the program. The program will then return the fitting results: the slope and intercept of lnV vs. time and the standard deviation of fitting.

Data Treatment

The data collected from charge pulse experiments were exponentially fit using Fit command in MEMBRN.FTN; 2 to acquire the relaxation time according to the equation:

 $\tau = 1/-SR$

where S : slope of lnV vs. t plot (V : membrane

potential; t : time)

R : data collection rate

The fit section of MEMBRN.FTN; 2 is an exponential curve fitting routine. The program linearizes the exponential data, calculates the proper weighting coefficients, and then calls a weighted linear least squares fitting subroutine.

The dimerization constant and partition coefficient of gramicidin in the membrane were acquired by fitting data (i.e. channel and gramicidin concentrations)

to equation (13) using KINFIT (74) on the MSU CDC-6500 computer.

For a given membrane forming solution of certain gramicidin concentration, τ is the average of at least 10 experiments, each performed on a new membrane. To calculate the channel concentration, equation (12) is used assuming a single channel conductance of 4.1 x $10^{-11} \,\Omega^{-1}$ (37) and a bilayer thickness of 32.0Å for hexadecane membranes. The thickness of other membranes is estimated from that of hexadecane membranes based on the ratio of their capacitances.

KINFIT requires that initial estimates for the parameters be given by the user. It is often a necessary condition for convergence that these initial estimates be fairly close to the actual values.

For n-tetradecane and n-hexadecane membranes, two variables (channel and gramicidin concentrations) were fit to equation (14) to acquire the dimerization constant and partition coefficient by use of KINFIT. For n-decane membranes, because of difficulties encountered in using KINFIT (error mode of negative numbers in square root operation despite various estimates for initial values), partition coefficient, D, was given as a constant in equation (14) and the standard deviation of fitting evaluated for a number of Ds. It turned out that when D=1, the fitting error is minimal.

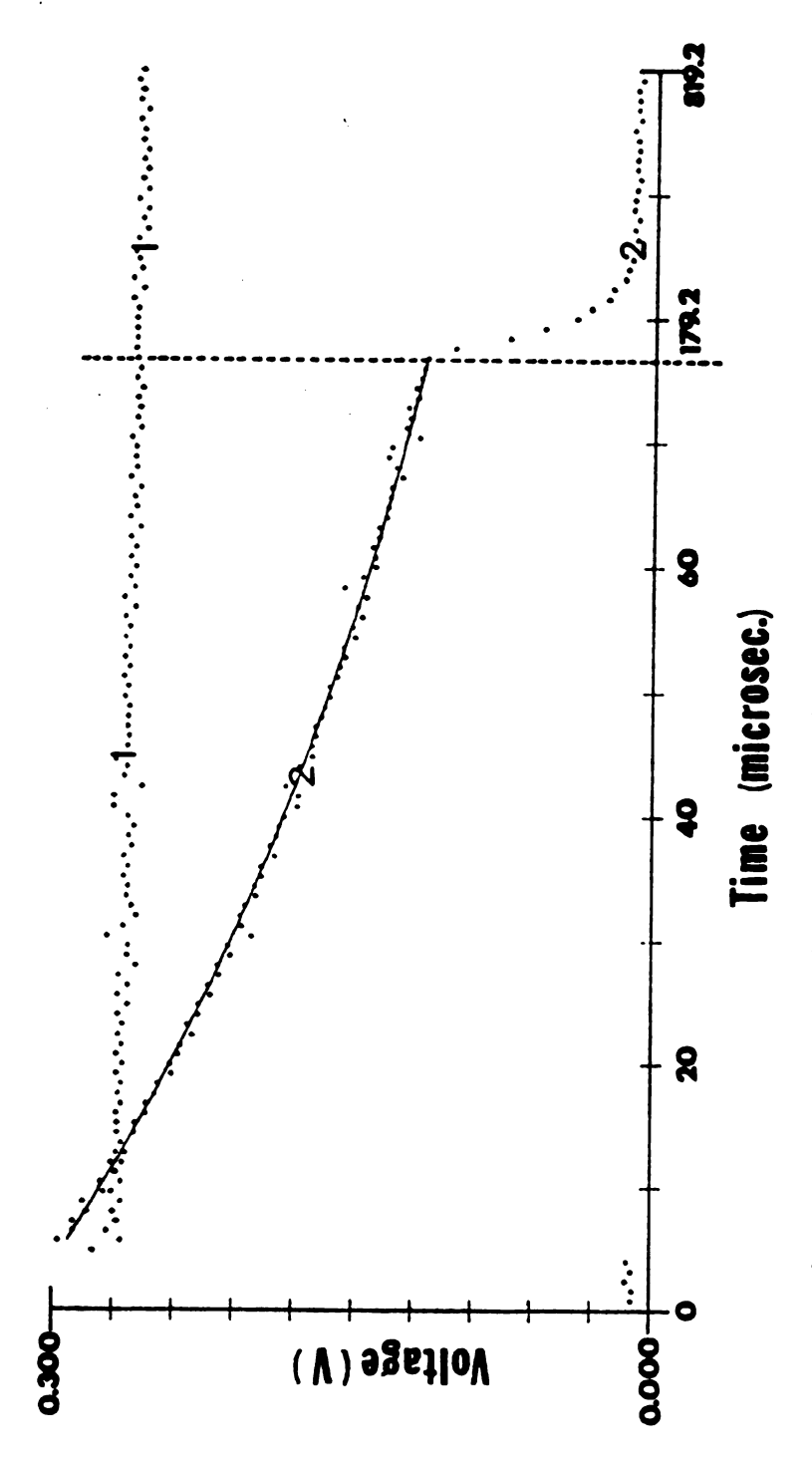
RESULTS AND DISCUSSION

Membrane Capacitance Measurement

To obtain membrane conductance by means of the charge injection method, a knowledge of the membrane capacitance is required.

Figure 3-1.1 shows the result of a pulse application to a GMO-cholesterol membrane with no external bleeder resistor. Two important facts can be recongnized from this figure. First, it is clear that discharge through the membrane or external circuitry is minimal, and therefore the membrane capacitance can be determined accurately by this method. Secondly, it shows that if any dielectric relaxation occurs in the membrane, it must either have a very small amplitude, or occur on a time scale which is either very much shorter or very much longer than the time scale of the charge pulse experiments. In either case, Figure 3-1.1 shows that the results of the membrane experiments will not be affected by a dielectric relaxation.

Figure 3-1.2 shows the transient resulting from the application of a pulse to the parallel combination of the membrane capacitance and a $10k \pm 0.1\%$ resistor. The solid curve is the result of a weighted linear least squares fit on the linearized exponential transient decay curve. The average of 7 such experiments, each performed on a new



THE COUNTY OF THE PARTY OF THE

Fig. 3-1 Voltage transients resulting from pulse application to 3% GMO- 1% cholesterol/n-tetradecane membranes in 1M KCl at 24 ± 1 °C. Solid curve represents exponential least squares fit to data. Discontinuity is due to data collection rate change from 1.25MHz to 39KHz. 1 ; unmodified BLM, 2 ; BLM inparallel with an external resistor $(10 \pm 0.1\% \text{kg})$.

Table 3-1 The thickness and capacitance of 3% GMO-1% cholesterol/n-alkane membranes (w/v).

Solvent	Capacitance (F·cm ⁻²)a	Thickness (Å)b
n-decane	$4.31 \pm 0.08 \times 10^{-7}$	46.5
n-tetradecane	$5.45 \pm 0.10 \times 10^{-7}$	36.8
n-hexadecane	$6.26 \pm 0.11 \times 10^{-7}$	32.0

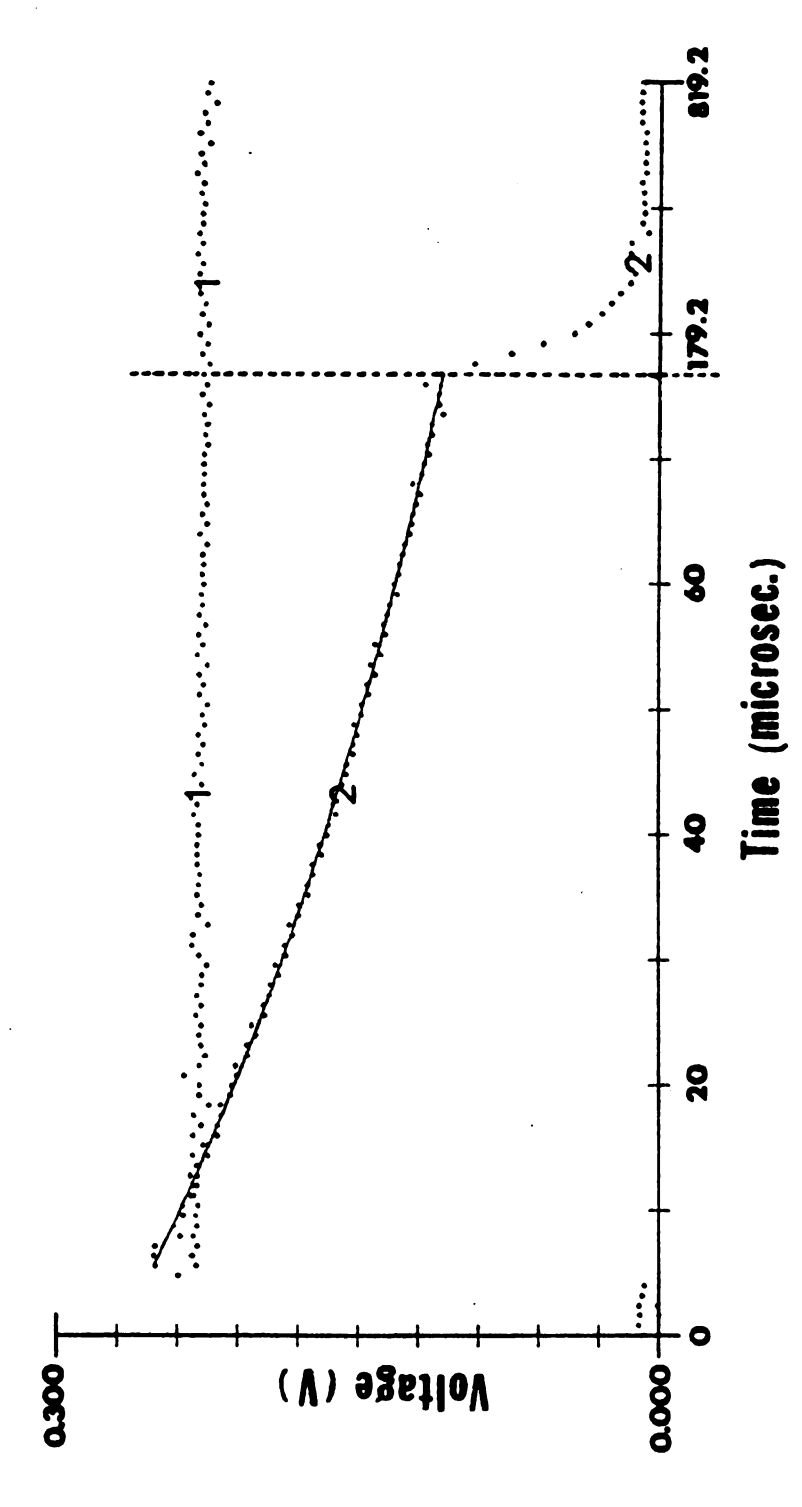
a: The membrane capacitance is the average of 5 measurements, each performed on a new membrane.

b: The thickness of n-hexadecane membranes was taken as 32.0Å according to reference (72-73). The thickness of other membranes was calculated from that of n-hexadecane membranes based on capacitance ratio.

membrane, resulted in a value of $(5.45 \pm 0.10) \times 10^{-7}$ F/cm² (this precision is comparable to the estimated error in the membrane area measurement).

In Table 3-1 are listed the capacitances and thicknesses of various n-alkane membranes. The bilayer thickness was calculated from the capacitance ratio assuming a 32.0A-thickness for hexadecane membranes (72). The variation of membrane capacitance and, in turn, the thickness as a function of chain length of the hydrocarbon solvents is in accordance with reported observations (72, 38). It simply implies that as the chain length of solvent in the film gets longer, the volume fraction of solvent in the membrane becomes smaller and, as a result, the film approaches the "true" bilayer membrane structure.

To measure the membrane capacitance of bilayers doped with gramicidin, we utilized the fact that gramicidin channels are not permeable to anions and divalent cations (38). Figure 3-2.1 shows the voltage transient resulting from a pulse application to a gramicidin-doped membrane in 0.5 M CaCl₂. It is evident that on the time scale of charge pulse experiments, no appreciable voltage discharge through the membrane occurs. Figure 3-2.2 shows the result of a pulse application to a gramicidin-doped membrane in parallel with an external resistor $(10k\Omega)$. The relaxation experiment results in value of 5.35×10^{-7} F/cm² for the membrane capacitance.



represents exponential least squares fit to data. Discontiuity is due to data collection rate change from 1.25MHz to 39KHz. Condition: 3%GMO-1% cholesterol/n-tetradecane membranes, Fig. 3-2 Voltage transients resulting from pulse application to gramicidin-doped membranes in 0.5M CaCl $_2$ at 24 \pm 1°C. Solid curve 1.07 x $10^{-6} M$ gramicidin in the membrane forming solution.

On the basis that the capacitance of unmodified BLM is equal to that of gramicidin-doped bilayers within experimental error, it is concluded that the former can be used to calculate membrane conductance from voltage relaxation time obtained from pulsing bilayers containing gramicidin.

Voltage Relaxation across Gramicidin-doped Membranes

Voltage transients resulting from pulse applications to gramicidin-doped membranes in 1 M KCl are shown in Figure 3-3. Both traces correspond to $8.32 \times 10^{-7} M$ gramicidin in the membrane forming solution. The slight vertical shift of curve 1 with respect to curve 2 and discontinuity of the curves is due to a difference in membrane area and a change in data acquisition rate, respectively. The solid curves result from exponential least squares fits. Two important conclusions can be drawn from this figure. First, gramicidin-mediated voltage relaxation is purely exponential in the submillisecond time range. The exponential nature of the decay suggests that the membrane conductance is independent of membrane potential. As a result, the channel concentration derived from the relaxation time represents the equilibrium dimer concentration in the bilayer prior to the charge perturbation. Second, the relaxation times for Figure 3-3.1 and 3-3.2 are 47.50×10^{-6} second and 42.6×10^{-6} second,

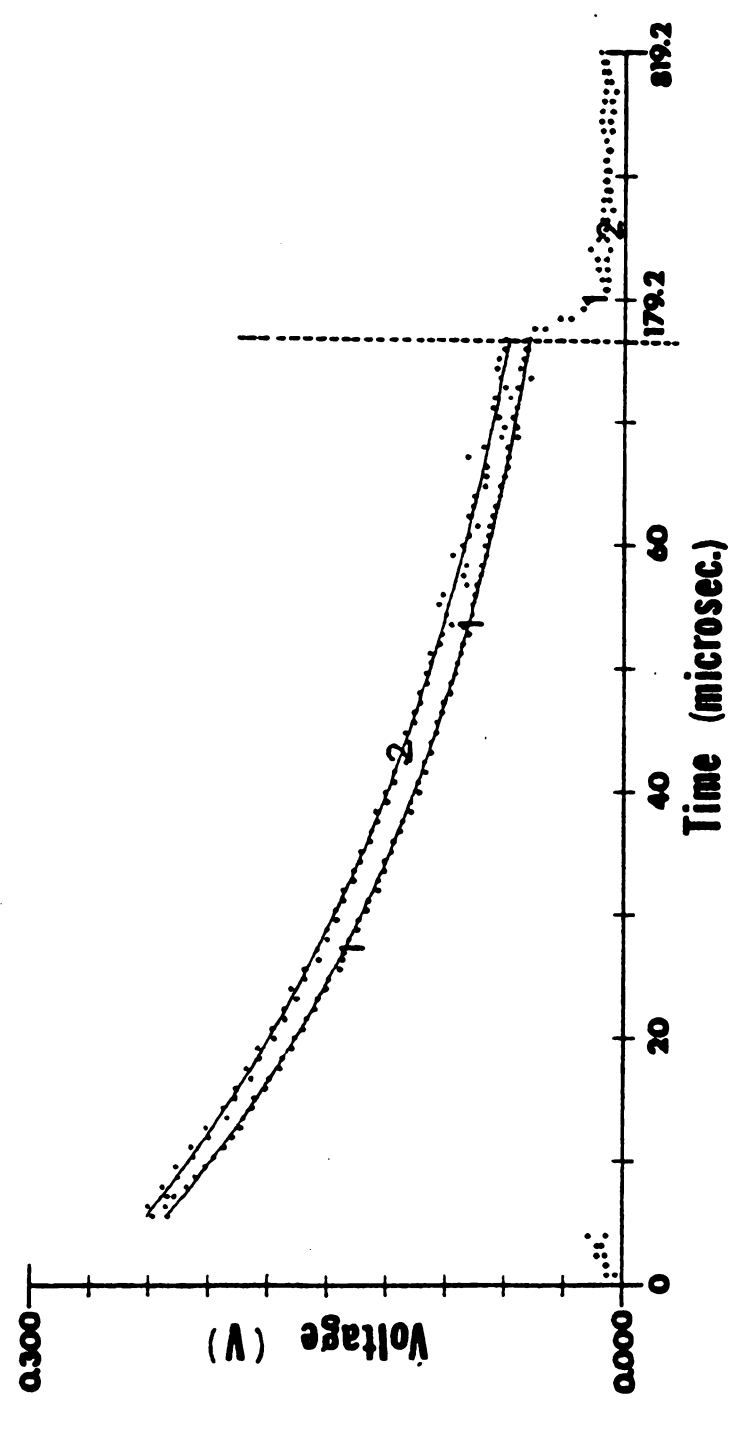


Fig. 3-3 Voltage relaxations resulting from pulse application to gramicidin-doped membranes in 1M KCl at 24 ± 1 °C. Solid curves represent exponential least squares fit to data. Discontinuity is Condition : 3% GMO- 1% cholesterol/n-tetradecane, 8.32 x 10-7M due to data collection rate change from 1.25MHz to 39KHz.

gramicidin in the membrane forming solution.

respectively, which amounts to a precision of about 8%. Although for some membranes a relative standard deviation of 20% in membrane conductance measurements was observed, the precidion of the charge injection technique is comparable to, if not better than, that of the voltage clamp method, as is evident from data presented in references (46), (47) and (70).

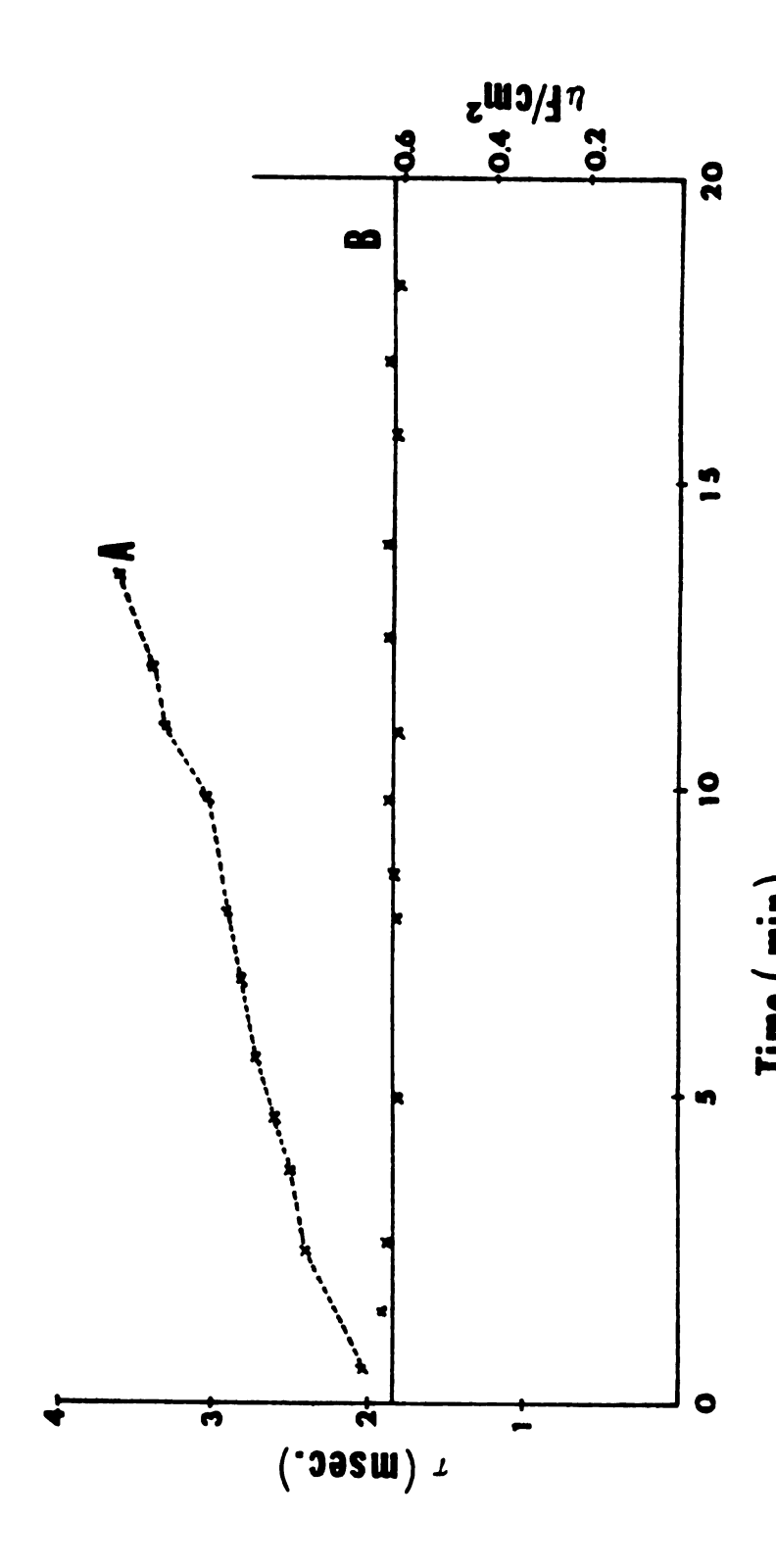
Figure 3-4 shows the capacitance and voltage relaxation time for gramicidin-doped membranes as a function of membrane age (t=0 at the instance the membrane is fully thinned). As pointed out by White and Thompson (71), to be a useful and valid model system for biological membranes, planar bilayer lipid membrane must assume a homogeneous equilibrium structure with a well defined stoichiometry. A reliance of membrane capacitance on membrane age implies a non-equilibrium bilayer structure which undergoes constant changes. Figure 3-4A shows a zero-order dependence of membrane capacitance on time, suggesting a stable configuration for gramicidin-doped GMO-cholesterol membranes. However, as the film aged, a slowdown in voltage relaxation obtained from pulsing the membrane was observed (Figure 3-4B). The rise in relaxation time is attributed to a decrease in membrane conductance because the membrane capacitance is constant. This finding is in accordance with the fact that gramicidin was added to the membrane phase only. The very poor correlation of

Figure 3-4A with Figure 3-4B again shows that the membrane capacitance is independent of gramicidin concentration in the membrane.

Formation Constant of Gramicidin Channels

The voltage relaxation times resulting from charge pulse experiments and the membrane conductance of various GMO-cholesterol membranes at different gramicidin concentrations are summerized in Tables 3-2, 3-3 and 3-4. The membrane conductance and channel concentration were calculated from relaxation time according to equations (10) and (11), respectively. The corresponding N₂ vs. B₂ plots and KINFIT fits to equation (13) are shown in Figures 3-5, 3-6 and 3-7. In Table 3-5 are listed the formation constants and partition coefficients resulted from curve fitting as well as literature values of these same parameters.

Several interesting features can be recognized from the figures and listed results. First, the relative standard deviations of relaxation time measurements for n-decane membranes are considerably larger than those for n-tetradecane and n-hexadecane membranes. This is probably due to the fact that for less permeable membranes, slight flaws in membrane structure such as microlenses (71) or air bubbles exert a greater effect on the membrane conductance than for highly permeable membranes. Second, except for



A i electrolyte i 1M KCl, gramicidin i 1.2 x 10^{-8} M. (relaxation time) Fig. 3-4 The voltage relaxation time and membrane capacitance of gramicidin-doped membranes (3% GMO-1% cholesterol/n-hexadecane). Time equals 0 at the instance the membrane is fully thinned.

electrolyte : 0.5M $CaCl_2$, gramicidin : $4.9 \times 10^{-7}M$. (capacitance)

.. M

Table 3-2 Relaxation time, membrane conductance and channel concentration of gramicidin-doped GMO-cholesterol/n-decane membranes at 24 ± 1 °C. Membrane conductance and channel concentration are calculated according to equation (10).

Gramicidin Concentration ^a	Relaxation Time	Membrane Conductance	Concentration	Calculated Channel Con.
M	Microseconds	Ω ⁻¹ .cm ⁻²	M	×
2.97 x 10 ⁻⁷ 5.95 x 10 ⁻⁷ 8.92 x 10 ⁻⁷ 1.19 x 10 ⁻⁶ 1.78 x 10 ⁻⁶ 2.38 x 10 ⁻⁶ 2.67 x 10 ⁻⁶ 2.97 x 10 ⁻⁶	7416 ± 874 3421 ± 612 1832 ± 314 1533 ± 459 934 ± 178 649 ± 72 493 ± 37 483 ± 11 272 ± 20	5.81 ± 0.68 × 10 ⁻⁵ 1.26 ± 0.22 × 10 ⁻⁴ 2.35 ± 0.40 × 10 ⁻⁴ 2.81 ± 0.84 × 10 ⁻⁴ 4.61 ± 0.88 × 10 ⁻⁴ 6.64 ± 0.74 × 10 ⁻⁴ 8.74 ± 0.66 × 10 ⁻⁴ 8.92 ± 0.20 × 10 ⁻⁴ 1.58 ± 0.35 × 10 ⁻³	5.06 ± 0.60 × 10 ⁻⁹ 1.09 ± 0.19 × 10 ⁻⁸ 2.05 ± 0.35 × 10 ⁻⁸ 2.45 ± 0.73 × 10 ⁻⁸ 4.02 ± 0.77 × 10 ⁻⁸ 5.78 ± 0.65 × 10 ⁻⁸ 7.76 ± 0.58 × 10 ⁻⁸ 1.08 ± 0.03 × 10 ⁻⁷ 1.38 ± 0.10 × 10 ⁻⁷	1.66 x 10 ⁻⁹ 6.53 x 10 ⁻⁹ 1.44 x 10 ⁻⁸ 2.51 x 10 ⁻⁸ 3.85 x 10 ⁻⁸ 5.40 x 10 ⁻⁸ 9.29 x 10 ⁻⁸ 1.15 x 10 ⁻⁷ 1.40 x 10 ⁻⁷

a : Concentration of gramicidin in the membrane forming solution.

Table 3-3 Relaxation time, membrane conductance and channel concentration of gramicidin-doped GMO-cholesterol/n-tetradecane membranes at 24 ± 1 °C. Membrane conductance and channel concentration are calculated according to equation (10).

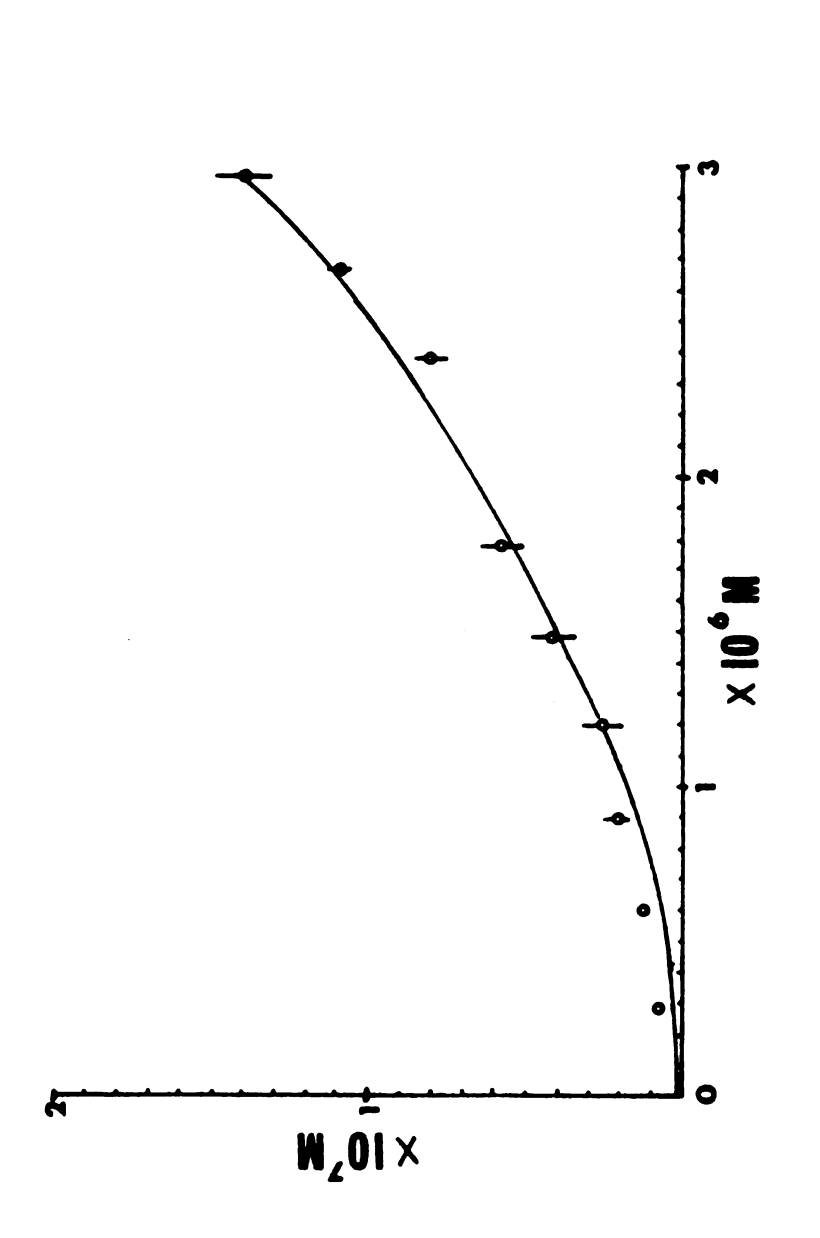
Gramicidin Concentration	Relaxation Time	Membrane Conductance	Concentration	Calculated Channel Con.
W	microseconds	Ω ⁻¹ .cm ⁻²	W	×
5.94 x 10 ⁻⁸ 1.19 x 10 ⁻⁷ 3.57 x 10 ⁻⁷ 4.76 x 10 ⁻⁷ 5.94 x 10 ⁻⁷ 8.32 x 10 ⁻⁷ 9.51 x 10 ⁻⁶ 1.07 x 10 ⁻⁶	1375 ± 303 374 ± 53.3 99.3 ± 15.1 66.4 ± 9.2 50.1 ± 7.1 34.7 ± 3.7 26.9 ± 1.8 22.4 ± 4.5	$3.96 \pm 0.87 \times 10^{-4}$ $1.46 \pm 0.10 \times 10^{-3}$ $5.49 \pm 0.83 \times 10^{-3}$ $8.21 \pm 1.14 \times 10^{-2}$ $1.09 \pm 0.15 \times 10^{-2}$ $1.57 \pm 0.17 \times 10^{-2}$ $2.03 \pm 0.13 \times 10^{-2}$ $2.43 \pm 0.48 \times 10^{-2}$	$4.36 \pm 0.96 \times 10^{-8}$ $1.60 \pm 0.23 \times 10^{-7}$ $6.04 \pm 0.91 \times 10^{-7}$ $9.01 \pm 1.20 \times 10^{-7}$ $1.20 \pm 0.17 \times 10^{-6}$ $1.73 \pm 0.18 \times 10^{-6}$ $2.23 \pm 0.15 \times 10^{-6}$ $2.68 \pm 0.53 \times 10^{-6}$	4.83 x 10 ⁻⁸ 1.41 x 10 ⁻⁷ 6.42 x 10 ⁻⁷ 9.23 x 10 ⁻⁶ 1.22 x 10 ⁻⁶ 1.84 x 10 ⁻⁶ 2.16 x 10 ⁻⁶ 2.48 x 10 ⁻⁶

a i see Table 3-2.

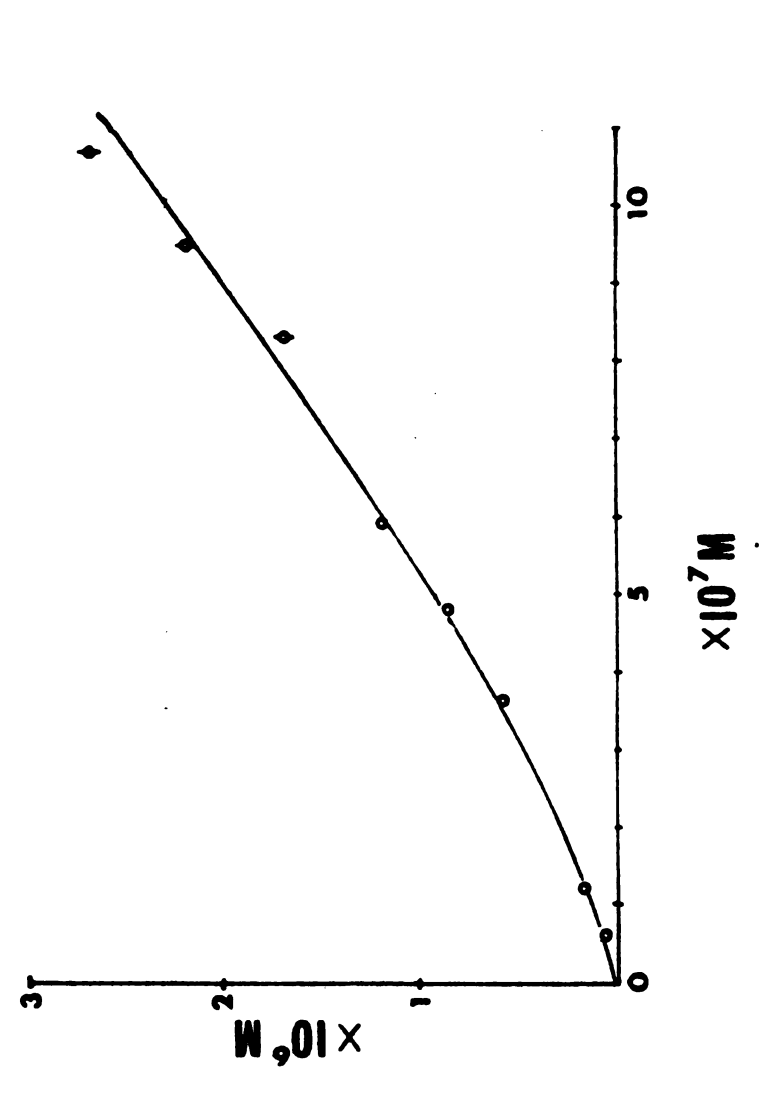
Table 3-4 Relaxation time, membrane conductance and channel concentration of gramicidin-doped GMO-cholesterol/n-hexadecane membranes at 24 ± 1 °C. Membrane conductance and channel concentration are calculated according to equation (10).

Gramicidin Concentration	Relaxation Time	Membrane Conductance	Channel Concentration	Calculated Channel Con.
W	microseconds	Ω ⁻¹ .cm ⁻²	W	W
2.43 x 10 ⁻⁸ 7.30 x 10 ⁻⁸ 9.73 x 10 ⁻⁸ 1.94 x 10 ⁻⁷ 2.92 x 10 ⁻⁷ 3.41 x 10 ⁻⁷ 3.89 x 10 ⁻⁷ 4.86 x 10 ⁻⁷	1206 ± 119 235 ± 12.3 198 ± 7.7 86.3 ± 6.3 45.7 ± 1.9 38.0 ± 2.0 34.9 ± 2.4 27.7 ± 2.5	5.19 ± 0.51 x 10 ⁻⁴ 2.66 ± 0.14 x 10 ⁻³ 3.16 ± 0.13 x 10 ⁻³ 7.25 ± 0.53 x 10 ⁻² 1.37 ± 0.06 x 10 ⁻² 1.65 ± 0.09 x 10 ⁻² 2.26 ± 0.20 x 10 ⁻²	6.56 \pm 0.65 \times 10 ⁻⁸ 3.37 \pm 0.18 \times 10 ⁻⁷ 4.00 \pm 0.16 \times 10 ⁻⁷ 9.19 \pm 0.67 \times 10 ⁻⁶ 1.73 \pm 1.07 \times 10 ⁻⁶ 2.09 \pm 0.11 \times 10 ⁻⁶ 2.27 \pm 0.16 \times 10 ⁻⁶ 2.86 \pm 0.25 \times 10 ⁻⁶	6.27 x 10 ⁻⁸ 2.94 x 10 ⁻⁷ 4.27 x 10 ⁻⁷ 1.00 x 10 ⁻⁶ 1.63 x 10 ⁻⁶ 1.95 x 10 ⁻⁶ 2.92 x 10 ⁻⁶ 2.92 x 10 ⁻⁶

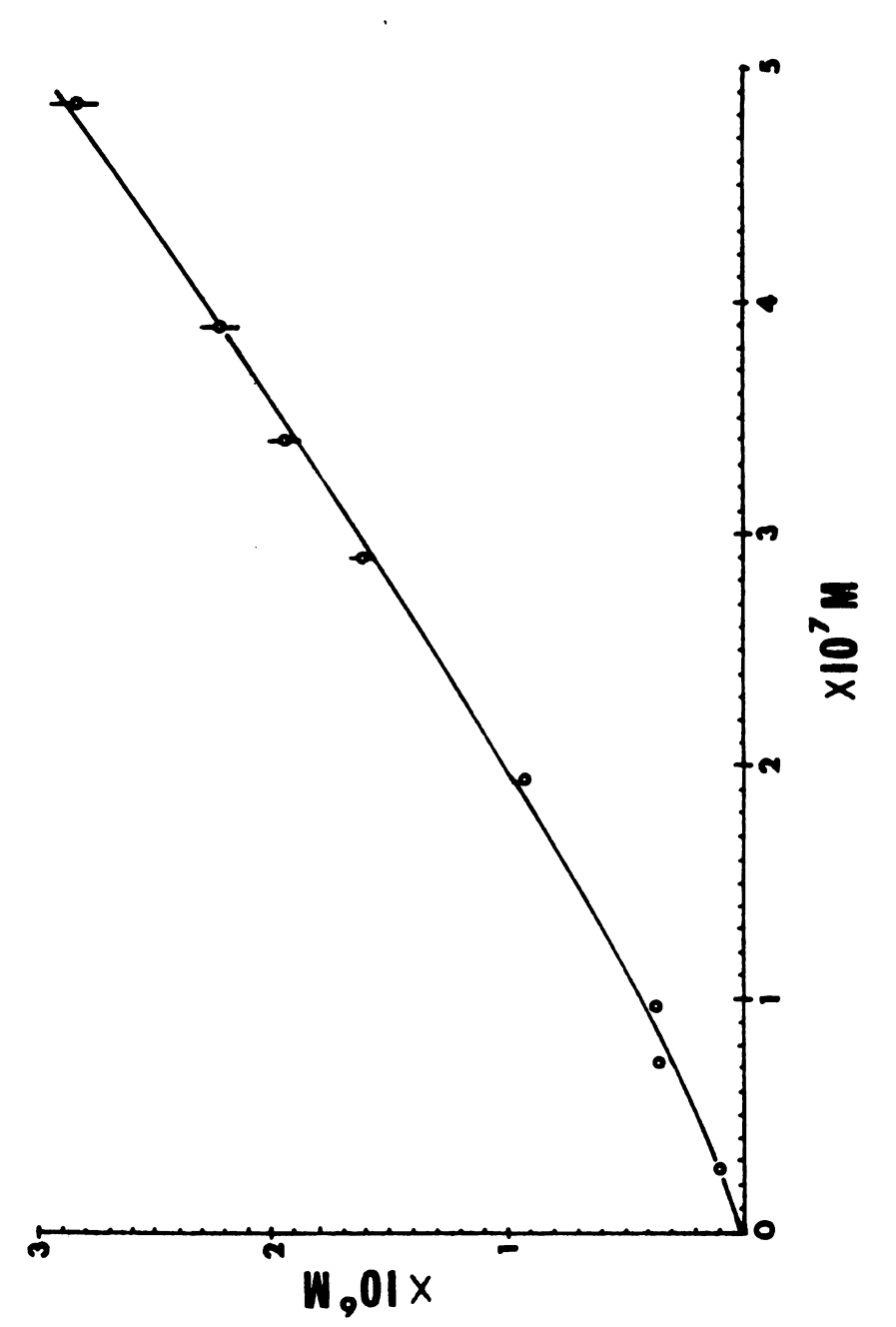
a : see Table 3-2.



gramicidin concentration, B, in GMO-cholesterol/n-decane membranes. Solid curve results from KINFIT fit to equation (12). $\rm N_2$ was Fig. 3-5 Dimeric channel concentration, N_2 , as a function of the calculated assuming a membrane thickness of $46.5\mbox{\AA}$ according to equation (10).



gramicidin concentration, B, in GMO-cholesterol/n-tetradecane membranes. Solid curve results from KINFIT fit to equation (12). Nowas calculated assuming a membrane thickness of 36.8Å according Fig. 3-6 Dimeric channel concentration, N_2 , as a function of the to equation (10).



gramicidin concentration, B, in GMO-cholesterol/n-hexadecane membranes. Solid curve results from KINFIT fit to equation (12). N_2 was calculated assuming a membrane thickness of $32.0\mbox{\AA}$ according to equation (10). Fig. 3-7 Dimeric channel concentration, N_2 , as a function of the

Table 3-5 Dimerization constants, K, and partition coefficients, D, of gramicidin in bilayer lipid membranes.

Solvent	Lipid	K (M ⁻¹)f	Q	Source
·	PC ^a	6.9 x 10 ⁴	1	(94)
•	PC	$1.6 \times 10^{5} (125 \text{ mV}^{\text{b}})$	i	(94)
	PC	$6.0 \times 10^4 \text{ (135 mV)}$	ı	(69)
n-decane	PC	$9.0 \times 10^3 (10 \text{ mV})^c$	ı	(44)
	GMO	47 (10 mV) ^C	21 ^d , 1.1 ^e	(44)
	GMO-cholesterol	1.9 ± 0.2 x 10 ⁴	П	this work
n-tetradecane	GMO-cholesterol	1.1 x 10^3 (10 mV) ^c 5.5 ± 1.8 x 10^5	7.0 + 9.9	(47) this work
n-hexadecane	GMO GMO-cholesterol	$\geqslant 3 \times 10^{4} (10 \text{ mV})^{\text{c}}$ 9.9 ± 4.8 × 10 ⁵	- (47) 15.6 ± 1.4 this work	(47) this work

Table 3-5 (continued)

a . PC = dioleoyl phosphatidylcholine.

b : Membrane potential at which the experiment was conducted.

c : Dansyl gramicidin C was used in the experiment.

d : D was calculated from data given in reference (47) based on their K, i.e., 47 M⁻¹.

e : Same calculation except our K being used (1.9 x 10^4 M⁻¹).

f ' The units for K were changed from those used by cited authors.

n-decane membranes, the fit of experimental data, B and N2, to equation (13) is very good as is judged from random deviations of channel concentrations from calculated values as well as from relatively small standard deviations of fitted results. Thirdly, the formation constant of gramicidin channels depends markedly on the thickness of the hydrocarbon core. Hladky and Haydon (38) found that the mean duration of a single channel increases monotonically with decreasing membrane thickness. They attributed this effect to a variation in the extent of local thinning or dimpling of the membrane in the vicinity of the conducting channel. Our data are consistent with their proposal. The nearly 52 fold decrease in the dimerization constant in going from a 32Å to a 46.5Å GMO-cholesterol membrane corresponds to an increase in the free energy of dimerization of 2.3 Kcal/mole. This free energy difference might represent the energy of deforming a small region of the 46.5Å membrane to match the length of the gramicidin channel. Fourth, for a given dimerization constant, the relative population of gramicidin channels rises as the total amount of gramicidin in the membrane increases. For n-decane membranes, based on our results, only 10% of gramicidin is in the channel form for a membrane forming solution nearly saturated with gramicidin. By contrast, more than 75% of the gramicidin in hexadecane membranes is in the active dimer form when the gramicidin concentration is six times less than the saturation concentration. This

implies that, for solvent-free membranes (such as lipid vesicles) which are even thinner than hexadecane membranes, practically all the gramicidin molecules in the bilayer are in the channel form. As will be discussed later in Chapter IV, this is used to advantage in attempts to photolabel gramicidin channels in lipid membranes.

Also listed in Table 3-5 are the literature values of the dimerization constant. Similar to our results, Veatch et al. (47) observed a dependence of channel formation constant on membrane thickness despite of the fact that dancyl gramicidin C, an active analog of gramicidin, was used in the study. It is noticed, however, that the present results are uniformly larger than the values reported by Veatch et al..

A careful examination of data given in Veatch et al.'s work results in the following findings:

- 1. In converting the observed fluorescence intensity to the absolute surface density of dancyl gramicidin a value of 1.0 was assigned to the relative efficiency of detection of the dancyl fluorescence without citing any reference. It was also assumed that both monomeric and dimeric gramicidin have the same excitation characteristics and quantum yield.
- 2. The dimerization constant of 9 \times 10¹³ M⁻¹ obtained from fluorescence measurements for

dancyl gramicidin C in dioleoyl phosphatidylcholine is a factor of five less than the value obtained using the voltage-jump technique for dancyl gramicidin C on the same membrane. Veatch et al. attributed this disagreement to the overestimate of the total gramicidin concentration by fluorescence measurements. They noticed that Raman scattering and fluorescence arising from the solution can give a much larger signal than the fluorescent species in the membrane. It was also reported that for a 26Å GMO membrane an average value of 1.4 was found for the ratio C_d'/C_d where C_d' is the gramicidin concentration calculated from membrane conductance (Cd'=2N2) and Cd the total gramicidin concentration obtained from fluorescence measurement. As the error resulting from conductance measurements is much smaller than that from fluorescence measurement and in principle the Cd'/Cd ratio should be equal to or less than one (the ratio equals 1 when all the gramicidin is in the dimer form), a value of 1.4 for $\mathbf{C_d}$ '/ $\mathbf{C_d}$ suggests an underestimate of total gramicidin concentration in the membrane by fluorescence measurements. However, no explanation was given for these apparently

conflicting results on the fluorescence measurements.

3. No statistical or mathematical means was utilized in data treatment. In fact, except for n-decane membranes, only ONE data point, i.e., one simulataneous measurement of membrane conductance and fluorescence, was reported for each type of the membrane. Consequently, it is rather difficult to estimate the reproducibility of the measurements and, in turn, the relibility of the inferred results.

Regardless of these findings, on the basis of rather strong fluorescence background emitted by plain membranes and solutions, it seems that the fluorescence technique provides a lower boundary for high dimerization constants.

Another interesting feature evident from Table 3-5 is the dependence of dimerization constant on membrane composition. Veatch et al. discovered a 200-fold increase in formation constant going from a GMO to a dioleoyl phosphatidylcholine membrane. Parallel correlation also exists between Lauger et al.'s and our results although the difference is less drastic. Since all these membranes are composed of neutral lipids with similar chain length and use same alkane solvents, factors other than bilayer thickness and charge distribution must be responsible for this

phenomenon. Consequently, the difference in bilayer composition might be another reason for the discrepancy between Veatch's and our results.

<u>Partition Coefficient of Gramicidin between the Membrane</u> and Torus Phases

Another important physical parameter obtained from our study is the partition coefficient of gramicidin between the membrane and torus phases. As is evident from Table 3-5, the partition coefficient also exhibits a strong dependence on membrane thickness. It increases from 1 for n-decane membranes to 15.6 for n-hexadecane membranes.

Recently, Sychev et al. (75) reexamined the spectral properties of gramicidin A and its analogs in dioxane (a nonpolar solvent) and obtained a value of $1x10^5 \text{ M}^{-1}$ for dimerization constant. On the basis of theoretical calculations in conjunction with observed dissociation rate constants for the dimers, they concluded that the predominant dimeric species in the nonpolar solvent is different from that in the membrane and thus suggested that the bilayer structure of a membrane has a greater influence on the dimer conformation than on the monomer's. If the torus region could be approximated by the dioxane solution and the gramicidin monomers assume similar structure in both membranes and nonpolar solvents,

the partition coefficient would then be a measure of stability of membrane dimers with respect to dimers in dioxane and the dimerization constant would represent the stability of dimers relative to monomers. In Table 3-6 are listed G's calculated from partition coefficients and dimerization constants according to equation (15):

where ΔG° : the change in standard free energy in Kcal·mole⁻¹

R : gas constant

T: temperature (24°C was used)

K : partition coefficient or dimerization constant

Since $\Delta G_{\mathrm{par}}^{\circ}$ equals zero for n-decane membranes, the standard free energy of dimers in dioxane solution and n-decane membrane should be the same. As a result, the following relation between $\Delta G_{\mathrm{dim.}}^{\circ}$'s and $\Delta G_{\mathrm{par.}}^{\circ}$ is derived:

where the alkane is either n-tetradecane or n-hexadecane. If the average of $\Delta G_{\text{dim.}}^{\circ}$'s for dioxane and

Table 3-6 Free energy of dimerization and partition of gramicidin in alkane membrane.

Phase	$K (M^{-1})$	ΔG ^o dim. ^D (Kcal/mole)	Ω	ΔG par. (Kcal/mole)
Dioxane solution (75)	1 x 10 ⁵	-6.8	I	I
Decane membrane	$1.9 \pm 0.2 \times 10^{4}$	-5.8 ± 0.1 , -6.3 ± 0.1^{d}),1 ^d 1	0
Tetradecane membrane	$5.5 \pm 1.8 \times 10^5$	-7.8 ± 0.3	4.0 + 9.9	-1.1 ± 0.1
Hexadecane membrane	$9.9 \pm 5.0 \times 10^5$	-8.2 ± 0.3	15.6 ± 1.4	-1.6 ± 0.1

The average of $\Delta G_{\text{dim.}}^{\circ}$'s for decane membranes and dioxane solution. **--**ਲ

b $AG_{dim.}^{\circ} = -RTlnK_{dim.}$ c $AG_{par.}^{\circ} = -RTlnD$

d : Data were collected at $24 \pm 1^{\circ}C$.

n-decane membrane is taken as the ΔG° dim., decane, it is evident that equation (16) holds within experimental error.

As shown in Table 3-5 only one set of data was available wherefrom D could be calculated. One major reason for the scarcity of literature values for this parameter is that in voltage-clamp experiments, the total concentration of gramicidin in the membrane is not needed for data treatment. Based on Veatch et al.'s dimerization constant (47 M⁻¹) for n-decane membranes, a value of 21 was obtained for D. If our dimerization constant (1.9 x 10⁴ M⁻¹) is used, D then equals 1.1. This finding demonstrates that our results are self-consistent even when their data is used.

Comments on the Assumptions

The agreement between the experimental data and the proposed model observed in reported studies as well as in our approach strongly supports the validity of the assumptions involved in the investigation. However, one additional condition was imposed in the present study, i.e., that the partition coefficient of gramicidin between the membrane and torus phases is a constant over the concentration range used in the experiments.

In analog experiments, Veatch et al. discovered a linear relation between the total amount of gramicidin in the membrane and the gramicidin concentration in the membrane forming solution as long as the latter is less

than 1×10^{-6} M. As shown in Tables 3-2 to 3-4, except for some n-decane membranes, all the solutions used are equal to or less than 1×10^{-6} M in gramicidin. It is also obvious from Tables 3-3 and 3-4 that the partition coefficient must be greater than one since the dimer concentrations obtained from conductance measurements are greater than the gramicidin concentration in the membrane forming solution.

In 1971, based on the measurements of interfacial tension, Fettiplace et al. (72) estimated the area per molecule occupied by glyceryl monocleate (GMO) in the alkane membranes. They found that the area covered by one GMO is almost independent of the solvent and has a value of 39.5Å^2 . If it is assumed that the same value applies for GMO-cholesterol membranes and the bilayer is solvent-free, a value of 4.5×10^5 for the lipid to dimer ratio is obtained for our most permeable membrane. It means two adjacent channels are separated by 670 lipid molecules. As a result, the interaction between channels should be minimal and single channel conductance could be employed to calculate the dimer density from conductance measurements.

Conclusion

We have successfully obtained the formation constants of gramicidin channels in lipid membranes as well as the partition coefficients of gramicidin between

the bilayer and torus phases by use of the charge injection technique. The results acquired are comparable to those found in literature. In addition, a correlation was found between the dimerization constant and partition coefficient. It is of interest to note that although relaxation experiments have been performed on the membranes, the resulting physical parameters represent the equilibrium values of the same parameters prior to the charge perturbation.

CHAPTER IV

PHOTOLABELING OF GRAMICIDIN CHANNELS IN LIPID MEMBRANES

INTRODUCTION

Since the discovery that ion transport across the lipid membrane is mediated by gramicidin via the pore mechanism (37), a number of studies (50, 58) have been conducted to determine the molecular architecture of gramicidin channels in lipid bilayers.

As described in Chapter I, four configurations exist as the possible structure of gramicidin channels. They are parallel double-stranded helix, antiparallel double-stranded helix, C-terminal-to-C-terminal single-stranded helix and N-terminal-to-N-terminal single-stranded helix. Results obtained from various investigations indicated that N-terminal-to-N-terminal helix is the major, if not sole, conformation of the transmembrane gramicidin channel.

A careful examination of the reported studies, however, shows one serious drawback, i.e., altered gramicidin or gramicidin analogs have been used in the experiments. It has been noted that some of these analogs

are not capable of inducing membrane conductivity and, for the "active analogues", their single channel conductance greatly depends on the polarity of the attached chemical groups. Consequently, in order to obtain unambiguous information regarding the structure of transmembrane gramicidin channels, a direct method based on the use of native gramicidin is highly desired.

In this chapter, we describe the effect of photolabeling on channel conductivity and its potential use in unraveling channel conformations.

Photolabeling

In the past ten years, photolabeling techniques (59) have found wide application in the studies of biochemical systems. Some typical examples are the mapping and identification of ligand binding sites on biomacromolecules (60, 61), the location of membrane constituents (62-66) and the topography of biopolymers (63).

In such methods, a photolabile probe which suits the needs of the system in question is selected. Upon illumination, the photogenerated reactive species covalently binds to the target. Subsequent analysis of the photo-altered target thus reveals the immediate chemical surroundings that are adjacent to the binding site.

Generally speaking, photolabeling has three major advantages over the conventional labeling. First of all,

photolabeling probes are inert until photolysis, which permits some experiments to be dome before irradiation without any irreversible interactions between the target and probe. Secondly, many photolabeling reagents can insert into carbon-hydrogen bonds. Thus, photolabeling probes can mark any reaction site which contains carbon-hydrogen bonds and which does not require the presence of particular reactive functional groups at the binding site. Thirdly, with an infarared filter, photolysis is practically free from introducing any heat into reaction vessel, which preserves the structural integrity of biological systems.

As such, photolabeling seemed to be an ideal method for our study. The reasons are two-fold.

- 1. Native gramicidin can be used in the experiments since, as memtioned above, photolabeling does not require the assistance of any special chemical groups at the reaction site.
- 2. Photolabeling probes could be tailored to mark certain moieties of the channel so that the analysis of photo-tagged gramicidin would yield information regarding the channel conformation in lipid membranes.

For a transmembrane polypeptide, the amino acid residues can be classified into two categories: those located near or on the membrane surface and those in the membrane interior. As gramicidin forms linear channels

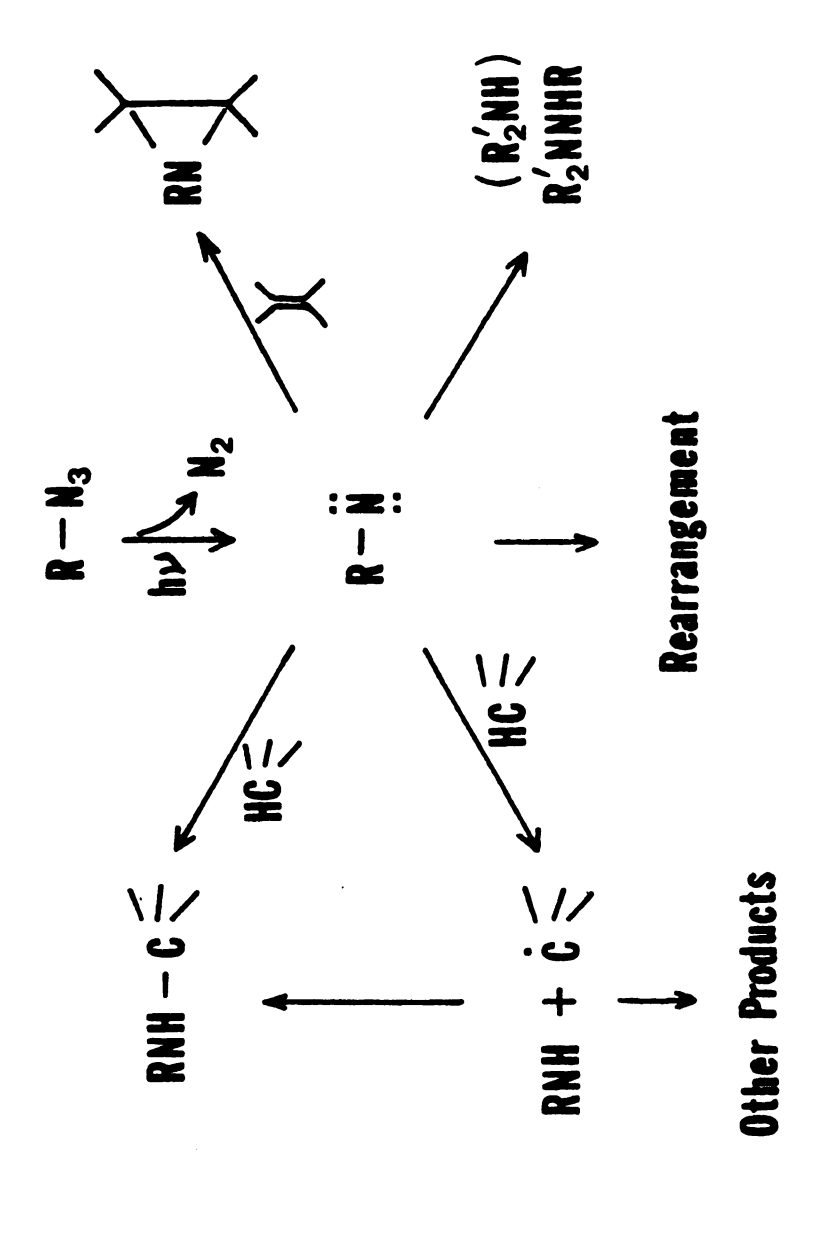
across lipid membranes, it is expected that a few of its 15 amino acid constituents would be exposed to the aqueous phase. It follows that labeling of gramicidin channels on the membrane surface would produce relatively simple photoproducts.

Arylazides

There are two common reactive species which meet the carbon-hydrogen bond insertion requirement of photolabeling technique: carbenes and nitrenes.

Carbenes can be generated by the photolysis of compounds such as diazoalkanes, diazirines, and -ketodiazo compounds, which produce the carbene on loss of nitrogen. Although it is very reactive, carbene has been ruled out as a good photolabeling reagent on the grounds that most of carbene precursors are not chemically inert and stable, and that α -ketocarbene produced from stable α -diazoketones, esters etc. readily undergoes the intramolecular rearrangement to a ketene, which is less reactive and subject to attack by nucleophiles.

In contrast, nitrenes can be produced from chemically inert azides by reactions similar to those forming carbenes. As illustrated in Figure 4-1, a nitrene could undergo a variety of reactions after its formation: abstraction (normally of hydrogen from carbon), cycloaddition, direct insertion (usually into carbon-hydrogen



Reactions open to a nitrene after its formation. Fig. 4-1

bonds), attack by nucleophiles, and rearrangement. Direct insertion, abstraction-coupling or addition reactions will result in covalent attachment of label to the target.

Rearrangement reactions can, as with carbenes, reduce the effectiveness of the reagent. Acylazides rearrange smoothly on photolysis to isocyanates; whereas arylnitrenes are much less susceptible to rearrangement.

In addition, alkyl azides have absorption maxima around 200 nm and it is not possible to effect photolysis without radiation damage to the polypeptides. With proper substitution on the aromatic ring, arylazides can be photolyzed to the arylnitrenes at wavelengths greater than 300 nm. Thus it appears that arylazides are appropriate reagents for photolabeling experiments.

2-Nitro-5-Azidobenzoic Acid

Of various arylazides, 2-nitro-5-azidobenzoic acid (NABA) has been chosen as the photolabeling reagent in our studies of gramicidin channels in lipid membranes. The introduction of an electron withdrawing group (-NO₂) into the aromatic ring shifts the absorption maximum and pKa of the benzoic acid to 315 nm and 3.6 respectively. It follows that, with proper buffering of the aqueous solution, arylnitrenes photolytically generated from NABA would essentially stay in the aqueous phase and covalently bind to gramicidin channels on the membrane surface.

2-nitro-5-azidobenzoic acid

NABA

EXPERIMENTAL

Reagents

All chemicals and solvents used were reagent grade and used without further purification. Freshly deionized water was used to prepare all solutions. The lipid used for liposome solutions was phosphatidylcholine (type V-E, from egg yoke, Sigma Chemical Company).

Gramicidin, a mixture of gramicidin A (85%), gramicidin B (4%), and gramicidin C (11%) (64), was purchased from Sigma and used as received. Sephadex G-50 (particle size 50-150 micro, pharmacia Fine Chemicals) was suspended in 0.1 M phorphate buffer, pH 10, for at least 6 hours before column packing. 2-Nitro-5-amino-benzoic acid was purchased from Pfaltz and Bauer; trifluoroacetic anhydride, trifluoroacetic acid and n-decane from Sigma; glyserolmonoo-leate (GMO) from Matheson, Coleman & Bell, and

N,N'-dinitroso-N,N'-dimethyl terephthalamide from Du Pont.

Apparatus

The UV and IR spectra were obtained by the use of a Beckman Gray 17 spectrometer and a Perkin-Elmer 457 spectrometer respectively. The mixture analysis was performed on a Finnigan 4000 automated gas chromatograph-EI/CI mass spectrometer with INCOS data system. Thin-layer chromatography was carried out on Analtech silica gel G plates of 1-mm thickness. PH measurements were made on a Heath EU-302A digital pH/volt meter with a Sargent combined glass electrode. For photolysis experiments, a Hanovia medium pressure 450 W mercury lamp with a Pyrex cooling jacket was used as the radiation source. All the reaction vessels for photolysis were of Pyrex glass, so that UV light less than 300 nm was absent. The sonication of lipid-gramicidin suspensions was achieved on a Mettler Electronics ME 4.6 bath sonicator. For voltage clamp experiments, a Heath Voltage Reference Source was used to provide membrane potential and a Kiethley 610A Electrometer to monitor resulting membrane current. Electrodes, electrolytic cells and charge injection instrument were described in Chapter III. Gas chromatogram was obtained by use of a Varian model 1400 FID gas chromatograph.

Procedure

1. Synthesis of 2-nitro-5-azido-benzoic acid (NABA)

2-Nitro-5-amino-benzoic acid (9.43 g, 0.05 mole) was suspended in aqueous H₂SO₄ (3.8 M, 95 ml) at -5°C. To the maxture was added dropwise NaNO2 (7g, 0.1 mole, in 35 ml of water at -5°C) followed by additional urea crystals (6 g, 0.1 mole) to destroy excess NaNO2. After stirring the solution for 15 minutes, NaNO3 (13.1 g, 0.2 mole, in 35 ml of water at -5°C) was added slowly over a period of 30 minutes. After N_2 evolution ceased, the mixture was stirred for additional 20 minutes and the solid product collected on a Buchner funnel. The product was washed once with ice water and recrystallized from $MeOH:H_2O$ (2:1 by volume) in a yield of 3.06 g (33%). The pKa of NABA was determined by titrating 18 mg of the product in 150 ml of water with 0.01 N NaOH. The course of the titration was followed by a pH meter. The pH of the solution at the midpoint of the titration was taken as the pKa of NABA.

The UV spectrum (0.1 M Na₂HPO₄, pH 7.4) showed max 315 nm (E9300); the IR spectrum (Nujol) showed: 2120 cm⁻¹ (S, -N₃), 3400 cm⁻¹ (S, broad, -OH); m.p. 163-166C(lit. 165-166 C); pKa 3.6.

2. Preparation of gramicidin-doped liposomes

Phosphatidylcholin (100 mg, 0.13 mmole, in 1 ml of CHCl₃) and gramicidin (24 mg, 0.013 mmole, in 0.5 ml of methanol) were mixed and evaporated first on a rotatory evaporator and then by a vacuum pump. The mixture was under vacuum for at least one hour to ensure the complete removal of organic solvents. NABA (31 mg, 0.15 mmole, in 4 ml of 0.1 M phosphate buffer, pH 10) was then added to the lipid-gramicidin mixture, vortexed for 10 minutes and sonicated for one hour. The resulting liposome solution was incubated in an oil bath for 8 hours at 55°C to establish the incorporation of gramicidin into the lipid membrane (65).

3. Photolysis

For liposome solutions, the irradiation lasted about 36 hours until the IR peak of azide group $(-N_3, 2120 \text{ cm}^{-1})$ of NABA completely disappeared.

4. Separation of gramicidin and its analogs from liposomes

The irradiated or control liposome solution was diluted two-fold with 0.1 M phosphate buffer (pH 10) and applied to a Sephadex G-50 column (1.3 cm x 27 cm) in two portions. The liposomes were eluted with 0.1 M phosphate buffer (pH 10) and the turbid fractions

collected. The recovered liposome solution was then carefully evaporated on a rotatory evaporator to about 0.5 ml followed by extractions with two 25-ml portions of methanol. After evaporation of the solvent, the extract was dissolved in minimal methanol and separated by thin-layer chromatography (solvent system: methanol). The fast moving band near the solvent front was eluted with methanol. The eluent showed a UV spectrum and imgration destance similar to authentic gramicidin and, thus, was gramicidin or its analog or their mixtures.

5. Partial hydrolysis and derivatization of gramicidin and its analogs

Gramicidin or its photolabeled analog were partially hydrolyzed with 2 ml of trifluoroacetic acid in constant distilled HCl $(1:1\ (V/V))$ at 110° C for 1.5 hour in an evacuated and sealed thickwall glass tube. The contents of the tube were then transferred into a 10 ml flask and evaporated on a rotatory evaporator.

To the resulting mixture was added ethereal diaxomethane freshly prepared by reacting 2 g of N,N'-dintroso-N,N'-dimethyl terephthalamide with 10 ml of 10% methanolic NaOH in 30 ml of dry ether at 0°C. After evaporation of excess diazomethane and ether, the methyl esters were transformed into their trifluoroacetyl-derivatives by treatment with 1 ml of trifluoroacetic

anhydride in 0.5 ml of CH₂Cl₂ for two hours. The resulting mixture was then evaporated and stored in the refrigerator.

6. GC-MS analysis

The derivatized bydrolysate of control or irradiated gramicidin was dissolved in 0.2 ml of acetone and 1 μ l of this solution injected into gas chromatograph-mass spectrometer. Glass columns (3') filled with 3% SE-30 on Gas Chrom Q (applied Science Lab.) were used in all experiments. The initial temperature was 80°; a linear temperature programming rate of 8°/min. was used to a final temperature of 290°. Electron impact (70 eV) was exploited to obtain the mass spectra.

RESULTS AND DISCUSSION

Photolysis of NABA

The UV-Visible spectrum of NABA (Figure 4-2) is characterized by a single peak at 315 nm. Upon photolysis with a medium pressure mercury lamp (\geqslant 320 nm), a stable spectrum was obtained that displayed two shoulders near 265 nm and 248 nm, and the major absorption peak was shifted (λ_{max} = 345 nm) toward higher wavelengths. This red spectral shift and creation of new spectral shoulders is attributed to a solvolysis reaction of the nitrene

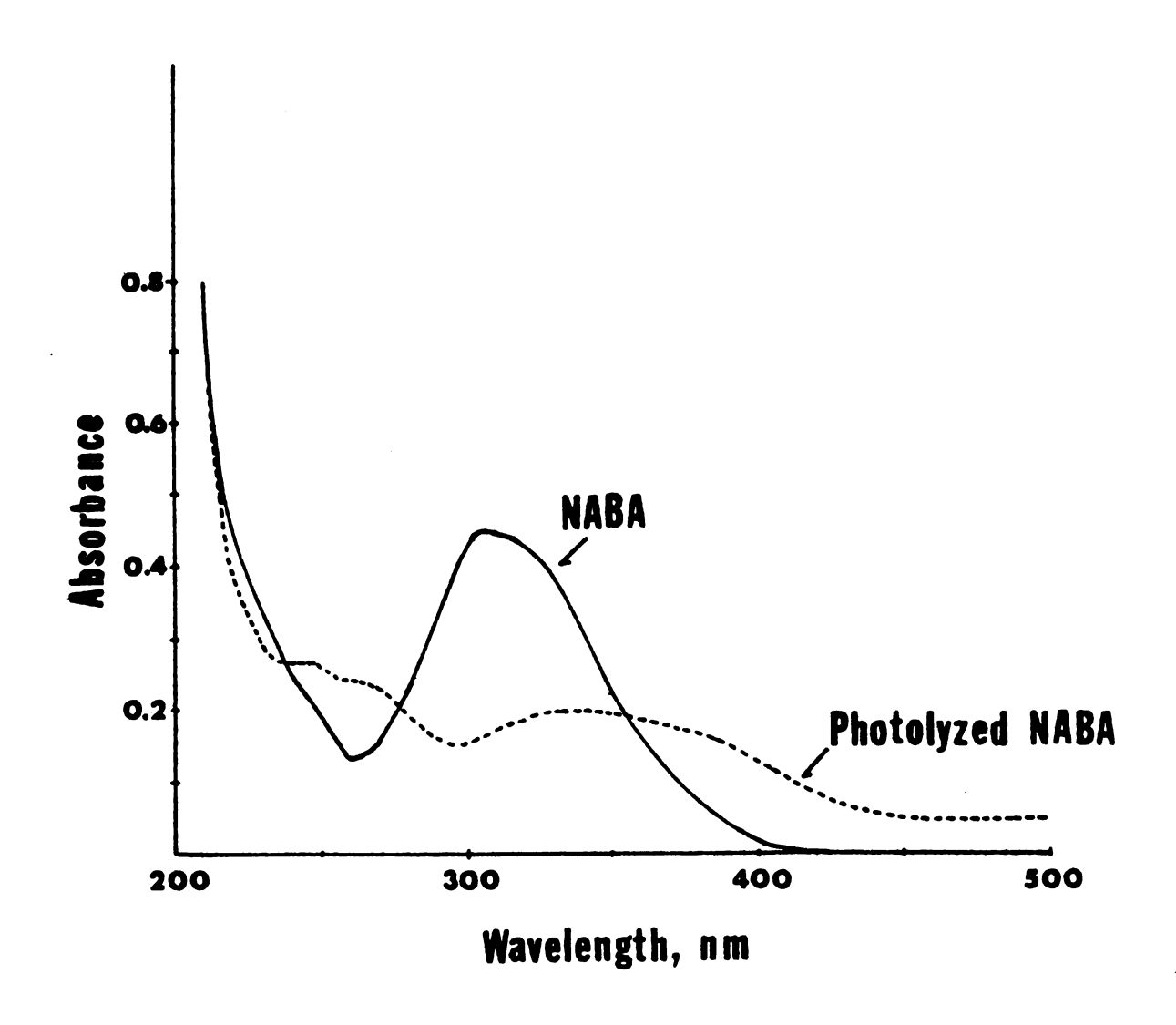


Fig. 4-2 The effect of photolysis at≥320 nm on the UV spectrum of NABA. NABA was dissolved in 0.1M phosphate buffer (pH 9.4) and irradiated at≥320 nm for 10 minutes until no further change in the spectrum.

intermediate photogenerated from NABA.

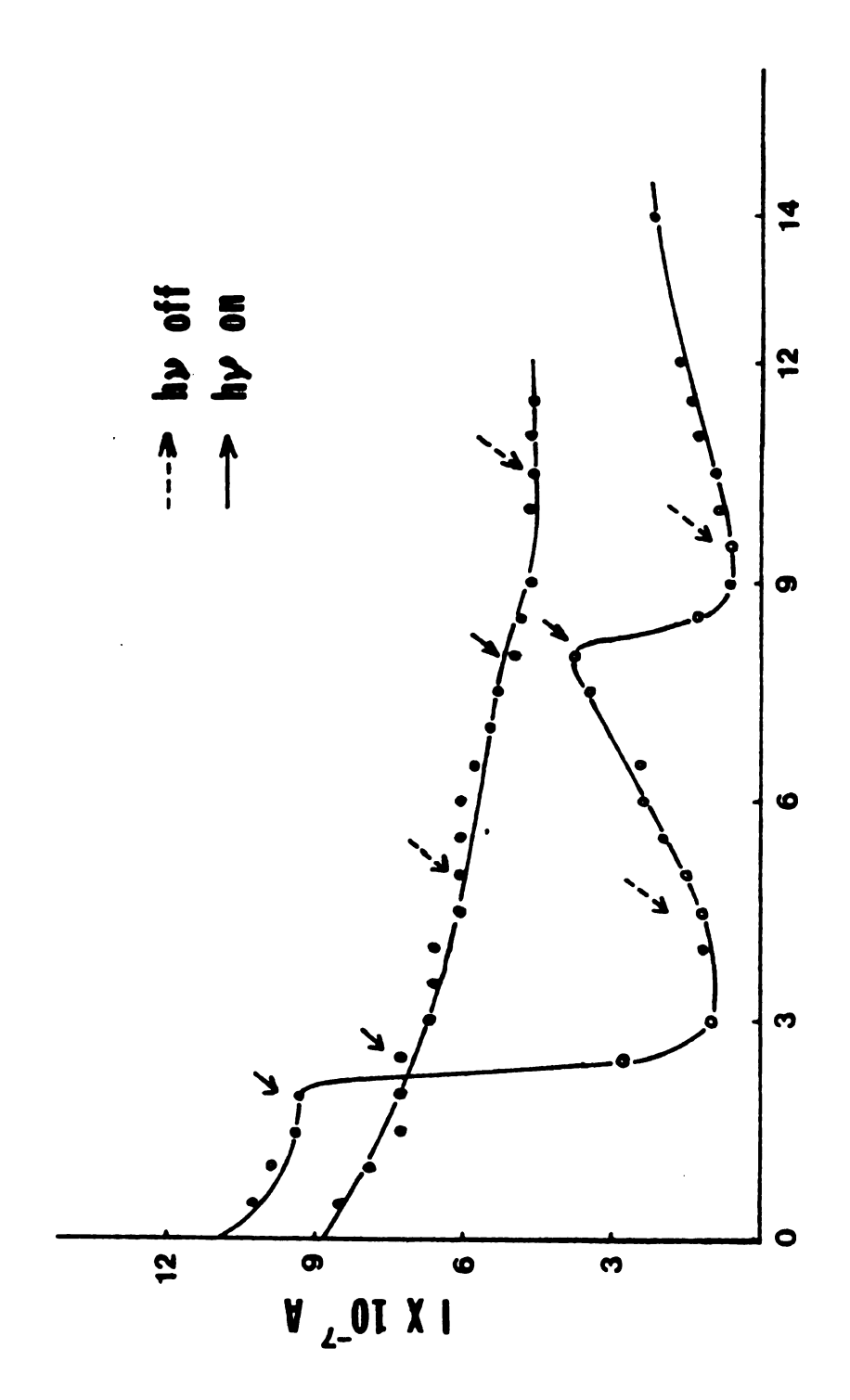
Spectral changes of NABA in infrared regions was also observed. The sharp absorption peak of azide group $(-N_3)$ at 2120 cm $^{-1}$ is destroyed upon illumination. In photolabeling experiments, the disappearance of this spectral peak was monitored to signal the end of the photolysis.

Effect of Photolysis of NABA on Gramicidin-mediated ion Transport

Two techniques have been employed to investigate the effect of photolysis of NABA on the membrane conductivity induced by gramicidin. They are the voltage clamp experiment and the charge injection experiment.

In voltage clamp experiments, lipid bilayers containing gramicidin were formed and the membrane current resulting from an externally applied potential was monitored. As the light was turned on and off, as shown in Figure 4-3, a small decline in membrane current in the dark is observed. Since the antibiotic was added to the membrane forming solution, the decline is attributed to the less lipid-bond gramicidin to the aqueous solution. It is evident from Figure 4-3 that in the absence of NABA irradiation does not cause any change in membrane conductance.

In the presence of NABA, however, a remarkable



The effect of photolysis on membrane conductance. n was added to the membrane forming solution (1% GMO-terol in n-decane). Membrane potential : 50mV; electrolyte Fig. 4-3 The ef Gramicidin was a 1% cholesterol 0.1M phosphate • no NABA; •

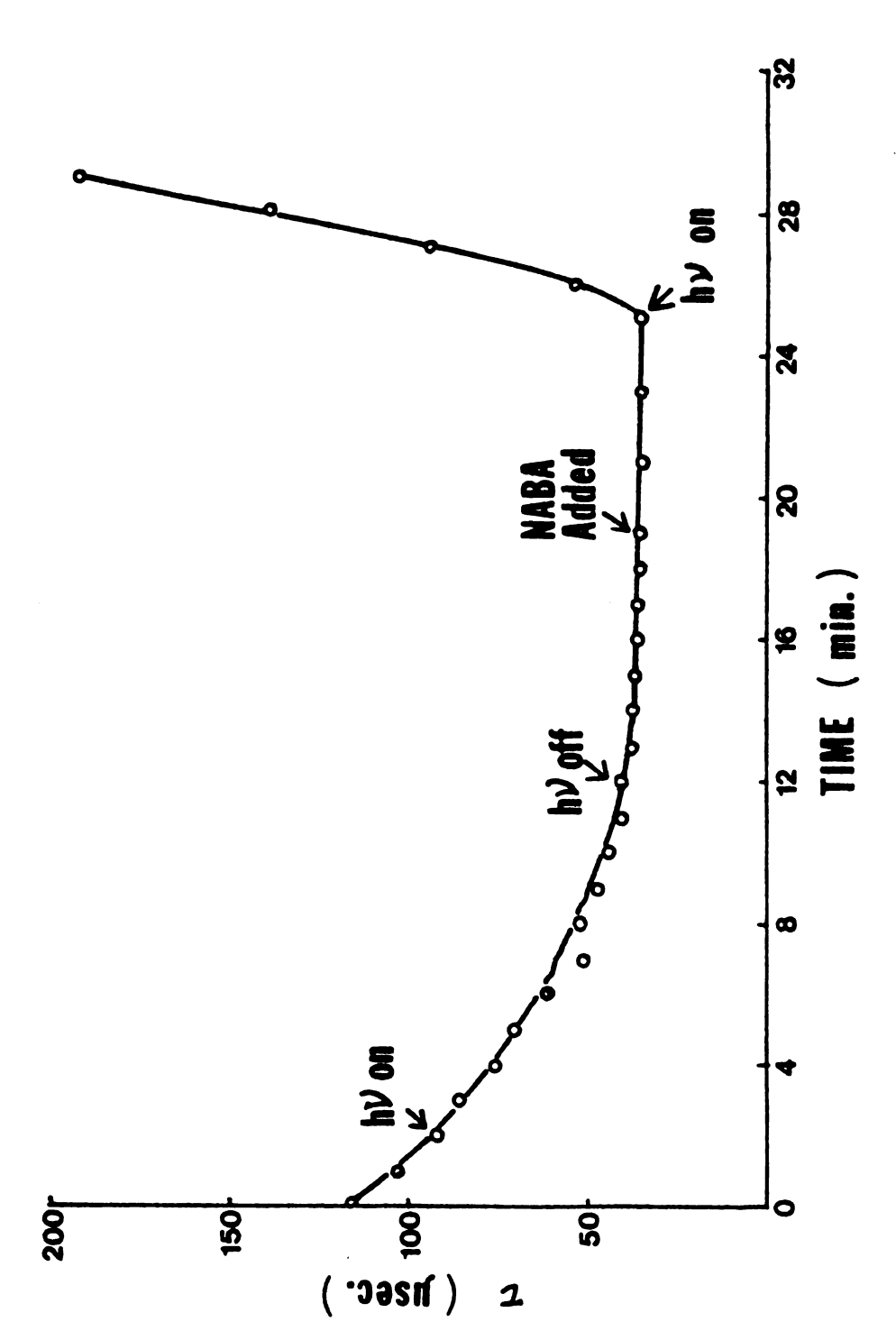
: NABA in aqueous phase.

change in membrane conductance is observed upon illumination. The membrane current drops more than 90% from 9.2 x 10^{-7} A to 9.0 x 10^{-8} A and reaches a steady state. As the membrane current is a manifestation of active gramicidin channels, its reduction reflects either a decrease in the number of open channels or a partial loss of channel activity. Upon discontinuing irradiation, a slow recovery in membrane conductance was registered. The membrane current enters another fall-and-rise cycle when one more round of on-and-off of radiation source is effected.

Similar results were also obtained from charge injection experiments.

As discussed in Chapter III, the relaxation time of voltage transient resulting from pulse applications to a membrane equals the ratio of membrane capacitance to membrane conductance. As membrane capacitance is voltage-independent and does not vary with time, the relaxation time is inversely proportional to the concentration of gramicidin channels in the membrane.

In the charge injection experiments, gramicidin was added to the aqueous solution. As shown in Figure 4-4, the relaxation time decreases as gramicidin diffuses into the lipid phase in the early stage of the experiment. It was observed that during this period irradiation exerts no effect on the membrane conductance. When the relaxation time reached a steady state, NABA was added and photolysis



transmembrane voltage relaxation was caused by applying charge pulse to the membrane (1% GMO-1% cholesterol/n-decane). Gramicidin was added to the aqueous phase (0.1M phosphate, pH 7.6) at the Fig. 4-4 The effect of photolysis on voltage relaxation time. The begining of the experiment.

effected. A rapid rise in relaxation was registered.

Unlike the voltage clamp experiments, explanations of changes in voltage relaxation time are a little more complicated. The attachment of negatively charged nitrene intermediates to membrane surface would inevitably modify the double layer structure and result in changes in membrane capacitance. In view of the five-fold increase in decay time, it is, however, unlikely that the entire change in relaxation time would be due to a variation in membrane capacitance. The depletion mechanism for membrane charge must somehow have been altered by photolysis of NABA.

There are reasons to believe that the photoinduced blocking of gramicidin channels arises from the binding of nitrene intermediates to the channel openings. In both experiments, NABA was kept in aqueous phase and denied its access to membrane interior by use of alkaline buffer (pH 7.6). With a channel diameter of 4Å plus the fact that gramicidin does not induce anion permeability, it is quite impossible for NABA to be present inside the pores. Consequently, the only place left on gramicidin channels that could be photolabeled by nitrene intermediates is channel termini near membrane surface. It thus appears that the reduction of membrane conductance upon photolysis of NABA is due to the steric hindrance introduced by the covalent attachments of nitrene intermediates to the channel orifice.

Chemical Characterization of Gramicidin Isolated from Irradiated Liposomes

If the blocking effect of photolysis of NABA on gramicidin-mediated ion transport is indeed a result of the covalent binding of nitrenes to channel mouth, structural analysis of gramicidin photolabeled while in its pore position would then reveal information regarding the channel conformation in lipid membranes.

Unfortunately, BLM experiments do not yield enough material for chemical characterization. One way to circumvent the difficulty is to employ gramicidin-doped lipid vesicles. The solvent-free nature of liposome bilayers provides an additional advantage over BLM, i.e., essentially all the gramicidin molecules in the membrane are in the channel form.

The search for a technique that suits our need was limited by four factors. First, even with the liposome approach, the amount of gramicidin available is in the milligram range. Second, the technique should be capable of yielding some structural information. Third, the method should allow mixture analysis. And last, it should be practical with resources available.

In view of these requirements, gas chromatographymass spectrometry appeared to be the best choice among the various techniques. The outline of the experiments is shown in Figure 4-5. Briefly, gramicidin-doped liposomes

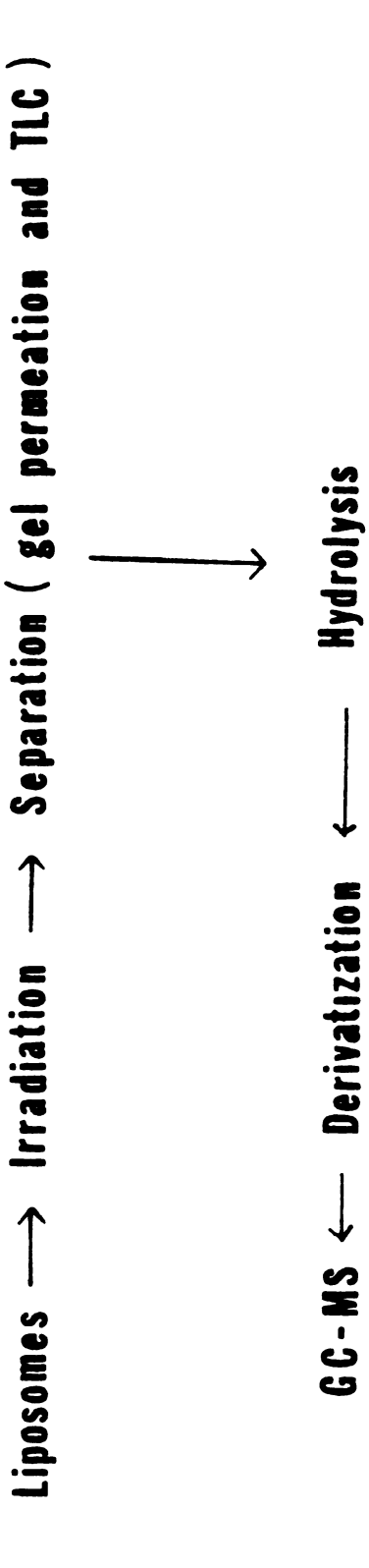


Fig. 4-5 Experiments that would result in substantial amount of photolabeled gramicidin for chemical characterization.

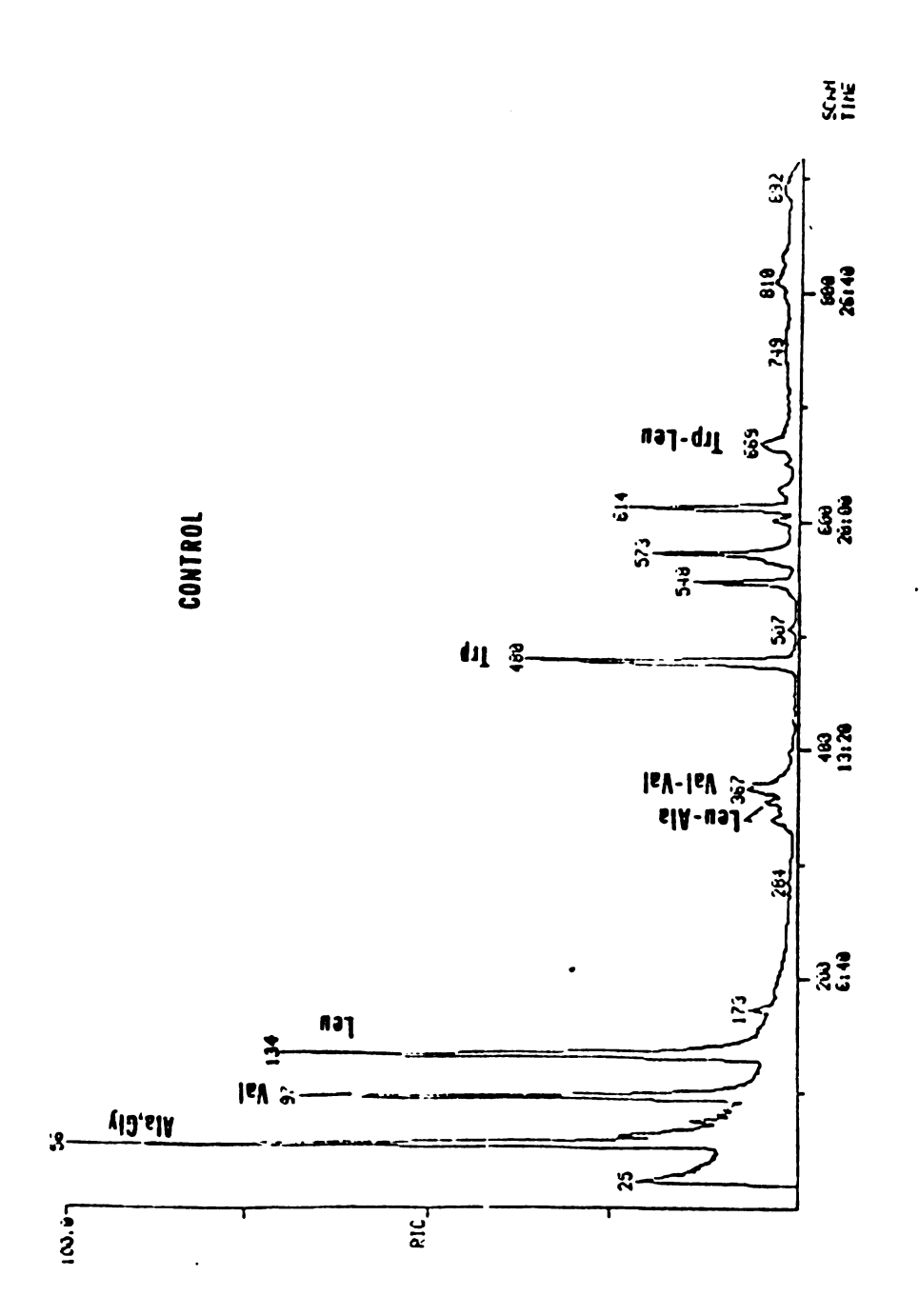
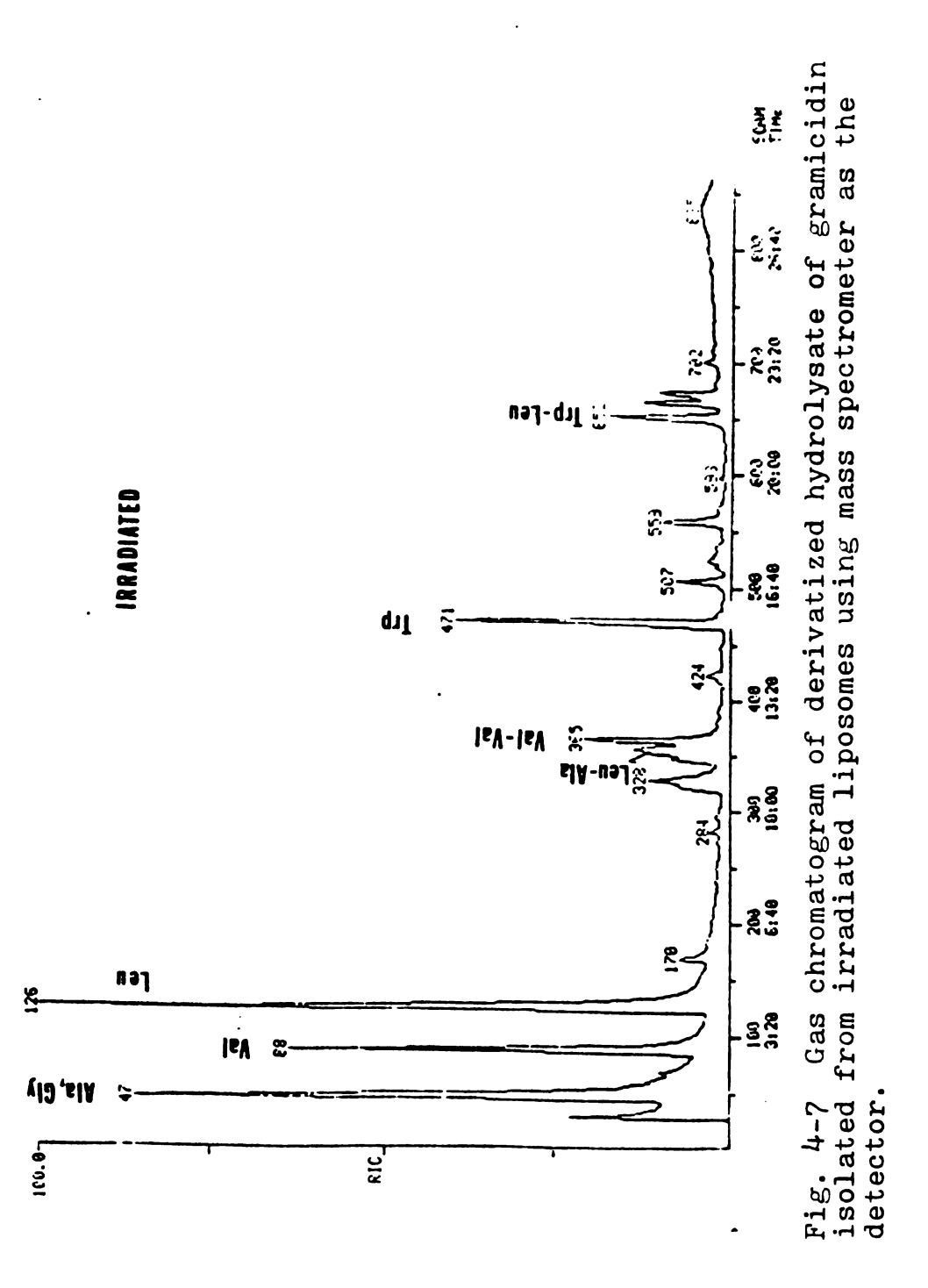


Fig. 4-6 Gas chromatogram of derivatized hydrolysate of gramicidin isolated from control liposomes using mass spectrometer as the detector.



where $\mathbf{R_1}$, $\mathbf{R_2}$ are the side groups of amino acids.

Species	M.W.	m/e					
Gly	185	126, 185	185				
Ala	199	140,	184,	199			
Val	227	168,	185				
Leu	241	182,	185				
Leu-ala	312	182,	210,	255			
Val-val	326	168,	213,	267,	787		
Trp	410	129,	226,	297,	351,	410	
Trp-leu	523	129,	226,	266,	297,		410

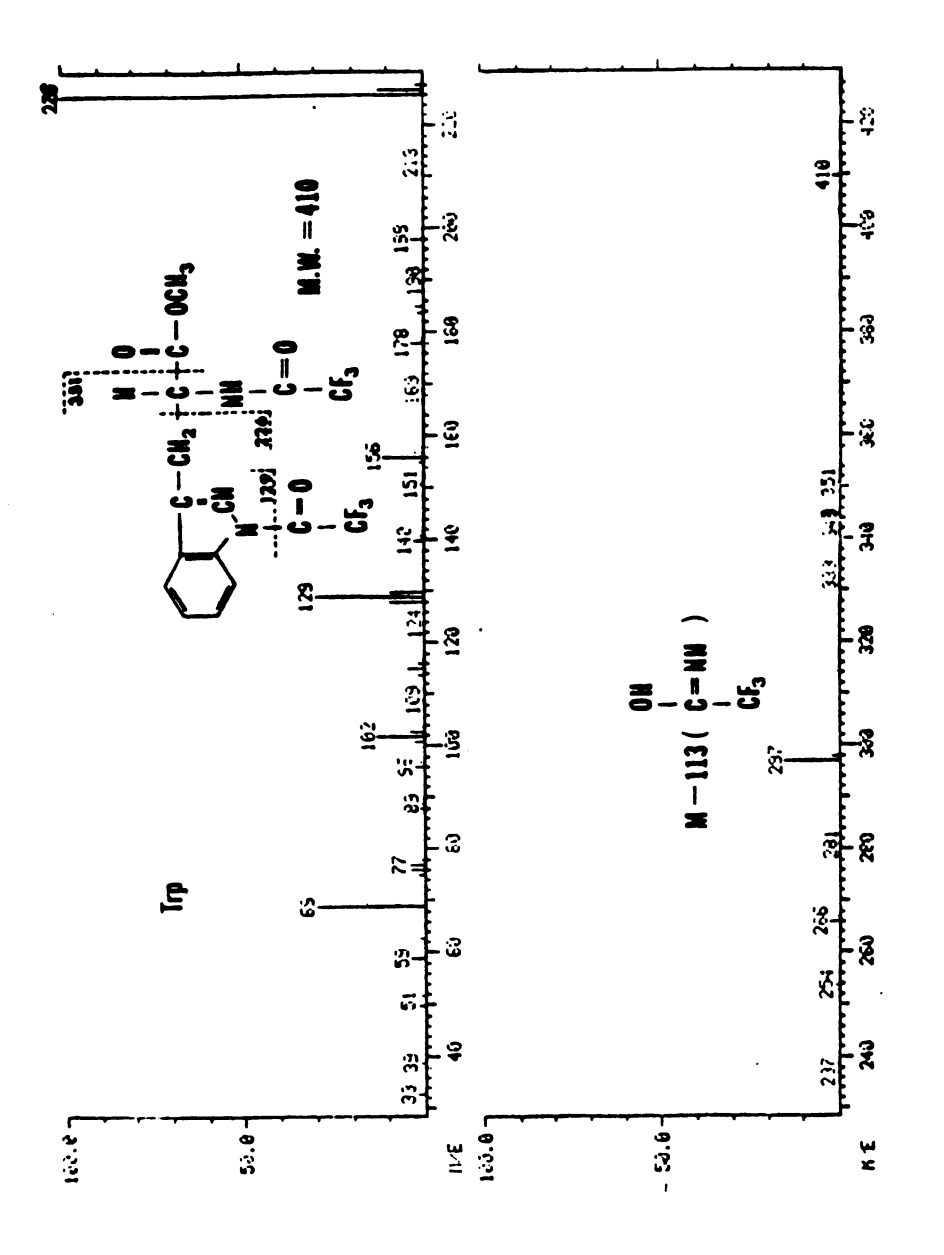


Fig. 4-8 The mass spectrum of derivatized tryptophan.

were prepared and photolyzed in the presence of NABA followed by the separation and hydrolysis of gramicidin. After transforming the hydrolysate into volatile species, GC-MS analysis was carried out.

The gas chromatograms for control and irradiated gramicidin, using mass spectrometer as detector, are shown in Figure 4-6 and 4-7, respectively. The compounds identified are listed in Table 4-1. A typical mass spectrum of an identified GC eluent is shown in Figure 4-8, which corresponds to the gragmentation pattern of derivatized tryptophan. It is of interest to note that the elution order of the compounds follow that of molecular weight. However, glycine was not separated from alanine partly because of their light molecular weights and partly because of their similar structures.

As is evident from GC-MS profile, the majority of high mass GC effluents are not identified. The reasons are two-fold.

- 1. Most of the mass spectra from the high mass fractions lack high mass peaks.
- 2. For eluents of similar retention time, similar mass fragmentation patterns were observed.

The situation is further complicated by the fact that although the retention time of each peak is very reproducible, the number of peaks after tryptophan is not always a constant.

To alleviate the first problem, chemical ionization

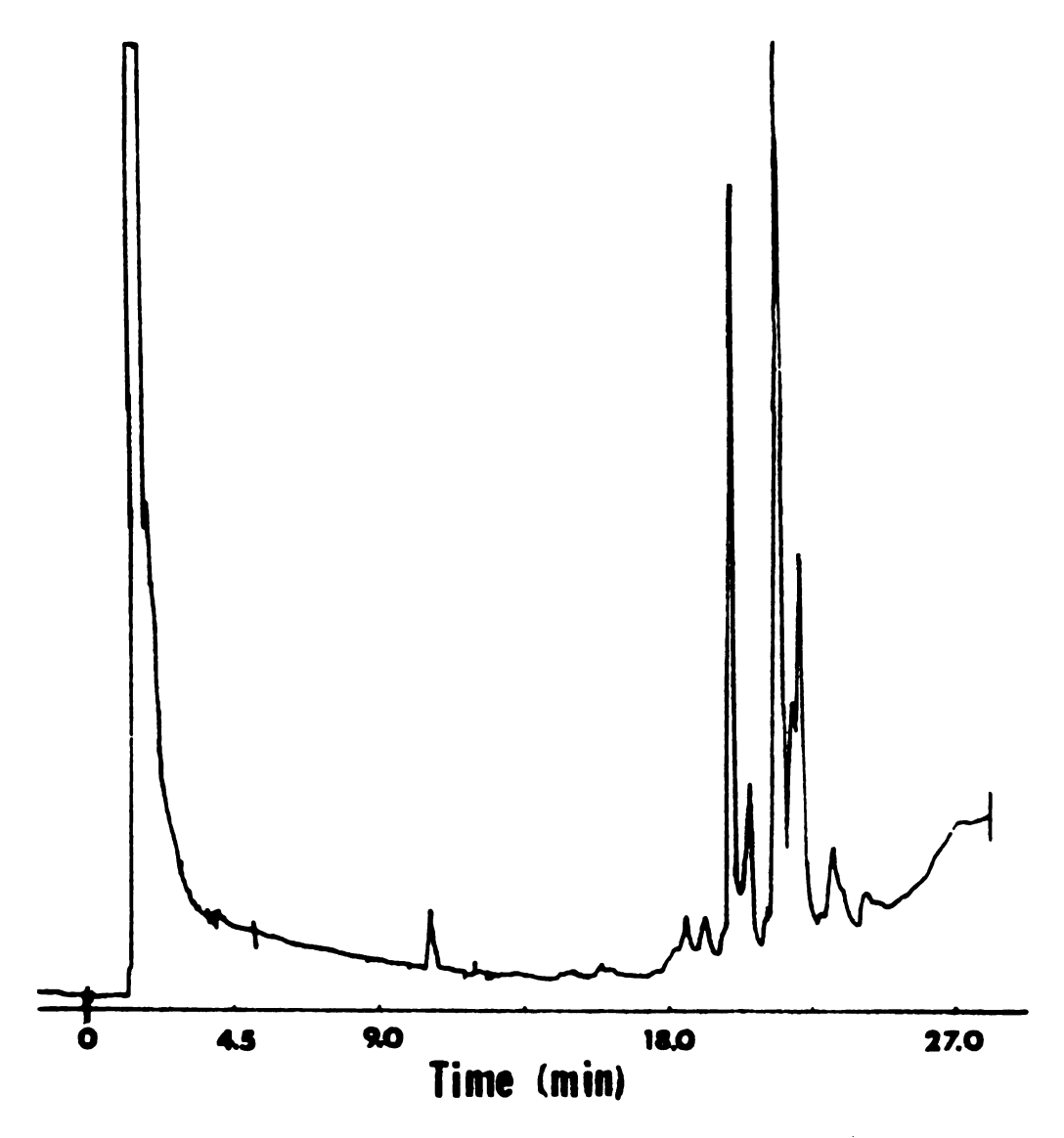


Fig. 4-9 GC trace of the derivatives of tryptophane which has been treated with trifluoro acetic acid-const. distilled HCl (1:1 by volume) at 110 C for 1.5 hours. Condition: column: 3% SE-30, temperature: 80-290°C at 8°C/min., detector: FID.

mass spectrometry was employed to elimenate the excessive fragmentation caused by energetic electron impact.

However, probably due to source fouling, the mass spectrometer consistently lost its sensitivity minutes after sample injection. As a result, no useful information was acquired.

Figure 4-9 shows the GC trace of the acid-treated tryptophan derivative which displays multiple peaks. The similarity of Figure 4-9 to the region between trp and trp-leu peaks in Figures 4-4 and 4-5 indicates that eluents right after trp in GC-MS chromatogram are the decomposed products of tryptophan during acid hydrolysis.

Although the determination of the molecular structure of GC effluents is of importance, the essence of the study, however, is to identify those eluents that are unique to either irradiated or control gramicidin.

Unfortunately, the comparison of the GC-MS profile of irradiated gramicidin to that of control gramicidin does not yield any significant difference. To reconcile this negative result with that obtained from BLM photolysis experiments, we postulate that the photolabeled constituents of gramicidin are such that they could not survive the harsh acid hydrolysis.

There is evidence to support our hypothesis. In 1978, in an attempt to photolabel membrane interior with lipophilic phenylazides, Knowles and Bayley discovered

that photogenerated phenylnitrene exhibits certain electrophilicity and prefer electron-rich reaction sites to C-H bonds (67). The current consensus on gramicidin channels is that the amino alcohol at N terminus is situated at the membrane surface. These two thoughts lead us to the belief that upon photolysis the nitrene intermediate reacts with the hydroxyl oxygen at the channel opening, forming a rather labile O-N bond (Scheme 4-1) which later breaks down during acid hydrolysis.

Scheme 4-1

To test the hypothesis, we could either adopt a milder protein degradation process to retain the labile bonds or find a carbene analog that would result in an acid-resistant etherlike linkage (C-0) to the antibiotic. Again, difficulties were encountered.

Because of its alternating D and L amino acid configuration, gramicidin is not subject to enzymatic cleavage by any presently known proteinase. A search for

chemical reagents that would break peptide bonds in less harsh conditions also failed.

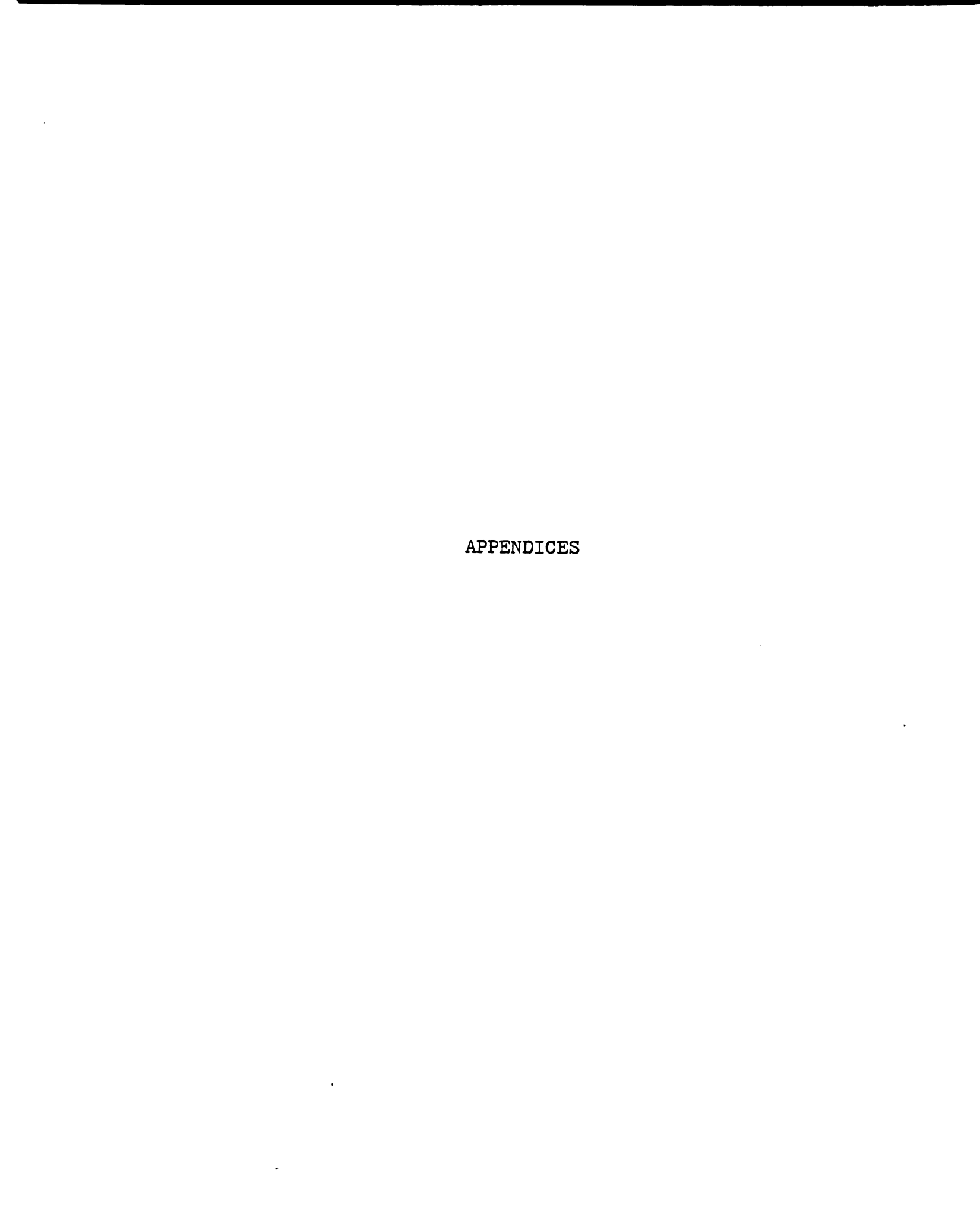
In 1975, Smith and Knowles (68) reported the synthesis of p-(carboxymethoxyphenyl)-3H-diazirine. Upon photolysis, diasirine generates a carbene intermediate which

diazirine

readily undergoes insertion into 0-H and C-H bonds and forms highly stable C-O and C-C linkages. Furthermore, diazirine is fairly stable in aqueous solutions at room temperature and has an absorption maxima at 362 nm. However, the reported yield (1%) of diazirine synthesis is too low to be of any practical value.

At this point, with reluctance, we abandoned the attempted chemical proof of the gramicidin orientation. The attempt was, however, not without value. We have demonstrated that the photolysis of NABA exerts a remarkable effect on ion transport mediated by gramicidin. It appears that the reduction in membrane conductance arises from steric hindrance imposed by photolabels at the channel opening. The failure to identify the photoproducts is attributed to the acid-labile linkage between gramicidin

and photolabel. It is believed that as the availability of various photolabeling reagents expands, the photolabeling technique will become an indispensable tool in biochemical studies.



APPENDIX A PERIPHERAL SCHEMATIC DIAGRAMS

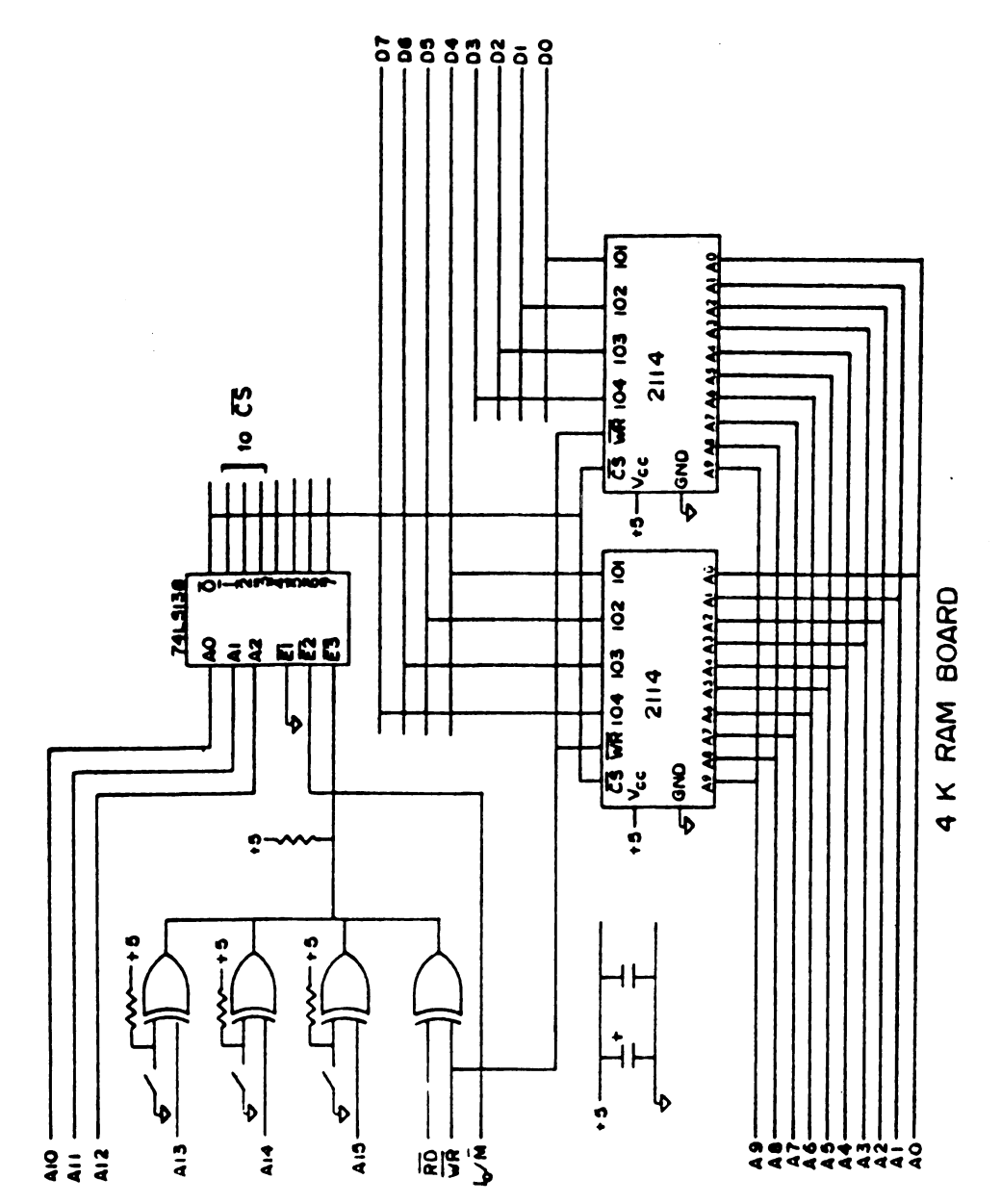


Figure A-1. 4K RAM board schematic diagram.

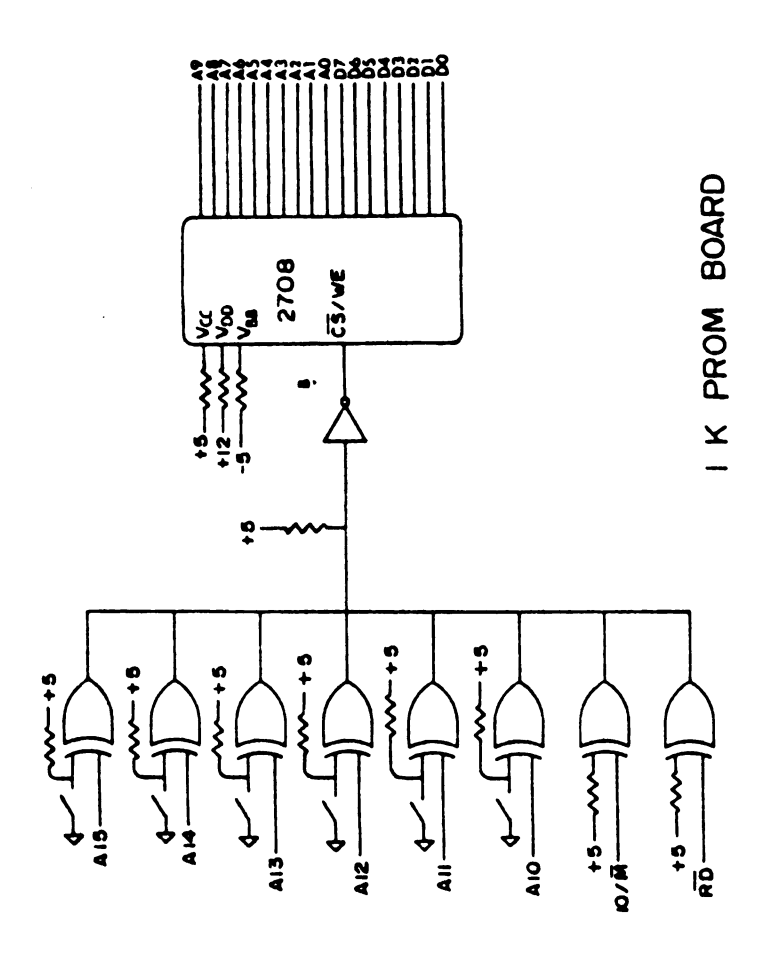


Figure A-2. 1K PROM board schematic diagram.

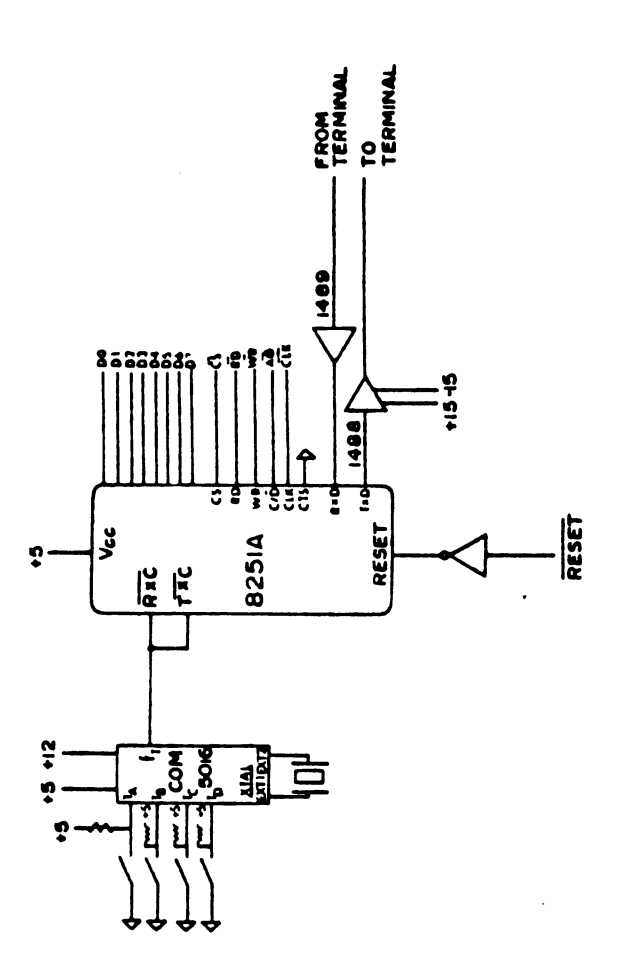


Figure A-3. USART board schematic diagram.

APPENDIX B PROGRAM LISTINGS

```
C
        MEMBRN. FNT; 2
C
        MANAGER PROGRAM FOR MEMBRANE ION TRANSPORT STUDY
        COMMON/VECTOR/XSCALE, YSCALE, IDEV
        COMMON/VOLAY/ XOFF, YOFF, XLAST, YLAST
        COMMON/VABS/
                       IX, IY
        COMMON/OFILE/ LUNIT
C
C
        BYTE FILNAM(32), DAT(9), TIM(8)
        DIMENSION A(500), B(100), C(10)
C
        A=DATA
                  ARRAY, B=BASELINE ARRAY, C=LINEARITY
        CORRECTION COEFF.
        INTEGER POINTS (500), OPTION, AUTO
        LUNTI = 5
C
C
        ** DISPATCHER **
C
        IQUE=200
C
        IGUE=200 MEANS DATA COLLECTION ROUTINE
C
        SHOULD BE INITIALIZED.
        CALL COLECT(NPTS, IPUSH, POINTS, IQUE, ISROPT)
10
        WRITE(LUNTI, 200)
200
        FORMAT(1X, ' OPTION: COLLECTION DATA, AVERAGE
        1, LIST DATA, PLOT DATA'/' STORE DATA,
        2, BASELINE PLOT, EXIT'/'
        3, EXPONENTIAL FIT (/ '$?')
        READ(LUNTI, 210) OPTION
210
        FORMAT(A1)
        IF (OPTION, EQ. 1HC) GOTO 20
        IF (OPTION. EQ. 1HL) GOTO 40
        IF (OPTION, EQ. 1HB) GOTO 59
        IF (OPTION. EQ. 1HP) GOTO 60
        IF (OPTION. EQ. 1HS) GOTO 80
        IF (OPTION. EQ. 1HA) GOTO 100
        IF (OPTION. EQ. 1HF) GOTO 600
        IF (OPTION. NE. 1HE) GOTO 10
        STOP
C
C
        ** DATA COLLECTION SECTION **
C
20
        WRITE(LUNTI, 300)
300
        FORMAT( '$ENTER # OF DATA POINTS(DEFAULT=128); ')
        READ(LUNTI, 310) NPTS
310
        FORMAT(14)
         IF (NPTS. LE. O) NPTS=128
        WRITE(LUNTI, 320)
350
        FORMAT ('$AUTO DR MANUAL?')
        READ(LUNTI, 210) AUTO
         IPUSH=0
         IF (AUTO, EQ. 1HA) IPUSH=1
```

```
WRITE(LUNTI, 325)
325
         FORMAT(1X, ' SET UP FAST DATA POINTS, FAST DATA
         1, RATE AND SLOW DATA RATE ()
C
C
        COLLECTION RATE OPTIONS:
C
C
        BITS
                   FUNCTION
C
C
                   SET # FAST DATA POINTS COLLECTED
        0-6
C
                   AFTER TRIG., MAX. = 98. (PRE-TRIG.
C
                   RECORD = 98 - # SET)
C
C
        8-10
                   SET FAST DATA RATE
C
                   RATE = 10 \text{ MHZ}/(2** *SET)
C
C
                   SET SLOW DATA RATE (A/D CONVERT
         11-13
C
                   RATE), RATE = 39.0625 KHZ/(2**
                    #SET)
        READ(LUNTI, 326) JSROPT
326
        FORMAT (06)
         CALL COLECT(NPTS, IPUSH, POINTS, IQUE, JSROPT)
C
        GO GET DATA
        DO 30 I=1, NPTS
        A(I)=FLOAT(POINTS(I))
30
        CONTINUE
        COTO 10
C
C
         ** DATA LISTING SECTION **
C
40
        WRITE(LUNTI, 330)
330
        FORMAT('SENTER DESTINATION (LP, KB): ')
        READ(LUNTI, 210) AUTO
         IVAR=5
         IF (AUTO, EQ. 1HL) IVAR=6
50
        WRITE(IVAR, 340)(A(I), I=1, NPTS)
340
        FORMAT(5(4X, F7, 2))
        WRITE(IVAR, 350) IQUE
350
        FORMAT(' NOISE QUE = 1/4/2X/2X/1')
        GOTO 10
C
C
         ** DATA PLOTTING SECTION **
C
59
        LB=1
        KPTS=100
        GOTO 61
60
        LB=O
        KPTS=NPTS
```

```
C
C
         INITIALIZE PLOT
C
61
         RKPTS=KPTS
         IDEV=1
         CALL VECTOR(XS, YS, -3)
         XSCALE=RKPTS/XS
         YSCALE=2048. /YS
         CALL VECTOR (0. 1, 0. 1, 0)
C
C
         DRAW AXES
C
         CALL VECTOR(0, 0, 2048, , 1)
         CALL VECTOR (0. 0, 0, 0, 2)
         CALL VECTOR (RKPTS, 0, 0, 2)
C
C
         PLOT POINTS
C
         DO 70 I=1, KPTS
         X = I
         Y=A(I)
         IF(LB, EQ. 1) Y=B(I)
         CALL VECTOR(X, Y, 1)
         CALL VECTOR (X, Y, 2)
70
         CONTINUE
         CALL VECTOR (0. 0, 0, 0, 4)
         COTO 10
C
C
         ** DATA STORAGE SECTION **
C
80
         IF (BASAVG. NE. O) GOTO 81
         WRITE(LUNTI, 355)
355
         FORMAT(' NO BASELINE--NO ACTION TAKEN')
         COTO 10
81
         WRITE(LUNTI, 360)
360
         FORMAT ( '$ENTER FILNAME: ')
         READ(LUNTI, 370) FILNAM
370
         FORMAT (32A1)
         CALL DATE (DAT)
         CALL TIME(TIM)
82
         CALL ASSIGN(4, FILNAM, 32)
         WRITE(4,380)NPTS
380
         FORMAT('NU', 15)
C
         BASELINE SUBTRACTION (ALLIGNS NOISE QUE FIRST)
         K=IQUE
         J=JBQUE
         IOFF=MOD(NPTS, 100)
         DO 84 I=1, NPTS
         A(K)=A(K)-B(J)+BASVAG
         K=K+1
         J=J+1
```

```
IF (K. GT. NPTS) GOTO 85
83
         IF (J. GT. 100) J=J-100
84
        CONTINUE
         GOTO 87
85
        K=K-NPTS
         J=J+100-IDFF
        COTO 83
87
        NTERMS=6
C
        LINEARITY COEFFICIENTS: (FROM POLFIT)
        C(1) = -0.00035
        C(2)=0.96329
        C(3) = -0.01033
        C(4)=0.01107
        C(5)=-0.00271
        C(6)=0.00024
        DO 90 I=1, NPTS
        Y=0. 0
         TERM=1. 0
         YI = (5.0/2048) *A(I)
C
        LINEARITY CORRECTION
        DO 88 N=1, NTERMS
        Y=Y+C(N) *TERM
         TERM=TERM*YI
88
        CONTINUE
        WRITE(4,390)I, Y
90
        CONTINUE
390
        FORMAT ('RD', I15, F15, 5)
        BASVAE=BASVAG*5. 0/2048
        WRITE(4, 392)
392
        FORMAT ('ED')
        WRITE(4,395)BASVAE, IQUE
        WRITE(4,400)JSROPT
395
        FORMAT('BA', F10. 6/'QU', I4)
400
        FORMAT ( 'SR ', 06)
        WRITE(4, 405)FILNAM
405
        FORMAT('FI', 1X, 32A1)
        WRITE(4,410)DAT
        FORMAT ('DA', 1X, 9A1)
410
        WRITE(4,420)TIM
420
         FORMAT('TI', 1X, 8A1)
         CALL CLOSE(4)
         GOTO 10
```

```
C
C
        ** BASE LINE AVERAGING SECTION **
C
100
        WRITE(LUNTI, 500)
500
        FORMAT ( '$HOW MANY SCANS?: ')
105
        READ(LUNTI, 505) NSCANS
505
        FORMAT(16)
        IF (NSCANS. LE. O) NSCANS=10
        DO 110 I=1,100
        B(I)=0.0
110
        CONTINUE
        DO 180 J=1, NSCANS
        CALL COLECT(100, 1, POINTS, JBQUE, 98)
        K=JBQUE
        DO 120 I=1,100
        B(I)=B(I)+FLOAT(POINTS(K))
        IF (K. GT. 100) K=K-100
120
        CONTINUE
180
        CONTINUE
        BASAVG=0.0
        DO 185 I=1,100
        B(I)=B(I)/NSCANS
        BASAVG=BASAVG+B(I)
185
        CONTINUE
        BASVAG=BASAVG/100.0
        JBQUE=1
        GOTO 10
C
C
        ** EXPONENTIAL FIT SECTION **
C
600
        WRITE(5, 605)
605
        FORMAT('$ENTER FILENAME: '/'$?')
        READ(5,610)FILNAM
610
        FORMAT (32A1)
        WRITE(5,615)
615
        FORMAT('$ENTER INITIAL AND FINAL POINTS')
        READ(5, 620) J. K
620
        FORMAT(215)
        CALL EXPFIT(FILNAM, J, K)
        GOTO 10
        END
```

```
. TITLE COLECT. MAG
         . IDENT /VO. 04/
         . GLOBL COLECT
        . NLIST BEX. TTM
        . PSECT COLECT, RW, REL
R0=%0
R1=%1
R2=%2
E%=ES
R4=%4
R5=%5
SP=%6
PC=%7
POINTR:
                 . WORD O
NPTS:
                 . WORD O
IPUSH:
                 . WORD O
SROPT:
                 . WORD O
POL:
                 . WORD O
COLECT: MOV @2(R5), R3
         MOV R3, NPTS
       MOV @4(R5), IPUSH
        MOV 6(R5), R4
         MOV R4, POINTR
        CLR CMR
         CMP @10(R5), #100
         BLOS PASS2
        MOV #30, DATO
        MDV #4000, CMR
         CLR @10(R5)
        MOV #1000, CMR
        RTS PC
PASS2:
         CLR POL
        MOV @12(R5), RO
        MOV RO, SROPT
         DEC RO
         MOV RO, DATO
        MOV #400, CMR
        MOV #10, R1
        MOV SROPT, RO
        SWAB RO
        MOV RO, R2
         BIC #177770, RO
         ASH RO, R1
         ASH #75, R2
         BIC #177770, R2
        MOV #20, RO
         ASH R2, RO
```

ADD RO, R1

ADD #20, R1

1\$:

SOB R1.1\$

MOV #2000, CMR

TST IPUSH

BEQ CHECK

MOV #1000, CMR

CHECK:

BIT #100000, FLAG

BEQ CHECK

MOV DATI, (R4)+
MOV #2000, CMR
SOB R3, CHECK

CLR R2

MOV POINTR, R4

STORE:

INC R2

MOV (R4), R1

COM R1

CUE:

CMP R2, #100

BHI OVER

BIT #40000, R1

BEG OVER

MOV R2, @10(R5)

OVER:

BIT #4000, R1

BEG POS

MOV #1, POL

POS:

BIC #174000,R1

MOV R1, (R4)+ CMP R2, NPTS BLO STORE

RTS PC . END

```
TITLE: MEMB. MAC - PROGRAM TO PERFORM MEMBRANE
                     EXPERIMENTS AND SEND DATA TO
                     PDP-11 THROUGH A SERIAL PORT
      AUTHOR: H. Y. GUH
               DEPARTMENT OF CHEMISTRY
               MICHIGAN STATE UNIVERSITY
               EAST LANSING, MI 48824
       DATE: 30-JUL-80
ITO USE THE PROGRAM, DATA COLLECTION RATE IS DEPOSITED
AT 2000H AND CHARGING VOLTAGE AT 2001H.
107==>15MHZ
; 06==>10MHZ
: 05==> 5MHZ
: 04==> 2MHZ
; 03==> 1MHZ
              REGISTER FUNCTION
; ADDRESS
; 8000/100000
             RATE DATA RATE
i 8040/100100
              CMD
                        BITO===>1: CLEAR FLIP FLOPS
                                  AND COUNTERS.
                         BIT1===>1: START EXP.
;8080/100200 VOLT
;80C0/100300 SWITCH
                         CHARGING VOLT. (0-10V)
                        BITO===>1: OPEN FEEDBACK SW
                         BIT2==>1: CLOSE CHARG. SW
#F000/170000 UDATA USART==>DATA
#F001/170001 UCMD USART==>CMD F
#C000/140000 DATADD FAST RAM(1K)
                       USART==>DATA REG.
                       USART==>CMD REG.
; E000/160000
                        RAM(4K)
       RATE = 100000
       CMD = 100100
       VOLT = 100200
       SWITCH = 100300
       UDATA = 170000
       UCMD = 170001
       DATADD = 140000
       . = 160000
                        STARTING ADD. OF 4K RAM
       INITIALIZATION OF SP AND USART
   SP, 20302
A, 116
UCMD
                              ; INITIALIZE STACK POINTER
 START: LXI
       MVI
                              ; SET UP USART - ASYN MODE
       OCMD
A, 5
STA
                             ; SET UP USART - ENABLE TX
              UCMD
                              ; AND RX
```

;						
•	INITIALIZATION OF REGISTERS					
;	XRA					
		A CMD	CLEAR CMD			
			AND UOLT			
			AND VOLT			
			AND SWITCH			
		A, 01 CMD	CLEAR COUNTERS AND FLIP			
			;FLOPS ;ALLOW COMPLETE ACTION			
		B, 05	ALLOW COMPLETE ACTION			
1	CALL					
, ,	SET UP EXPERIMENT					
•	LXI	H, 20000	GET RATE FROM 2000(H)			
	MOV					
	STA	RATE	·			
	LXI	H. 20001	GET CHARGING VOLTAGE FROM			
	MOV		; 2001(H)			
	STA	VOLT				
	MVI	A, 04	CHARGE UP CAPCITOR			
	STA	SWITCH				
	MVI	B, 10	DELAY SOMEWHAT TO ALLOW			
	CALL	DELA	COMPLETE CHARGING			
	MVI	A, 01	; OPEN CHARGING AND FEEDBACK			
	STA	SWITCH	; SWITCH			
		B. 5	; ALLOW COMPLETE ACTION			
		DELA				
•	START EXPERIMENT AND DATA COLLECTION					
, ======	MVI		; DUMP CHARGE AND COLLECT			
		CMD	; DATA			
; ======	*******	**********				
;;	TRANSFER DATA TO 11					
;	SET UP DATA BYTE COUNTER					
	MVI		GET TIME DELAY			
			SET BYTE COUNTER: 1K BYTES			
		E, 0				
	CALL		CHECK PROMPT FROM 11			
;;	TRANSFER DATA BLOCK					
;		U BATARR	. CET UD BATA BLOCK ASS			
MOBYT.			SET UP DATA BLOCK ADD.			
MUBTI:	MOV		FETCH A DATA BYTE			
	CALL		; AND SEND IT OFF TO 11			
	CALL	UCLA	DELAY FOR A WHILE			

```
INX
                             JUPDATE ADD. POINTER
            Н
      DCX
                             JUPDATE BYTE COUNTER
            D
      MOV
             A, D
                             ; ALL THE BYTES SENT ?
      ORA
             E
      JNZ
            MOBYT
                            ; IF NO, SEND ANOTHER BYTE
      RST
                            SOFT RESET
      SDCO - SEND OUT A BYTE AND CHECK ECHO
SDCO:
              UDATA
                             ; SEND BYTE OUT
      STA
              UCMD
RD1:
      LDA
                            ; CHECK ECHO
      ANI
             2
                            RXRDY FLAG SET?
             RD1
      JZ
                            ; NO; CHECK AGAIN
              UDATA
                            YES; RESET FLAG
      LDA
      RET
      DELA - KEEP CPU IN LOOP FOR SOME TIME
      A, B, C, ARE USED
DELA:
      MOV
            A, B
              C, B
DELAO: MOY
DELA1: DCR
            С
      JNZ
          DELA1
      DCR
            A
      JNZ
            DELAO
      RET
```

. END

```
LOAD. MAC - READ MESSAGES FROM PDP-11 AND STORE IT
                INTO MICRO'S MEMORY WHICH STARTS AT E000(H)
                /160000(D).
               LOAD, OBJ STARTS AT A000/120000(EPROM).
       UCMD=170001
       UDATA=170000
       . =120000
       LXI
               SP, 20302
                         ; INITIALIZE STACK POINTER
       MVI
               A. 116
                          ; DEFINE USART MODE:
               UCMD
                          ; ASYN MODE
       STA
       MVI
               A, 5
                          ; ENABLE TX AND RX
       STA
               UCMD
                         ; SET UP ADD. POINTER OF
       LXI
               H, 160000
RDUS:
       LDA
               UCMD
                          ; MESSAGE BLOCK, AND READ
       ANI
               2
                          ; USART STATUS, AND MASK OUT
               RDUS
                          ; RXRDY FLAG, AND IF RX NOT
       JZ
                          ; READY, BACK TO RDUS, AND
       LDA
               UDATA
       VOM
                          FREAD THE BYTE AND STORE IT
               M. A
       STA
               UDATA
                          ; ECHO THE BYTE
       INX
               Н
                          ; UPDATE ADD. POINTER
       JMP
               RDUS
                          GET NEXT BYTE
```

. END

```
DOWNLD. FTN - READ A BLOCK OF DATA AND SEND IT
                TO A REMOTE TERMINAL
        BYTE IDATA(512), F(32), NAM(8), TT5(8)
        INTEGER*2 NBYTE, ICNT, IERCN, ITABLE (96)
        DATA LUNIN/1/, LUNTIN/2/, NAM/8*' '/
        DATA TT5/2*'T', '5', ': ', 4*' '/
        GET FILENAME AND SET UP I/O PORT; DEFAULT PORT
C
        - TT5:
        WRITE(5, 150)
 5
        FORMAT ( ' NAME OF THE FILE THAT WILL BE COPIED
 150
        1, INTO THE ARRAY ')
        READ(5,110) F
 110
        FORMAT(32A1)
        WRITE(5, 130)
 130
        FORMAT('$1/0 PORT (DEFAULT - TT5: ) : ')
        READ(5, 135) NAM
 135
        FORMAT(8A1)
        IF (NAM(1), NE. 32) GO TO 140
        DO 200 I=1.8
200
        NAM(I)=TT5(I)
 140
        CALL ASSIGN(2, NAM)
        OPEN THE FILE - READ MODE
        CALL UNFORM(O, IERR, ITABLE, F, O, 3, LUNIN)
        IF (IERR. NE. 0) GO TO 9001
        NERR=0
        MBYTE =0
        NRD=0
 120
        NBYTE = 512
C
        READ ONE RECORD OFF THE FILE INTO ARRAY 'IDATA'
        RETURN THE LENGTH OF THE RECORD IN NBYTE
        CALL UNFORM(1, IERR, ITABLE, IDATA, NBYTE)
        IF (IERR. EQ. -1) GO TO 1100
        IF (IERR. GT. 0) GO TO 9000
        IF (NBYTE, NE. 2) GD TD 60
        GO TO 120
        WRITE(5,8500)
 1100
 8500
        FORMAT(' END OF FILE')
        GO TO 8503
 9000
        WRITE(5,8501)
        FORMAT(' ERROR IN READ')
 8501
        GU TO 8503
```

C	
C	SEND DATA TO THE REMOTE TERMINAL
70 C	CALL SEND(IDATA, NBYTE, IERCN, LUNTIN) NRD=NRD+1 WRITE(5,70) NRD FORMAT(' NUMBER OF RECORDS READ : ', I3) NERR=NERR+IERCN GO TO 120
C C C	MORE FILE TO OPEN? IF YES, GO BACK AND DO IT ALL OVER AGAIN
_	WRITE(5,300) NERR, MBYTE FORMAT(' TOTAL NUMBER OF TRANSMISSION ERRORS 1, = ',16/'TOTAL NUMBERS OF BYTES = ',16) WRITE(5,90)
90	FORMAT('\$FILE IS CLOSED; MORE FILE TO OPEN 1,? Y OR N ') READ(5,95) B
95	FORMAT(1A1) IF (B.EG.'Y') GO TO 5 CALL CLOSE(2) STOP END
8502 8503	WRITE(5,8502) FORMAT(' ERROR OPENING FILE') CALL UNFORM(2,IERR,ITABLE) GO TO 15
C	ADJUST BYTE COUNT AND DATA ARRAY
60	NBYTE=NBYTE-2 MBYTE=MBYTE+NBYTE DO 50 I=1,NBYTE IDATA(I) = IDATA(I+2)

0	SUBROUTINE SEND (IDATA, NBYTE, IERCT, LUNTIN)
C======= C C C	SEND. FTN - SEND INFORMATION TO A REMOTE TERMINAL
C	IDATA - ARRAY OF DATA TO BE SENT NBYTE - NUMBER OF DATA BYTES IERCT - NUMBER OF TRANSMISSION ERRORS
C	INTEGER*2 ISBTN(2), IPARTN(6), IERCT BYTE LBUFF(2), IDATA(NBYTE), NBUFF, ISERR EQUIVALENCE (ISERR, ISBTN(1)) DATA RRRR, WWWW/'TO11', 'TO85'/ DATA IEFNTN/10/ DATA IDATT, IDDET, IORPR/01400, 02000, 04432/
C	ATTACH I/O PORT; SET UP ERROR COUNTER
C	CALL WTGIO(IDATT, LUNTIN, IEFNTN, , ISBTN, IPARTN, 1, IDERTN) IERCT=0
_	SEND OUT DATA AND GET ECHO
8500 10 C	IF (NBUFF.EQ.LBUFF(1)) GO TO 10 IERCT=IERCT+1 CONTINUE
C	DETACH AND CLOSE I/O PORT
·	CALL WTGIO(IODET, LUNTIN, IEFNTN, ISBTN, IPARTN, 1, IDERTN) RETURN END

```
TITLE: DATAIN. FTN - PROGRAM TO FETCH DATA
C
               FROM A REMOTE INTELLIGENT TERMINAL
C
               THROUGH USE OF 'LISTEN'
       AUTHOR: H. Y. GUH
C
               DEPARTMENT OF CHEMISTRY
C
               MICHIGAN STATE UNIVERSITY
               EAST LANSING, MI 48824
C
C
       DATE: 31-JUL-80
        REAL BUFF (1024), POINT (1024), PHYS (8)
       INTEGER*2 NBYTE, IDATA(1024)
       BYTE ITIME(8), IDATE(10), F(32), NAM(8), TT5(8)
       DATA IDATE(10)/' '/, NAM/8*' '/
       DATA TT5/2*'T', '5', ': ', 4*' '/
       DATA IDATT, IDDET, IDRAL
        /01400,02000,01010/
       DATA LUNTIN/1/
       SET UP I/O PORT; DEFAULT PORT - TT5:
       WRITE(5, 130)
 130
       FORMAT('$1/0 PORT(DEFAULT - TT5:) : ')
       READ(5, 135) NAM
 135
       FORMAT (8A1)
       IF (NAM(1). NE. 32) GO TO 140
       DO 200 I=1,8
 200
       NAM(I)=TT5(I)
 140
       CALL ASSIGN(1, NAM)
 70
       WRITE(5, 100)
 100
       FORMAT('$COLLECT, PLOT, STORE, EXIT,
     1 BASELINE: ')
       READ(5, 110) A
 110
       FORMAT(A1)
       IF (A. EG. 'B') GD TD 500
       IF (A. EQ. 'C') GD TD 80
       IF (A. EQ. 'P') GO TO 120
       IF (A. EQ. 'S') GO TO 170
       IF (A. EQ. 'E') GO TO 450
       GO TO 70
       FETCH DATA
       CALL LISTEN(LUNTIN, IDATA, NBYTE, IERR)
 80
       GO TO 70
```

```
BASELINE AVERAGING
500
       CALL LISTEN(LUNTIN, IDATA, NBYTE, IERR)
       SUM=0
       DO 505 I=1, NBYTE
505
       SUM=FLOAT(IDATA(I))+SUM
       BASAVE=SUM/FLOAT(NBYTE)
       WRITE(5,510) BASAVE
       FORMAT ('BASELINE AVERAGE = ', F10. 6)
510
       GO TO 70
       PLOT DATA ARRAY
120
       DO 300 I=1, NBYTE
       BUFF(I)=FLOAT(IDATA(I))
300
       POINT(I)=FLOAT(I)
       PHYS(1)=0.0
       PHYS(2)=8.0
       0.0=(E) 2YH9
       PHYS(4)=6.0
       CALL ASSIGN(3, 'TTO: ')
       IDDEV=1
       WRITE(5,330) NBYTE
330
       FORMAT('$NUMBER OF POINTS: MAX. ', 14, ' ')
       READ(5,340) NPNT
340
       FORMAT(16)
       IMODE=1
       PHYS(5)=0. 0
       PHYS(6)=FLOAT(NPNT)
       PHYS(7)=0.0
       PHYS(8) = 256.0
       CALL PLOT (POINT, BUFF, NPNT, PHYS, IDDEV, IMODE)
       WRITE(5,370)
370
       FORMAT('$PLOT DATA ON LP: ? N OR Y ')
       READ(5,380) A
380
       FORMAT(A1)
       IF (A. NE. 'Y') GO TO 70
       IDDEV=3
       CALL PLOT (POINT, BUFF, NPNT, PHYS, IDDEV, IMODE)
       GD TD 70
```

```
STORE DATA IN ENKE FORMAT
170
       WRITE(5, 150)
150
       FORMAT('$FILENAME: ')
       READ(5, 160) F
160
       FORMAT(32A1)
       F(32)=0
       OPEN (UNIT=2, NAME=F, TYPE='NEW')
       CALL TIME (ITIME)
       CALL DATE (IDATE)
       WRITE (2,8501) IDATE, ITIME
8501
       FORMAT ('; ', 10A1, 8A1)
       WRITE(5, 420)
420
       FORMAT('$DATA COLLECTION RATE AND CHARGING
       VOLTAGE ', 14)
    1
       READ(5,430) IRATE, IVOLT
430
       FORMAT(214)
       WRITE(2,440) IRATE, IVOLT
440
       FORMAT('; DATA RATE(MHZ) ', I4/';
    1
       CHARGING VOLTAGE (, 14)
       DO 40 I=1, NBYTE
       BUFF(I)=FLOAT(IDATA(I))
40
       WRITE(2,50) FLOAT(I), BUFF(I)
50
       FORMAT ('RD', 2E15. 6)
       WRITE(2,60)
60
       FORMAT ('ED')
       WRITE(2,55) BASAVE
55
       FORMAT ('BA', F10. 6)
       CLOSE (UNIT=2)
       GO TO 70
450
       CALL CLOSE (1)
       STOP
       END
```

	SUBROUT 1	NE LISTEN (LUNTN, IDATA, MBYTE, IERR)			
_					
C					
C	TITLE:	LISTEN. FTN - SUBRUTINE TO INPUT AN			
C		ARRAY OF BYTES FROM A REMOTE			
C		INTELLIGENT TERMINAL			
C					
C	AUTHOR:	T. V. ATKINSON			
C		H. Y. GUH			
C		DEPARTMENT OF CHEMISTRY			
C		MICHIGAN STATE UNIVERSITY			
C		EAST LANSING, MI 48824			
C					
C	DATE:	25-JUL-80			
C					
C					
C C	LOCTON	HALL LINES MICT DE ATTACUES BEEGGE			
C		LOGICAL UNIT LUNTH MUST BE ATTACHED BEFORE			
C	ENIERING	ENTERING			
C					
C					
Č	ARGUMENT	ritet			
Č	HROUNCIA				
č	LUNTN	LUN FOR PORT FOR REMOTE			
Č	F014114	DATA INPUT			
C		DATA INFOT			
Č	IDATA	; INTERGER BUFFER TO			
Č		RECEIVE DATA			
Č		WEGETAE BHILL			
Č	MBYTE	NUMBER OF BYTES OF DATA			
Č		TO BE RECEIVED			
C	IERR	; ERROR FLAG (=0 FOR NO			
C		ERROE)			
Ċ					
C====					
	INTEGER	*2 IPARRX(6), ISBRX(2), IDATA(1024)			
	INTEGER	*2 NBYTE, KDATA(1024)			
		JFF(1024), ISERX, ICSOT, IBUFF(2048)			
	EQUIVAL	ENCE (ISERX, ISBRX(1)), (LBUFF(1), NBYTE)			
	EGUIVALE	ENCE (IBUFF(1), KDATA(1))			
	DATA ICS	SOT/'#'/, IEFNRX/10/			
	DATA IO	ATT, IODET, IORAL, IOWAL, IORPR			
	1 /01400	02000, 01010, 00410, 04410/			
C					
С	GET NUMI	BER OF BYTES			
C					
		GIO(IOATT, LUNTN, IEFNRX,, ISBRX, IPARRX			
	1,, IDER				
	WRITE(5	, 200)			

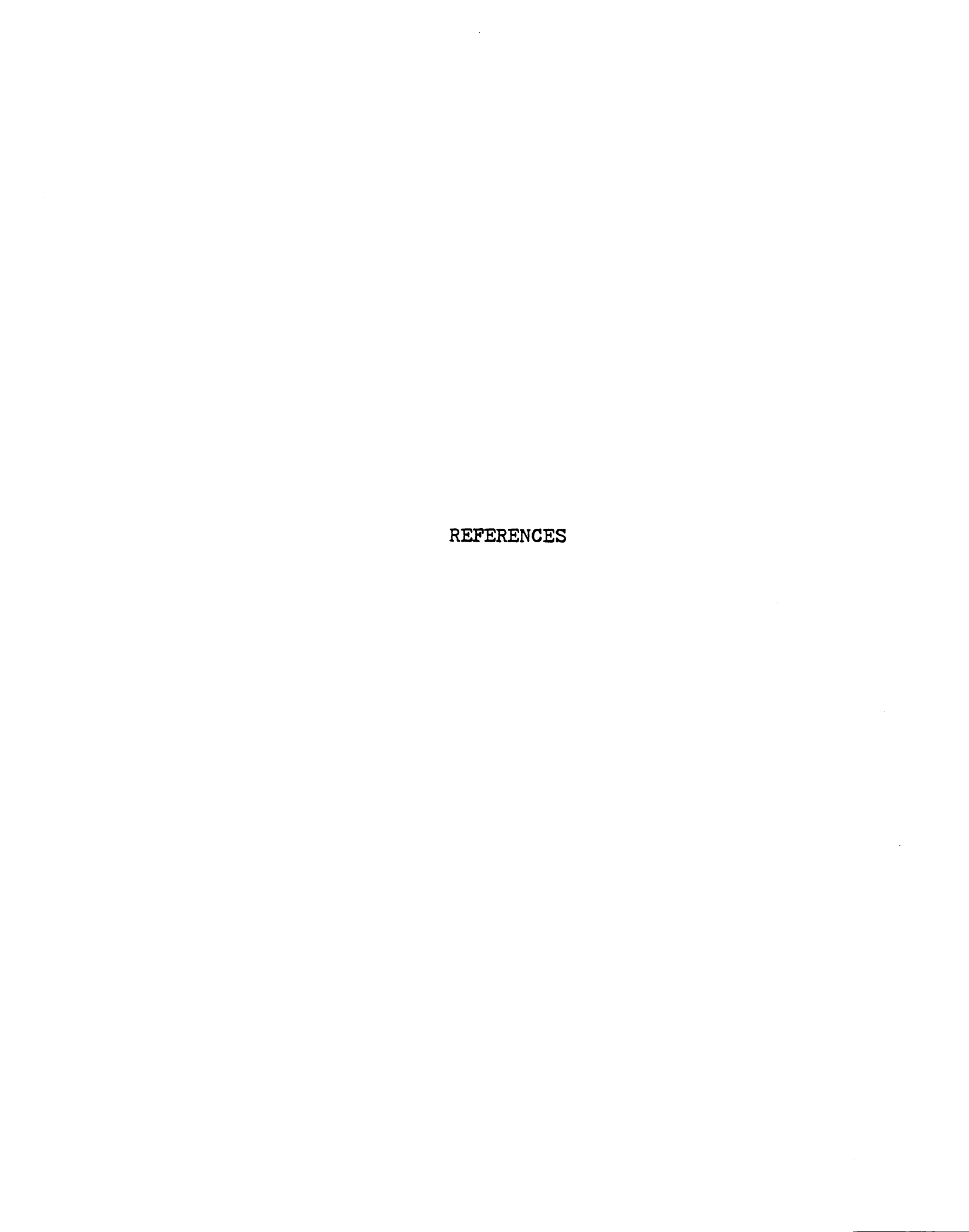
```
200
        FORMAT(' WTGIO ATTACHED')
        CALL GETADR(IPARRX(1), LBUFF(1))
        WRITE(5, 220)
 220
        FORMAT('$NUMBER OF BYTE -- ')
        READ(5,230) MBYTE
 230
        FORMAT(14)
C--
        GET BUFFER OF CHARACTE
        CALL GETADR(IPARRX, ICSOT)
        IPARRX(5)=1
         IPARRX(2)=MBYTE
        WRITE(5, 210)
        FORMAT(' GOING TO CALL WTGIO-RPR')
 210
        CALL GIO(IORPR, LUNTN, IEFNRX, , ISBRX, IPARRX
         1,, IDERRX)
         IF (ISERX, NE. 1. DR. IDERRX, NE. 1) GO TO 9000
        WRITE(5, 140)
        FORMAT( ' WAITING TO KILL: ')
 140
        READ (5,9878) III
 9878
        FORMAT (18)
        CALL GIO("12, LUNTN, IEFNRX, , ISBRX, IPARRX
         1,, IDERRX)
         WRITE (5,9868) ISBRX
         FORMAT (' ISBRX: ',208)
 9868
C
         CONSTRUCT DATA ARRAY - CONVERT ONE-BYTE
C
         DATUM INTO TWO BYTE INTEGER
C-
         WRITE(5,130)
         FORMAT(' DATA ARE IN')
 130
         DO 110 I=1, MBYTE
         J=2+I
         K=J-1
         IBUFF(K)=LBUFF(I)
         IBUFF(J)=0
         IDATA(I)=KDATA(I)
 110
         CONTINUE
         WRITE(5,120) (IDATA(I), I=1, MBYTE)
 120
         FORMAT(' IDATA=',5(1X, I4))
         GO TO 9999
C
         END OF TRANSFER
 9000
         IERR=1
         WRITE(5,170)
 170
         FORMAT(' ERROR FROM WTGIO')
 9999
         CALL WTGIO (IDDET, LUNTN, IEFNRX,, ISBRX, IPARRX
         1,, IDERRX)
         RETURN
         END
```

```
C
        EXPFIT. FTN
        PROGRAM TO LINEARIZE DECAYING EXPONENTIAL DATA
C
        AND CALL THE LINEAR LEAST SQUARES SUBROUTINE
C
C
        AUTHOR: H. Y. GUH
C
        DATE:
                 AUG-BO
C
C
        READS A STANDARD ENKE FILE
C
        RETURNS THE SLOPE, INTERCEPT, AND THEIR STD. DEV.
C
        CREATES A FILE REPRESENTING THE FIT TO EXP(-X)
C
C
C
        J : INITIAL POINT
C
        K : FINAL POINT
C
C
        DIMENSION X(1024), IBAD(50)
        BYTE FILNAM(32), DAT(9), TIM(8), FILE(32)
        WRITE(5,605)
 605
        FORMAT('$ENTER FILENAME: ')
        READ(5,610)FILNAM
 610
        FORMAT (32A1)
        WRITE(5, 615)
        FORMAT('$ENTER INITIAL FINAL POINTS: ')
 615
        READ(5, 620) J, K
 620
        FORMAT(215)
        CALL DSTRIP(FILNAM, X, NPTS, ICUE, ESROPT, BASE, DAT, TIM)
C
        LOCATE NOISE IN DATA FILE AND PLACE THE LOCATIONS
C
        IN IBAD
        N=1
        DO 300 I=J+2,K
        DEL=X(I-1)-X(I)
        DELTA=(ABS(DEL))/X(I-1)
        IF (DELTA, LT. 0, 15) GO TO 300
        X(I)=2*X(I-1)-X(I-2)
        IBAD(N)=I
        N=N+1
 300
        CONTINUE
```

```
C
        FIT EXPONENTIAL DATA
        CALL TLLSQ(J, Y, XDEV, YDEV, 1)
        N=1
        DO 20 I=J, K
        IF (I.EG. IBAD(N)) GOTO 25
        Y=ALDG(X(I)-BASE)
        Z=FLOAT(I-J)
        YDEV=3. 2/(350*X(I))
        CALL TLLSQ(Z, Y, XDEV, YDEV, 2)
        60 TO 20
25
        N=N+1
20
        CONTINUE
        CALL TLLSQ(Z, Y, XDEV, YDEV, 3)
        WRITE(5, 104) Z, Y, XDEV, YDEV
104
        FORMAT(' SLOPE =', F10. 7,' INTERCEPT =', F10. 7,
        1, 'SDEV =',F10.7,' IDEV=',F10.7)
        WRITE(5, 200)
        FORMAT(1X//// STORE EXPFIT DATA? - TYPE Y OR N')
200
        READ(5, 205) IOPT
205
        FORMAT(A1)
         IF (IOPT. EQ. 1HY) GOTO 210
        QOTO 110
210
        WRITE(5, 215)
215
        FORMAT(1X//' ENTER DEV AND FILENAME'/' ')
        READ(5, 220) FILE
220
        FORMAT (32A1)
        CALL ASSIGN(4, FILE, 32)
        A=EXP(Y)
        DO 30 I=J, K
        V=A*EXP(Z*(I-J))+BASE
        WRITE(4,105)FLOAT(1), V
105
        FORMAT ('RD', 2F15.7)
30
        CONTINUE
        WRITE(4, 106)Z, Y, XDEV, YDEV
106
        FORMAT('ED'/'; ', 4F10. 7)
        WRITE(4,107)FILNAM
107
        FORMAT (32A1)
        CALL CLOSE (4)
110
        STOP
        END
```

```
SUBROUTINE DSTRIP (FILNAM, D, NPTS, ICUE, ISROPT
      1 , BASE, DAT, TIM)
         BYTE LINE(80), FILNAM(32), DAT(9), TIM(8)
        DIMENSION D(1024)
        EQUIVALENCE (JFLAG, LINE(1))
C
C
        FLAGS:
                 NU =
                         DATA POINTS
C
                  RD = REAL DATA, FIELD WIDTH = 15
C
                  QU = NOISE INDEX PULSE
C
                  SR = SWITCH REGISTER OPTIONS
C
                 DA = DATE
C
                 TI = TIME
C
                 ED = END OF DATA BLOCK
C
C
        K=0
        CALL ASSIGN(4, FILNAM, 32)
10
        READ(4, 110, END=200) LINE
         IF (JFLAG. EQ. 2HRD) GOTO 30
         IF (JFLAG. EQ. 2HNU) GOTO 20
         IF (JFLAG, EQ. 2HQU) GOTO 40
         IF (JFLAG. EQ. 2HDA) GOTO 50
         IF (JFLAG. EQ. 2HTI) GOTO 60
         IF (JFLAG. EQ. 2HSR) GOTO 70
         IF (JFLAG. EQ. 2HBA) GOTO 80
        COTO 10
200
        CALL CLOSE(4)
        RETURN
110
        FORMAT (80A1)
20
        DECODE (7, 120, LINE) NPTS
120
        FORMAT(2X, I5)
        COTO 10
30
         K=K+1
         DECODE (32, 130, LINE) D(K)
        FORMAT (2X, 15X, F15, 5)
130
         GOTO 10
40
        DECODE (6, 140, LINE) ICUE
140
         FORMAT(2X, 14)
         Q0TO 10
50
        DECODE(12, 150, LINE) DAT
150
        FORMAT(3X, 9A1)
         COTO 10
60
        DECODE(11, 160, LINE) TIM
160
        FORMAT(3X,8A1)
         COTO 10
70
         DECODE(8, 170, LINE) ISROPT
170
         FORMAT(2X, 06)
         GOTO 10
80
         DECODE(12, 180, LINE) BASE
180
         FORMAT (2X, F10. 6)
         GOTO 10
         END
```

```
SUBROUTINE TLLSQ(X, Y, XDEV, YDEV, MODE)
C
        LINEAR LEAST SQUARES FOR Y=MX+B
C
C
MODE:
                 1=ZERO SUMS
                 2=ACCUMULATE SUMS
                 3=CALCULATE VALUES
        VALUES GIVEN: X, Y, YDEV (= ERROR ESTIMATE)
                          , MODE
        VALUES RETURNED:
                 X=SLOPE
                 Y=INTERCEPT
                 XDEV=SLOPE STANDARD DEVIATION
                 YDEV=INTERCEPT STANDARD DEVIATION
C
        GO TO (1,2,3) , MODE
1
        A1=0. 0
        A2=0.0
        B1=0. 0
        B2=0. 0
        C1=0. 0
        C2=0. 0
        RETURN
2
        SIG=YDEV
         A1=A1+X**2/SIG**2
         A2=A2+X/SIG**2
         B1=B1+X/SIG**2
         B2=B2+1/SIG**2
        C1=C1+(Y*X)/SIG**2
         C2=C2+Y/SIG**2
         RETURN
3
         D=A2*B1-B2*A1
         X = (B1 + C2 - B2 + C1)/D
         XDEV=SQRT(-B2/(A2**2-A1*B2))
         Y=(A2*C1-A1*C2)/D
         YDEV=SGRT(-A1/(A2**2-A1*B2))
         RETURN
         END
```



REFERENCES

- 1. Hodgkin, "The Conduction of the Nervous Impulse", Liverpool University Press, Liverpool (1964).
- Ashley in "Membrane and Ion Transport", Vol. 2,
 Ed. Bittar, pp. 1-23, Wiley, NY (1970).
- 3. Lehninger, "Biochemistry", Ch. 28, Worth, NY (1975).
- 4. F. Alverado, and A. Mahmood, Biochem., V. <u>13</u> (14), 2882 (1974).
- 5. Jain, "The Bimolecular Lipid Membrane", Ch. 7, Van Nostrand, NY (1972).
- 6. E. Overton, Vjsehr. Naturf. Ges. Zurich, <u>44</u>, 88 (1899).
- 7. I. Langmuir, J. Amer. Chem. Soc., 39, 1848 (1971).
- 8. E. Gorter, F. Grendel, J. Exptl. Med., 41, 439 (1925).
- 9. J. Danielli, H. Davson, J. Cell Phys., 5, 495 (1935).
- 10. S. Singer, and G. Nicholson, Science, 175, 720 (1972).
- 11. A. D. Bangham, M. W. Hill, N. G. Miller, Methods Memb. Biol., 1, 1 (1974).
- 12. P. Mueller, D. Rudin, H. Tein, W. Wescott, Nature, 194, 979 (1962).
- 13. H. T. Tien, "Bilayer Lipid Membranes (BLM): Theory and Practice", Ch. 6-7, Marcel Dekker Inc., NY (1974).
- 14. H. T. Tien, "Photosynthesis in Relation to Model Systems", Ed. J. Barber, pp. 116-173, Elsevier/North Holland Biochemical Press, Amsterdam (1979).
- 15. H. T. Tien, Separation Science and Tech., <u>15</u>, 1035 (1980).
- 16. W. Knoll, G. Stark, J. Memb. Biol., 37, (1977).
- 17. R. Benz, P. Lauger, J. Memb. Biol., 27, 171 (1976).

- 18. F. Gambale, A. Gliozzi, M. Robello, Biochim. Biophys. Acta. 330, 325 (1973).
- 19. W. Knoll, G. Stark, J. Memb. Biol., 25, 249 (1975).
- 20. G. Stark, R. Benz, P. Lauger, Biophys. J., <u>11</u>, 981 (1971).
- 21. D. Levitt, Biophys. J., 22, 221 (1978).
- 22. B. Hille, J. Gen. Physiol., <u>66</u>, 535 (1975).
- 23. P. Lauger, Biochim. Biophys. Acta., 455, 493 (1976).
- 24. E. Neher, J. Sandblom, G. Eisenman, J. Memb. Biol., 40, 97 (1978).
- 25. E. Neher, J. Sandblom, G. Eisenman, J. Memb. Biol., 31, 383 (1977).
- 26. S. Hladky, J. Harris, Biophys. J., 7, 535 (1967).
- 27. P. Lauger, Biochim. Biophys. Acta., 311, 423 (1973).
- 28. J. Hagglund, J. Sandblom, B. Enos, G. Eisenman, Biophys, J., 21, 26a (1978).
- 29. A. Finkelstein, A. Cass, J. Gen. Physiol. <u>52</u>, 145 (1968).
- 30. M. Shemyakin, V. I. Ivanov, V. K. Antonov, J. Memb. Biol., <u>1</u>, 402 (1969).
- 31. G. Szabo, G. Eisenman, S. Ciani, J. Memb. Biol., <u>1</u>, 346 (1969).
- 32. E. Bamberg, K. Janko, Biochim. Biophys. Acta., <u>426</u>, 447 (1976).
- 33. S. Schein, M. Colombim, A. Finkelstein, J. Memb. Biol., 30, 99 (1976).
- 34. K. F. Schnell, J. Memb. Biol., 37,99 (1976).
- 35. M. Eisenberg, J. Kolb, J. Memb., <u>14</u>, 143 (1973).
- 36. G. Boheim, H. Kolb, J. Memb. Biol., <u>38</u>, 99 (1978).
- 37. S. Hladky, D. A. Haydon, Nature, 225, 491 (1970).
- 38. S. B. Hladky, D. A. Haydon, Biochim. Biophys. Acta., <u>274</u>, 294 (1972).

- 39. S. Krasre, G. Eisenman, G. Szabo, Science, <u>174</u>, 412 (1971).
- 40. H. Eyring, B.I. Zwolinski, C. E. Reese, J. Phys. Chem., <u>53</u>, 1426 (1949).
- 41. R. D. Hotchkiss, R. J. Dubos, J. Biol. Chem., <u>141</u>, 155 (1941).
- 42. R. Sarges, B. Witkep, J. Amer, Chem. Soc., <u>87</u>, 2011 (1965).
- 43. V. B. Myers, D. A. Haydon, Biochim. Biophys. Acta., 274, 313 (1972).
- 44. D. C. Tosteson, T. E. Andreoli, M. Tieffenberg, P. Cook, J. Gen. Physiol., 51, 3733 (1968).
- 45. M. C. Goodall, Biochem. Biophys. Acta., 219, 471 (1970).
- 46. E. Bamberg, P. Lauger, J. Memb. Biol., 11, 177 (1973).
- 47. W. R. Veatch, M. Ersengerg, L. Stryer, R. Mathies, J. Mol. Biol., 99, 75 (1975).
- 48. H. A. Kolb, P. Lauger, E. Bamberg, J. Memb. Biol., <u>20</u>, 133 (1975).
- 49. R. Koeppe, J. M. Berg, K. O. Hodgson, L. Stryer, Nature, <u>279</u>, 723 (1979).
- 50. P. W. Urry, Proc, Natl. Acad. Sci. U.S.A. <u>69</u>, 1610 (1972).
- 51. R. J. Bradley, D. W. Urry, K. Okamoto, R. Rapaka, Science, 200, 435 (1978).
- 52. W. R. Veatch, E. T. Fossel, E. R. Blout, Biochemistry, 13, 5249 (1974).
- 53. W. R. Veatch, E. R. Blout, Biochemistry, <u>13</u>, 5257 (1974).
- 54. E. T. Fossel, W. R. Veatch, A. Yu, Biochemistry, <u>13</u>, 5246 (1974).
- 55. H. J. Apel. E. Bamberg, H. Alpes, P. Lauger, J. Memb. Biol., <u>31</u>, 171 (1977).
- 56. E. Bamberg, H. J. Apel, H. Alpes, Proc. Natl. Acad. Sci. U.S.A., 74, 2402 (1977).

- 57. D. W. Urry, M. C. Goodal, J. D. Glickson, D. F. Meyers, Proc. Natl. Acad. Sci. U.S.A., <u>68</u>, 1907 (1971).
- 58. S. Weinstein, B. A. Wallace, E. R. Blout, J. S. Morrow, W. Veatch, Proc. Natl. Acad. Sci. U.S.A., 76, 4230 (1979).
- 59. J. R. Knowles, Accounts of Chem. Res., 5, 155 (1972).
- 60. J. M. Stadel. D. B. Goodman, R.E. Galardy, H. Resmussen, Hiochemistry, 17, 1403 (1978).
- 61. R. E. Galardy, L. C. Craig, J. D. Jannieson, M. P. Printz, J. Biol. Chem., <u>249</u>, 3510 (1974).
- 62. T. Bercovici, C. Gitler, Biochem., 17, 1484 (1978).
- 63. P. R. Matheson, E. Vanwart, A. W. Burgess, L. I. Weinstein, H. A. Scheraga, Biochemistry, 16, 396 (1977).
- 64. R. B. Pepinsky, G. W. Feigenson, Anal. Biochem., <u>86</u>, 512 (1978).
- 65. D. W. Urry, A. Spisni, A. Khaled, Biochem. Biophys. Res. Comm., 88, 940 (1979).
- 66. J. V. Staros, F. M. Richards, Biochem., 13, 2720 (1974).
- 67. H. Bayley, J. R. Knowles, Biochemistry, <u>17</u>, 2414 (1978).
- 68. R. A. Smith, J. R. Knowles, J. Chem. Soc., Perkin Trans., 2, 686 (1975).
- 69. E. Bamberg, R. Benz, Biochem. Biophys. Acta., 426, 570 (1976).
- 70. H. J. Apeel, E. Bamberg, H. Alpes, P. Lauger, J. Memb. Biol., <u>31</u>, 171 (1977).
- 71. S. M. White, T. E. Thompson, Biochem. Biophys. Acta., 323, 7 (1973).
- 72. R. Fettiplace, D. M. Andrews, D. A. Haydon, J. Memb. Biol., <u>5</u>, 277 (1971).
- 73. R. Benz, O. Frolich, P. Lauger, M. Montal, Biochim. Biophys. Acta., 394, 323 (1975).
- 74. V. A. Nicely, J. L. Dye, J. Chem. Ed., 48, 443 (1971).
- 75. S. V. Sychev, N. A. Nevskaya, S. T. Jordanov, E. N. Shepel, Bioorg. Chem., 9, 121 (1980).

- 76. S. Feldberg, G. Kissel, J. Memb. Biol., 20, 269 (1975).
- 77. T. A. Last, C. G. Enke, Anal. Chem., 49, 19 (1977).
- 78. T. A. Last, Ph. D. Thesis, Michigan State University (1977).

